CLEEN
Cluster for Energy and Environment

Research Report nr D509
Helsinki 2013

Calin Cosma and Nicoleta Enescu
Vibrometric Oy

D509 Report on the reprocessing of the borehole seismic data collected at Ketzin in 2007-2011

ccsp
Carbon Capture and Storage Program

CLEEN LTD
ETELÄRANTA 10
P.O. BOX 10
FI-00130 HELSINKI
FINLAND
www.cleen.fi

ISBN XXX-XX-XXXX-X
ISSN XXXX-XXXX

Cleen Ltd.
Research Report nr D509

Calin Cosma and Nicoleta Enescu
Vibrometric Oy

D509 Report on the reprocessing of the borehole seismic data collected at Ketzin in 2007-2011

ccsp
Carbon Capture and Storage Program

Cleen Ltd
Helsinki 2013

Report Title: Report on the reprocessing of the borehole seismic data collected at Ketzin in 2007-2011

Key words: Borehole seismic, VSP, MSP, Crosshole, Monitoring of CO2 injection

Abstract

The main objective for the seismic characterization and monitoring activities for a CO2 geological storage facility is to provide a thorough understanding of the structural geometry and flow pathways of the reservoir prior to development, during operation and after closure.

This report documents the reprocessing and interpretation of recent and vintage seismic data sets from the Ketzin research facility in Germany, in the light of newly developed data enhancement and imaging techniques for analysis of time-lapse surveys. The data evaluated here was collected at a saline aquifer site with size and properties comparable to the potential sites envisaged by CLEEN. Development and testing of seismic imaging techniques was done in order to include these to the methodological package of storage sites testing.

In order to enhance the spatial resolution around the injection and to assess alternatives to the logistically and financially demanding 3D surveys, 2D reflection surveys were performed on seven profiles around the injection site (2D Star). The baseline and repeat surveys took place in 2005, 2009 and 2011, respectively. The same profiles were also used for the surface-to- hole MSP and VSP surveys. While the 2D reflection profiles basically image the same structures as do the 3D surveys, VSP and MSP surveys are characterized by a higher resolution at reservoir depth, and they are capable of imaging steeply dipping structures which are usually ignored by surface measurements alone.

Wide-band seismic data is increasingly recognized as a fundamental requirement for efficient and qualitative CO2 reservoir monitoring. Various seismic data acquisition tools and processing techniques have been evaluated and directions of further development towards improved technical capability and economic efficiency are recommended.

Helsinki, 03 2012

Table of contents

1 Introduction

Subsurface monitoring is necessary for any CO_2 geologic storage facility in order to control and optimize injection and build the safety case. The underlying assumption for using seismics for monitoring CO_2 geologic storage is that the acoustic impedance (the product of the density and acoustic velocity) decreases when CO_2 is injected in the storage formation. The evolution of the plume can therefore be followed by observing variations of the acoustic impedance in time-lapse seismic surveys. Table 1 summarizes the seismic investigation methods used for characterizing and monitoring of a CO_2.

Table 1. Seismic investigation methods for CO2 storage characterization.

Seismic investigation method	Factors that may affect the survey time-lapse repeatability	Factors that may affect the survey sensitivity	Expected output
2-D seismic profiling	Source repeatability Variations in set-up and processing flow. Changed weather conditions	Limited frequency band Uneven or off-target receiver layout Large static errors Low signal-to-noise ratio	Stratigraphic sequence, bed thickness, depth Change in impedance and velocity with change in CO2 saturation
Walk-away VSP / 3D VSP	Changed receiver array Variations in processing flow	Limited horizontal coverage	High vertical resolution Velocity vs. depth maps Direct imaging of steep faults
3-D seismic survey	Source repeatability Changed weather conditions	Limited frequency band Large static errors Low signal-to-noise ratio	3D imaging of stratigraphic sequence Change with time of spatial distribution of impedance and velocity with change in CO_2 saturation

The distribution in the injection reservoir of sufficiently large amounts of CO_2, i.e. enough to produce an observable change in the subsurface, can be mapped using active source **time-lapse seismic methods** from surface. Smaller amounts of CO_2 can be mapped, if **time-lapse borehole seismic methods** are used. The limit of detectability in terms of quantity injected has been studied (Enescu et. al., 2011b).

From Table 1, it appears that the main characterization and monitoring objectives are more closely met by the surface 3D surveys. Possible difficulties are related to the

deployment of the receivers on ground surface: decreased high frequency content due to absorption in the near-surface weathered zone, static errors due to large local variations of surface conditions and environmental noise. These difficulties are normally easily avoided. Regarding repeatability, difficulties with repeatability can appear due to changed water saturation, snow, frost and vegetation between time-lapse sessions and to variations of source coupling amongst the numerous shot locations.

The 2D surveys produce similar vertical results with 3D, but with uneven horizontal coverage and resolution. The main advantage is that frequent time-lapse repeats are easier to perform. Variations of source and receiver positions due to changed access between time-lapse sessions are more critical with 2D than with the 3D case. Changed layouts can also require changes in the processing flow, which could complicate the comparative time-lapse analysis. Planning the surveys based solely on unconfirmed modelling results can have dire consequences, if the subsequent evolution of the CO_2 plume does not follow the model predictions. It is therefore advisable to perform an extended-coverage baseline survey.

3D and 2D-VSP surveys in boreholes have definite advantages over the surface counterpart, such as the derivation of a velocity field at the site scale, and the direct imaging of faults, even if the vertical displacement is small or hidden in the stratigraphic complexity. The approximately double vertical resolution compared with the surface methods is also important, but it is somewhat shadowed by the horizontal coverage limited to a cylinder around the survey borehole with a diameter roughly equal to the borehole depth. The repeatability is less likely to be affected by changing surface conditions but varying technical conditions, e.g. measuring in a pressurized well after the start of the injection may require the receiver array to be modified between time-lapse sessions.

The repeatability of the surveys is very important and efforts are being made with all techniques to mitigate all factors that could influence it.

The distribution in the injection reservoir of sufficiently large amounts of CO_2, i.e. enough to produce an observable change in the subsurface, can be mapped using active source **time-lapse seismic methods** from surface. Smaller amounts of CO_2 can be mapped, if **time-lapse borehole seismic methods** are used. The limit of detectability in terms of quantity injected has been studied (Enescu et. al., 2011b).

1.1 The CO_2SINK project and the Ketzin site in Germany

As a founding member of the CO_2SINK consortium Vibrometric has privileged access to project data. The CO_2SINK project (www.co2sink.org) has been the first onshore European CO_2 injection experiment, made possible with funding from the EU commission (SES6-CT-2004-5025599), under the FP6 framework and the industry (Statoil, RWE, Vattenfall, and VNG).

The CO_2SINK site is located at Ketzin, west of Berlin, Germany. Three wells were drilled, one serving as the CO_2 injection well and the other two as observation wells (Figure 1).

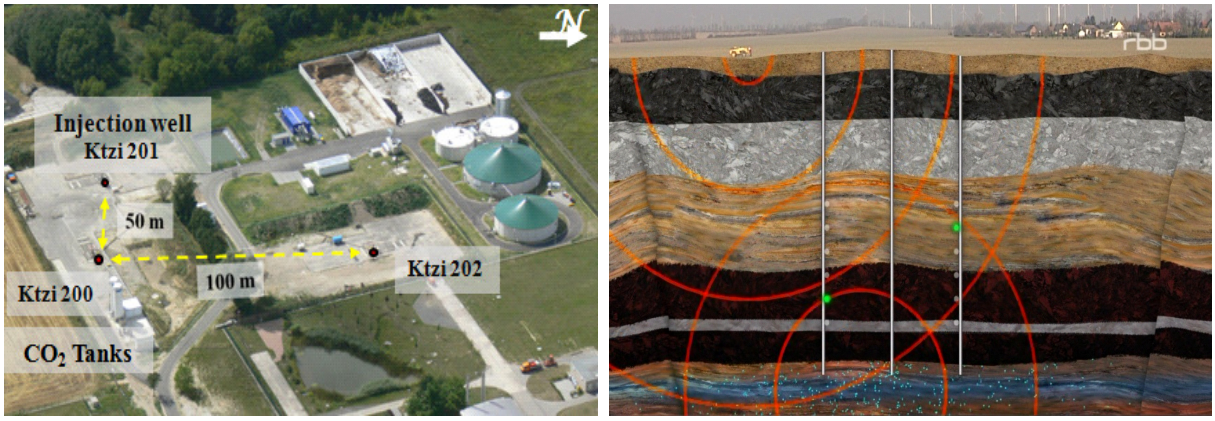

Figure 1. Ketzin site and cartoon illustrating the monitoring concept by reflection seismics from surface and boreholes.

The CO_2 is injected into a saline aquifer in the heterogeneous Upper Triassic Stuttgart Formation which is located at approximately 630-650 m depth in the injection well. The Stuttgart Formation is about 80 m thick and is comprised of siltstones and sandstones interbedded with mudstones. The saline sandstone aquifers vary in thickness from 1 m to 30 m (Norden et al., 2008). The caprock for the CO_2 reservoir is comprised of the Weser and Arnstadt Formations, containing almost 210 m of mudstone and evaporate. A 10-20 m thick high velocity anhydrite layer (K2) is present at the top of the Weser formation (Figure 2).

The injection started on 30.06.2008, and as of 31.07.2011, at the end of the CO_2SINK project, 51,231 tons of CO_2 have been injected in the underground. The injection rates and cumulative mass of injected CO2 are illustrated in Figure 3.

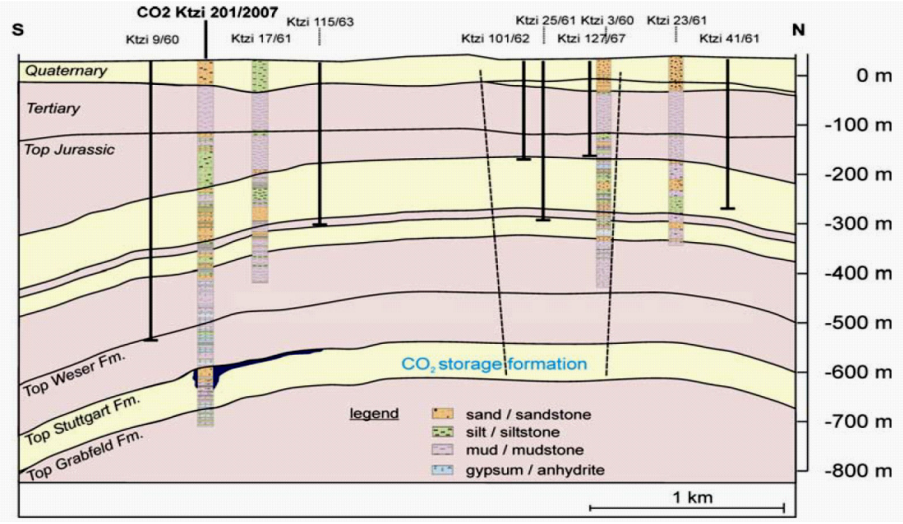

Figure 2. Simplified stratigraphic and lithologic section of the Ketzin Anticline *(*after Förster et al. (2006)) with lithology of the injection well CO2 Ktzi 201/2007.

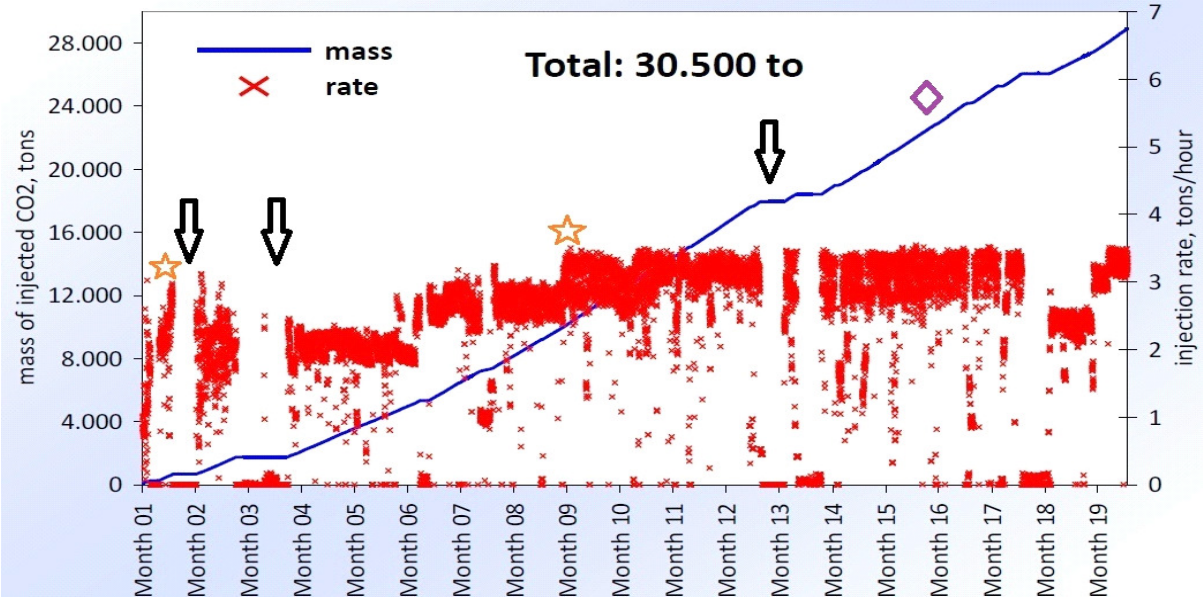

Figure 3. Injection rates and cumulative mass of injected CO2 at Ketzin, from July 2008 (Month 1) until Feb 2010 (Month 19) (Möller, 2010). Orange stars: break-through to KTZI-200 observation well (530 tons, 15 days) and to KTZI-202 observation well (11050 tons, 263 days). Black arrows: timing of the 3 cross-well repeats in July 2008, Aug 2008 and July 2009. Purple rectangle: timing of the first 3D repeat survey (Oct 2009).

1.2 Seismic monitoring at Ketzin, Germany

The seismic characterization of CO_2 storage at Ketzin consisted of several investigation and monitoring elements covering different experimental scales mutually validating and potentially complementing each other (Figure 4). Within the Stuttgart Formation, the CO_2 has been expected to migrate away from the injection point at distances of the order of one kilometer through channels tens of meters wide and a few meters thick. The intention was to cover with the seismic measurements the kilometer scale encompassing the region where the CO_2 could migrate, while resolving at a meter scale the potential heterogeneities of the aquifer, especially in the vicinity of the injection site.

The general objective was to contribute to the understanding of the structural geometry of the site by performing baseline surveys with all the methods listed in Table 1 and then to monitor the expansion of the CO_2 plume with time. The program has been structured so that the wide-coverage more costly items e.g. the 3D survey, were scheduled to be repeated at longer time intervals, while more frequent time-lapse repeats were planned for the focused and less costly items.

The proposed scope of the seismic investigation plan contained the following elements:

- baseline 3D
- multi-line 2D ‘Star’ survey; pre-injection baseline, repeat during injection, repeat after injection
- MSP (Moving Source Profiling); pre-injection baseline, repeat during-injection, repeat after injection, same source locations as with 2D ‘Star’

- VSP (Vertical Seismic Profiling); pre-injection baseline, repeat during-injection, repeat after injection, selected source locations along the 2D 'Star' lines.
- Four cross-hole sessions between Ktzi200 and Ktzi202 (baseline and three time-lapse repeats during injection).

Budgetary and scheduling reasons lead to the elimination of the VSP repeat during injection. Reduced area 3D repeats after injection end, as well as other investigations without a pre-injection baseline, have been performed, outside the frame of the CO_2SINK project.

The measuring program has been realized as follows:

a) **3D-Seismic**: baseline (Sept-Dec 2005), 1st repeat (Sept-Nov 2009) and 2nd repeat (Sept-Nov 2012)

The main purpose of the 3D measurements has been to provide a model of the geology around the injection well. The results of the measurements showed also detailed information from a fault and graben system ~2 km North of the injection and indications of residual gas in shallower layers formerly used for gas storage.

b) **Pseudo-3D (Star) Survey and MSP (Moving Source Profiling)**: baseline (Nov-Dec 2007), 1st repeat (Sept 2009) and 2nd repeat (Feb 2011)

The main objectives of the "star" surveys were to identify changes in the seismic response related to the injection of CO_2 between the repeat surveys and baseline survey and to compare these results with those from the 3D seismic data. Similarly, MSP measurements were made from sources of the "star" survey on surface to receivers down-hole, placed nearer to the injection layer in an attempt to provide a higher resolution image than what can be obtained from surface alone. Eight receivers were used for baseline MSP measurements, while the repeats were done with only one receiver, because of access limitations in the observation well, that had to be kept pressurized during the injection.

c) **VSP (Vertical Seismic Profiling)**: baseline (Nov-Dec 2007) and 1st repeat (Feb 2011)

Similarly with the MSP surveys, VSP was done from surface to borehole, but the entire length of the borehole was covered with receiver stations at 5 m intervals.

d) **Cross-hole** (between holes Ktzi-201 and Ktzi-202): baseline (May 2008), 1st repeat (Jul 2008), 2nd repeat (Aug 2008) and 3rd repeat (Jul 2009)

The crosshole measurements were meant to cover the smallest scale of all measurements performed, between wells approximately 100 m apart. Crosshole tomographic surveys were repeated between the observation wells located at 50m and 120m from the injection well in order to provide a high-resolution model for the reservoir near the injection and to observe the change of seismic velocities between the observation wells.

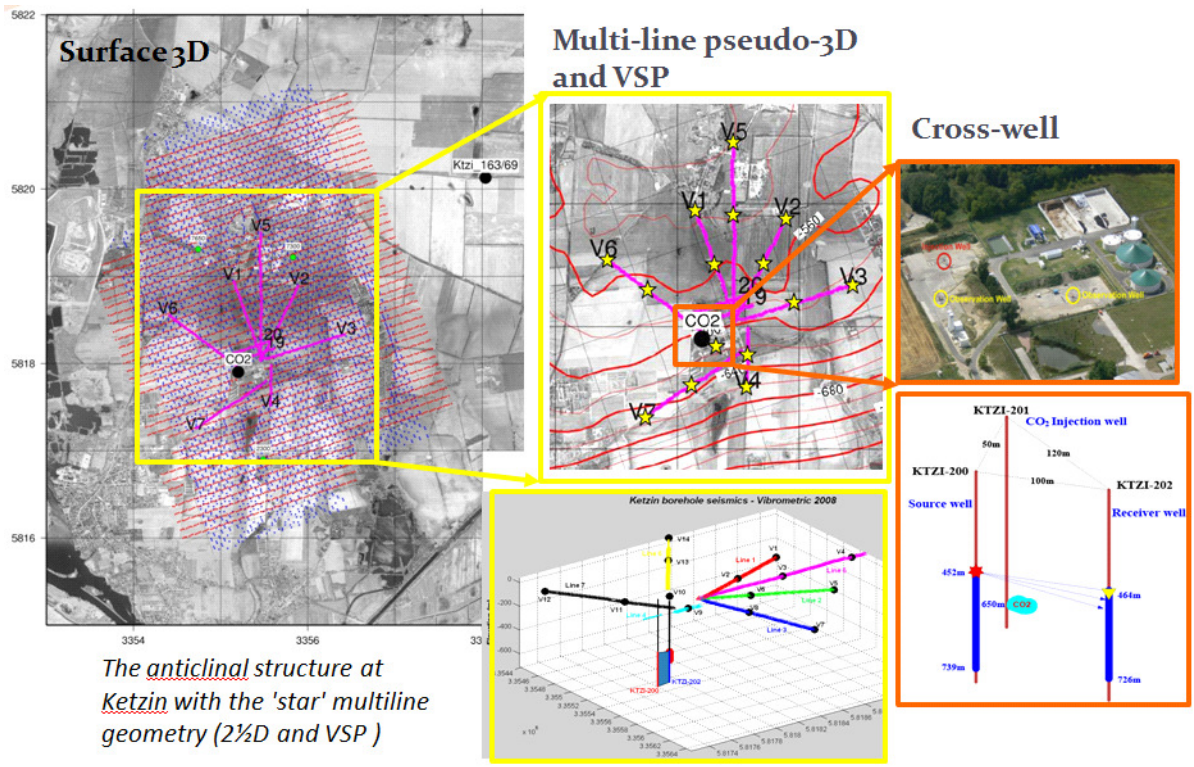

Figure 4. Seismic monitoring methods that have been applied at the Ketzin site comprise baseline and repeat observations at various scales.

1.2.1 Seismic data used for testing of new imaging techniques

The seismic data collected at Ketzin were re-analysed and used as a means of testing the methods and techniques studied and developed within subtask 5.1.3. The sizeable amount of data collected and the diversity of the measuring techniques used offered a valuable and comprehensive perspective on the seismic methods. The analyses were aimed at qualifying the methodology in the specific context of CCS projects. One question addressed has been how to describe in better detail the evolution with time of the reservoir after commencing the injection of CO_2 by performing frequent time-lapse repeats or continuous measurements while maintaining however costs at a reasonable level. The results of this study are presented in Section.1.3. Other topics presented further on in this report concern various improvements and further development of data processing and interpretation techniques to increase their efficiency for CCS applications.

1.3 Seismic modelling for CO_2 detection and optimal survey configuration

The modelling study undertaken in the CLEEN - CCSP framework and in collaboration with the MUSTANG project (Enescu et. al., 2011a and Enescu et. al., 2011b) is aimed to clarify optimum survey geometry (numbers of source and receiver stations) to be used for seismic monitoring of CO_2 geological storage sites and possibly the detection of a CO_2 leak.

The MUSTANG consortium, of which Vibrometric is a member, was established in 2009 under the EU FP7 and attempts to develop and disseminate tools and methodologies for the identification, assessment, characterization and evaluation of deep saline aquifers for CO2 storage. The Heletz area is located in Israel, in the southern part of the Mediterranean Coastal Plain, about 7 km from the sea shore. The target CO_2 storage layer is heterogeneous and consists of sandstone, low-permeability sandstone and shale. Approximately 1400 tons of CO_2 are planned to be injected at a depth of approximately 1600 m. The diameter of the plume is expected to be of the order of 100m. It is not expected that conventional surface seismic reflection surveys produce an image of a plume of this size. Diffractions and a non-coherent backscattering may however appear as local changes of amplitude and phase. The approach discussed is to detect, as opposed to delineate, a small CO_2 plume, by means of limited and/or sparse seismic arrays. Such arrays could reasonably be installed permanently or semi-permanently, to allow cost-effective active and passive measurements from surface and boreholes.

Seismic modeling studies were carried out in support of determining suitable source and receiver geometries and most appropriate seismic source frequencies. The main reason for carrying out these studies is that 3D surface seismic surveys are expensive and time consuming to perform and borehole methods only provide data in the vicinity of the boreholes. Migrated images of surface lines and VSP profiles were generated from synthetic data. The CO_2 plume intersected at the correct depth and displayed the correct lateral extent (as shown in Figure 5 and Figure 6). The surface source and receiver spacing was 12 m and borehole receivers were 80, placed at 5 m intervals, with the same relative geometry as the one used for the surveys done at Ketzin. Modeling results showed that a relatively small number of active sources and receivers can be used to detect subsurface changes that may be induced by injection of a relatively small amount of CO_2. Pseudo 3D coverage could be obtained with relatively sparse coverage from surface & borehole.

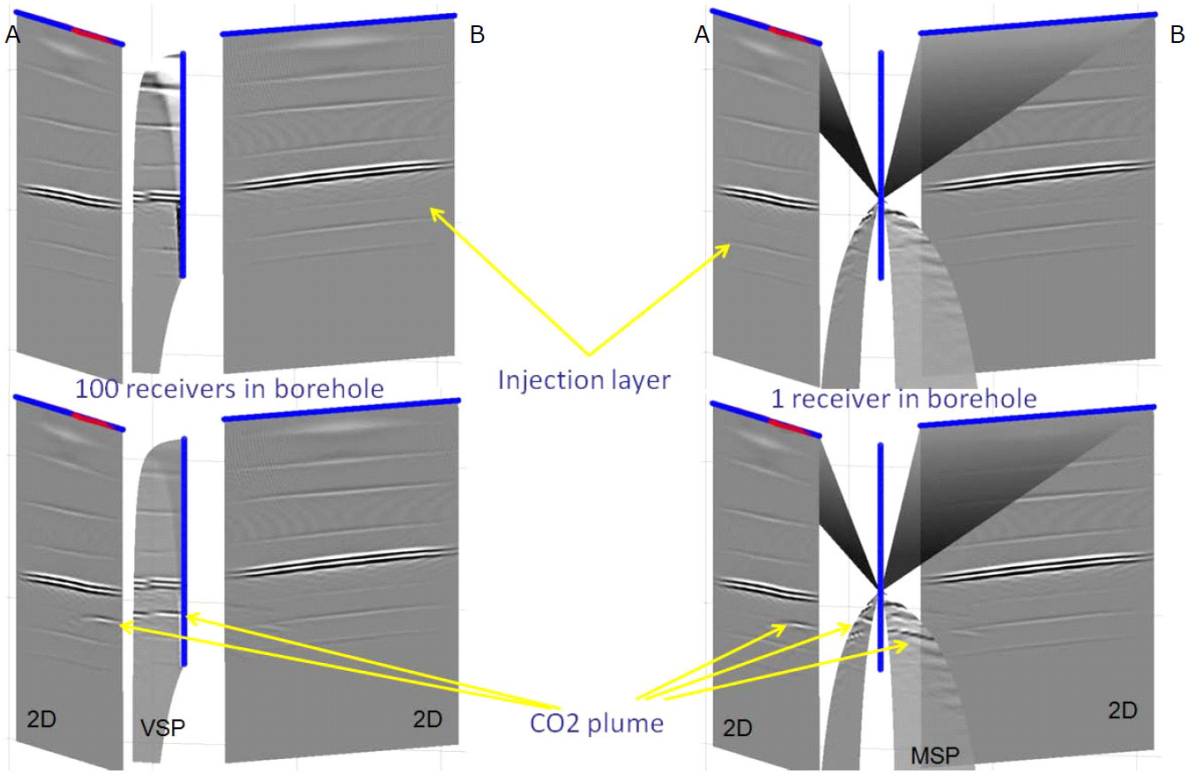

Figure 5. Reflection imaging from surface and borehole, 2D & VSP/MSP (assuming 100 Hz source signals), before and after injection of CO_2. Survey geometry and site characteristics mimics the monitoring done at Ketzin, with the simulated plume of the same size as the one detected by first 3D repeat done in 2009 (Enescu et. al., 2011b).

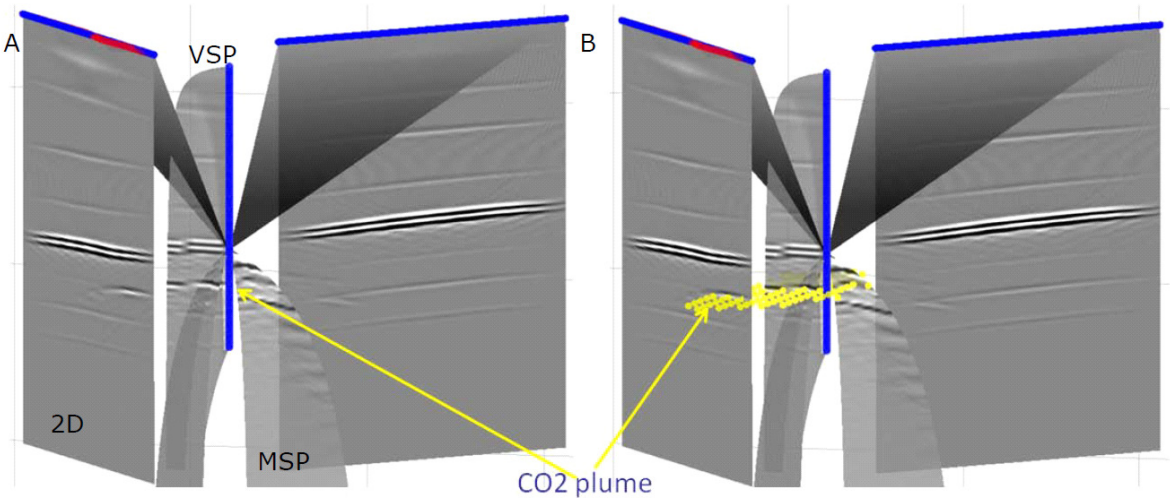

Figure 6. Combined imaging of the CO_2 plume from multi-line surface 2D and borehole measurements, VSP & MSP. Pseudo 3D coverage can be obtained with relatively sparse coverage from surface and borehole (Enescu et. al., 2011b).

Pairs of profiles were modeled without and with the CO_2 plume, as generated by sources with centre signal frequencies from 10 Hz to 100 Hz. Above 50 Hz the caprock layer and the CO_2 plume become clearly distinct (Figure 7). However, frequencies above 80-90 Hz were required to detect non-ambiguously the plume. At

Ketzin, such frequencies were typical for the borehole measured data, when a VIBSIST source was used. However, it is expected that at Heletz, such frequencies can be difficult to obtain using surface sources and receivers, considering the depth of the reservoir and the near surface conditions. Therefore, it is recommended that borehole seismics should be used at Heletz or at similar sites.

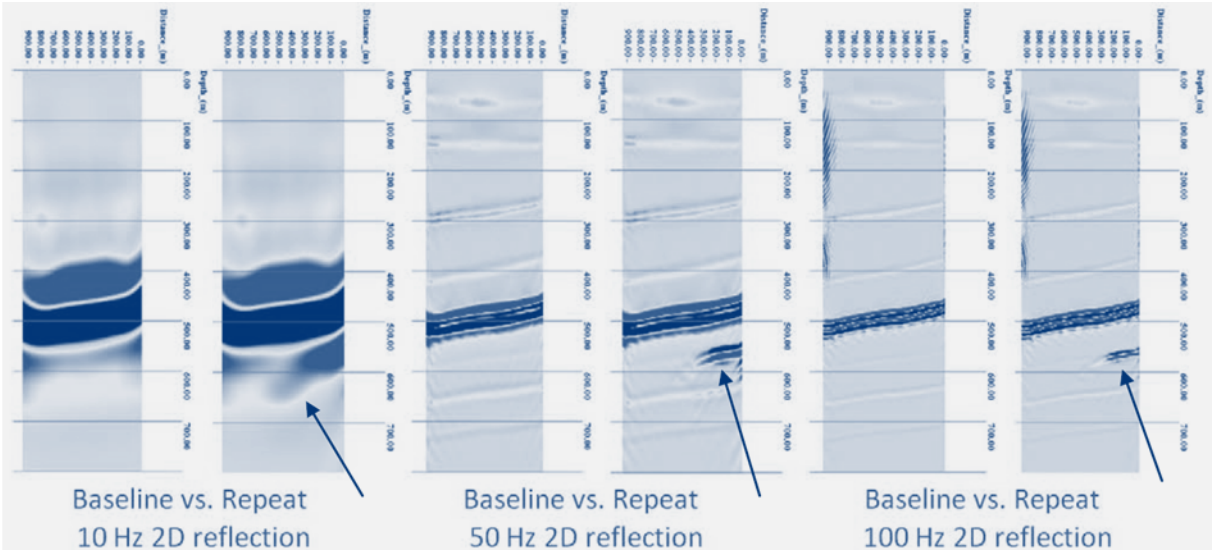

Figure 7. 2D reflection imaging (Line 6 or the Ketzin 2D Star array) before and after injection of CO2 assuming different frequency content of the seismic signals. This 2D profile is also shown on the left side in Figure 5 and Figure 6.

At the cost of reduced resolution, low frequencies allow larger volumes to be probed. The capability of producing and recording high frequencies should also be conserved for detailed monitoring whenever possible.

Changes of environment and climatic conditions rank high as causes of time-lapse noise and it is reasonable to assume that the noise is higher near the earth surface. Surface and borehole seismic surveys were simulated to evaluate the influence of four types of near surface conditions onto the complexity of recorded seismic signals. The physical properties in the near surface layers were varied as illustrated in Figure 8. This also displays records from sources and receivers placed on surface, assuming near surface conditions change from "very good" to "poor".

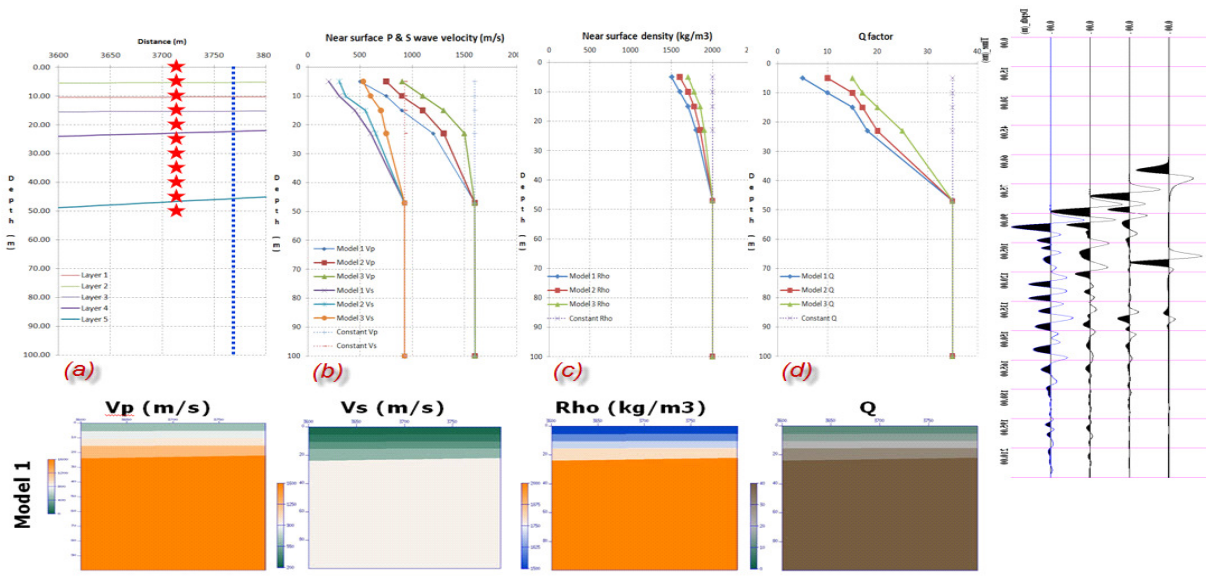

Figure 8. Seismic modeling for evaluation of the influence of changing near surface conditions on the repeatability of seismic imaging from surface and boreholes. Geometry (a) and physical properties used for four sets of 2D and VSP simulations meant to test the effect of variations in the near surface conditions. P wave velocities vary from 500m/s to 900m/s in the top surface layer to 1600m/s in the deeper layer (b), S wave velocities vary from 200m/s to 530m/s in the top surface layer to 925m/s in the deeper layer (b), densities vary from 1500kg/m3 to 1700kg/m3 in the top surface layer to 2000kg/m3 in the deeper layer (c) and Q factors vary from 5 to 15 in the top surface layer to 35 in the deeper layer (d). A case of constant properties was also considered, where velocities, density and Q factor values were set to equal those in the deeper layer, for the entire geometrical model.

Another illustration of the same phenomenon is shown in Figure 9 and Figure 10 where the complexity of the scattered seismic field is depicted for a synthetic VSP survey, with the source placed at various depths within and under the disturbed near-surface zone, showing that the complexity of the records in the near-surface increases with the degradation of the physical properties in the near-surface layers, the weaker the layers, the more complex the records.

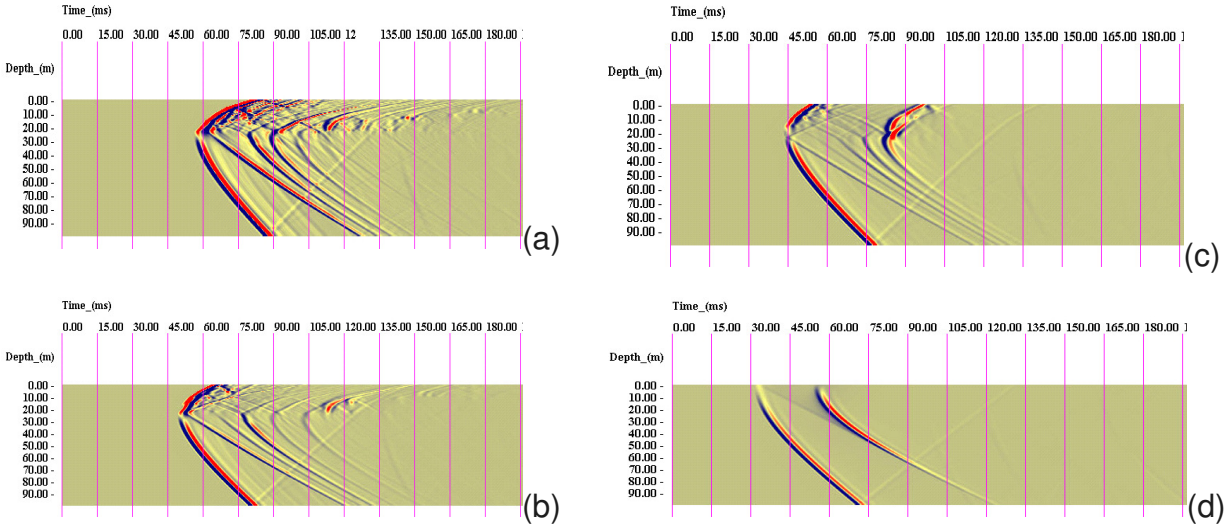

Figure 9. Noise free vertical component receiver layouts recorded for the VSP geometry, when the source is placed on the surface, at a 50m offset with respect to the receiver borehole. The profiles were obtained using the Model 1 (a), Model 2 (b), Model 3 (c) and constant properties model (d), as described in Figure 8.

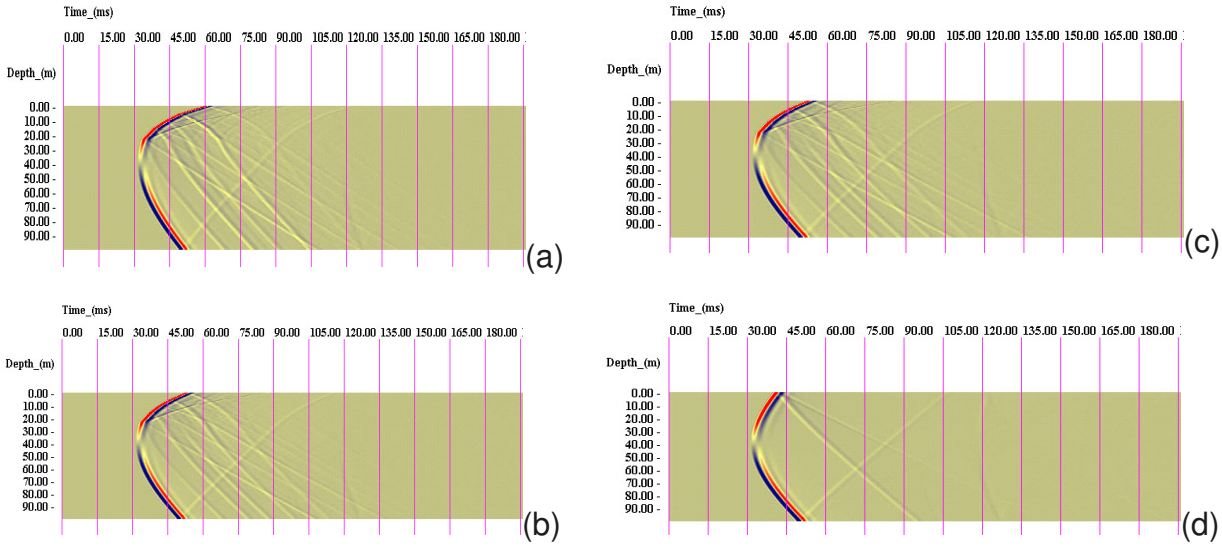

Figure 10. Noise free vertical component receiver layouts recorded for the VSP geometry, when the source is placed at 40m below the surface and at a 50m offset with respect to the receiver borehole. The profiles were obtained using the Model 1 (a), Model 2 (b), Model 3 (c) and constant properties model (d), as described in Figure 8.

As the surface conditions are difficult to control and may vary siginificatly at different moments in time, placing sources and receivers beneath the surface seems to be the only consistent way of mitigating the near-surface influence on the data quality. This conclusion falls in line with the attention given in Subtask 5.1.3. to borehole and subsurface seismic sources and receivers.

The potential of surface seismic methods to monitor small amounts of CO_2 is exemplified on a model created by assuming a 200 m wide plume at ~ 2000 m depth, as illustrated in Figure 11.

a)

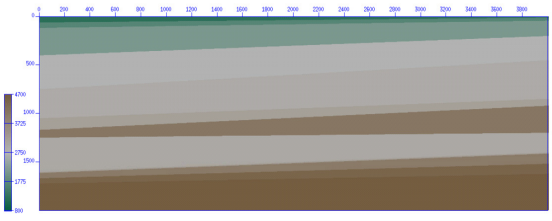

P wave velocity, variation from 1200m/s to 4700m/s.

b)

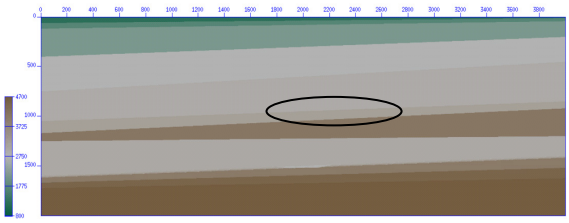

P wave velocity, assuming a 5% decreased in the zone affected by CO_2 injection.

Figure 11. Physical properties (P wave velocity) for the "Baseline" (a) and "Repeat" (b) simulated surveys.

CDP stacks are shown in Figure 12 (a) and (b). Little difference is observed between the baseline and repeats stacks when inspected individually. However, when the baseline result is subtracted from the repeat survey a clear anomaly due to the CO_2 plume is observed in Figure 12 (c). The anomaly roughly outlines the extent of the plume. However, when random shifts are introduced into the repeat data of +/- 4 milliseconds prior to processing it is not possible to identify the plume in the difference stack, as shown in Figure 12 (d). Differences in timing are often observed in real data acquired on land on repeat surveys due to changes in near-surface

conditions. This study supports the idea of installing sensors and sources below the near-surface.

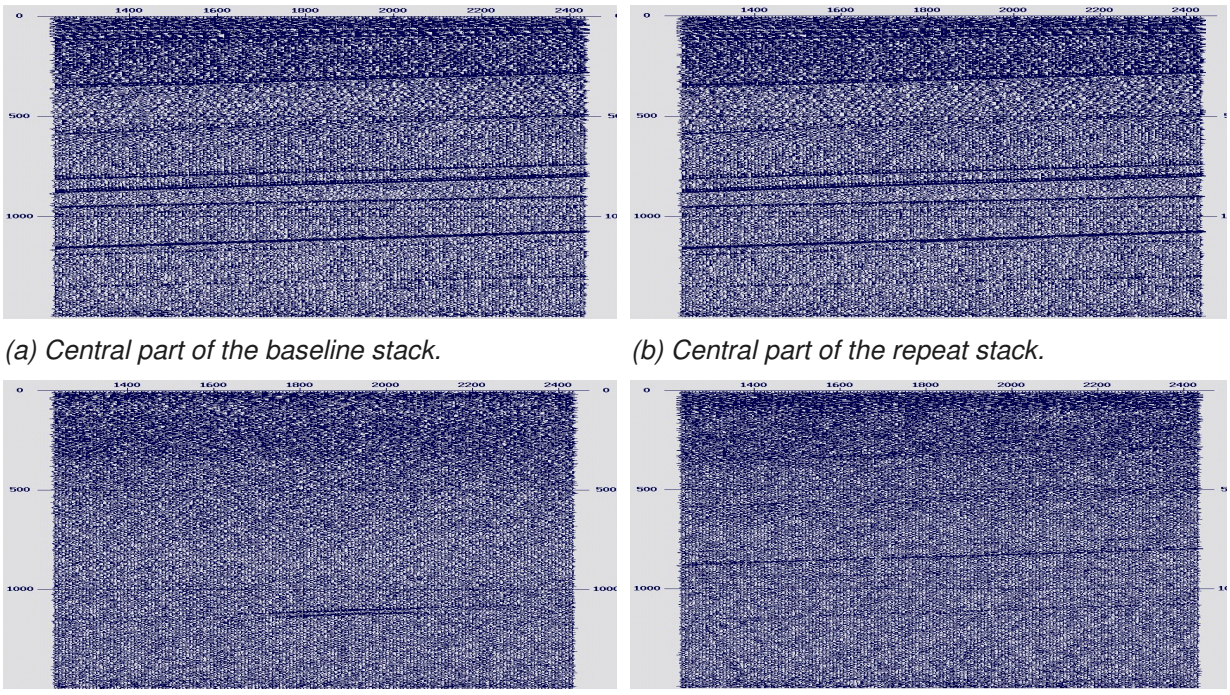

(a) Central part of the baseline stack.

(b) Central part of the repeat stack.

(c) Central part of the difference stack (repeat - baseline) for the 200 m wide plume model.

(d) Central part of the difference stack (repeat - baseline) for the 200 m wide plume model when random shifts of +/- 4 ms were introduced into the repeat data.

Figure 12. CDP stacks for evaluation of noise and near surface conditions variation on detectability of a small CO2 plume. Vertical axis is time in miliseconds, horizontal axis is distance along the model in meters. Injection point is at about 2000 m.

1.4 Main results from the 3D and 2D Star seismic site characterization at Ketzin

The main results, regarding monitoring of the CO2 in the Ketzin acquifer, of the baseline 3D site characterization and time-lapse analysis obtained from the first two 3D seismic surveys done at Ketzin were reported by (Juhlin, 2007 and Juhlin, 2010 - personal communication) and are shown in Figure 13 and Figure 14.

Up to the time of the 1st 2D Star repeat survey in September 2009 a relatively small amount of CO2 had been injected (22-25 kilotons) and by the time of the 2nd repeat survey in February 2011 about 45 kilotons had been injected. (Ivandic, 2012) reports the pseudo-3D processing of the 2D Star data. The main results obtained from the Star collection of 2D lines, as compared with real 3D time-lapse data, are shown in Figure 16.

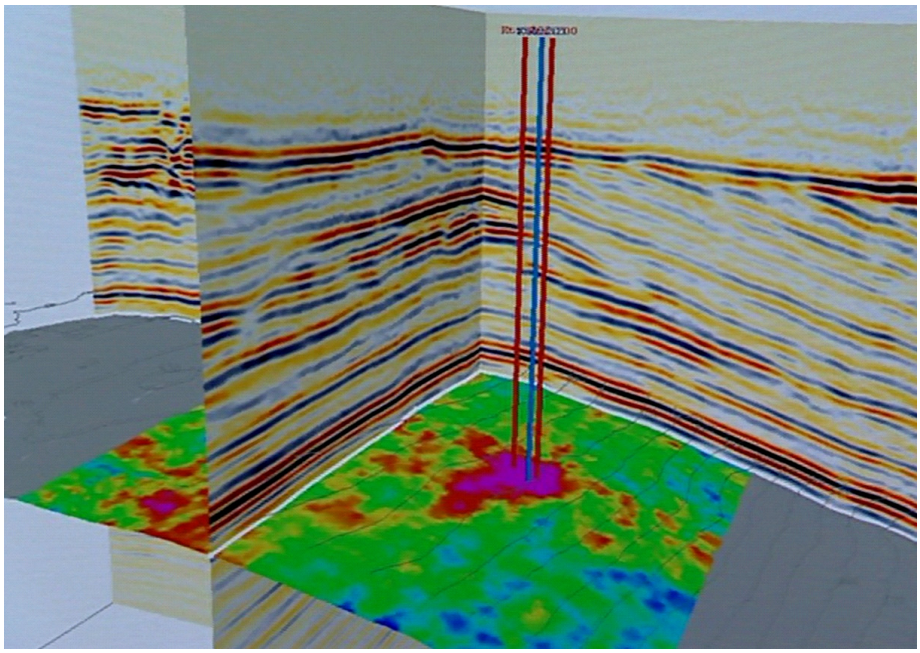

Figure 13. 3D map of the normalized time-lapse amplitude at the top of the CO2 injection layer. The time-lapse amplitude (color coded) is projected onto topography of the top of the reservoir. The injection well (KTZI-201/2007) is indicated by a blue vertical line. Two red vertical lines indicate the observation wells (KTZI-200/2007 and KTZI-202/2007).

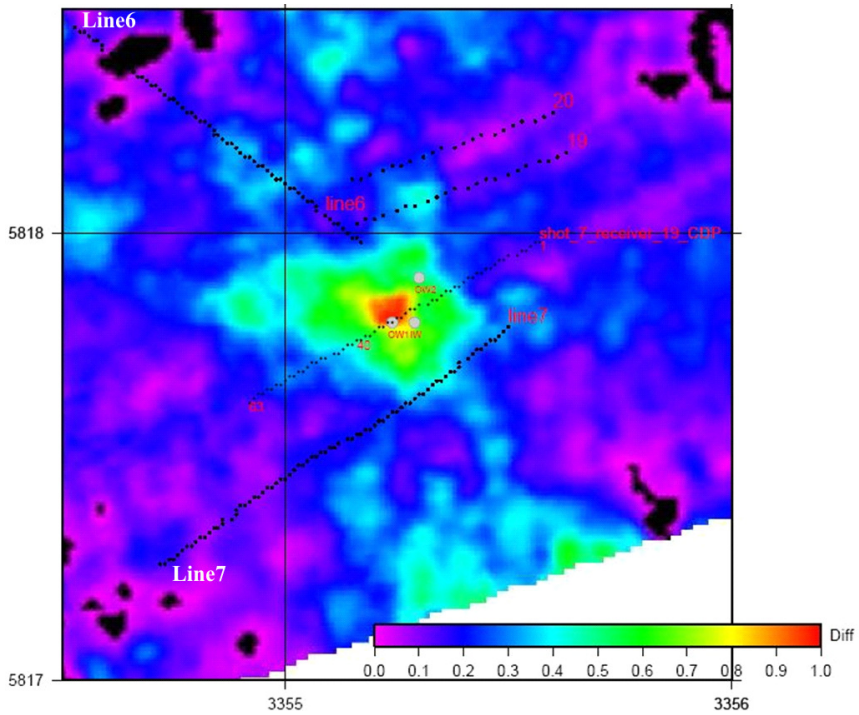

Figure 14. Detail of the difference map for the baseline minus the 2009 repeat for a horizon located 42 ms below the peak of the K2 reflection (Juhlin, 2010). This horizon approximately corresponds to the top of the injection zone. The map shows the locations of the injection well (KTZI-201/2007) and the two observation wells (KTZI-200/2007 & KTZI-202/2007) as grey dots. The anomaly in the south is due to the low fold in that area. Additionally, some of the sub-surface reflection points of the 2D seismic lines are plotted on top. Most of the 2D lines do not have sub-surface coverage of the CO_2 plume as mapped from the 3D seismic data. Only shot-receiver combinations of lines located on opposite sides of the anomaly are able to image the CO_2 plume.

According to (Bergmann, 2011), who compared results of independently processing the 2D lines that formed the Star survey (first repeat, in 2009) with the first repeat , also in 2009 of the 3D survey, it appears that both types of investigation do image the subsurface with local differences, attributed mainly to the difference in the acquisition geometry and source types in use. Time-lapse interpretation of the 2009 data set showed, that no CO_2 related time-lapse signature is observable where the 2D lines allow monitoring of the reservoir. This finding is consistent with the time-lapse results of the 3D surveys, which show a reflectivity increase centred around the injection well. Further investigation by AVO analysis confirmed that during the period of the 2009 repeat survey the CO_2 did not propagate as far as the 2D lines (Figure 15).

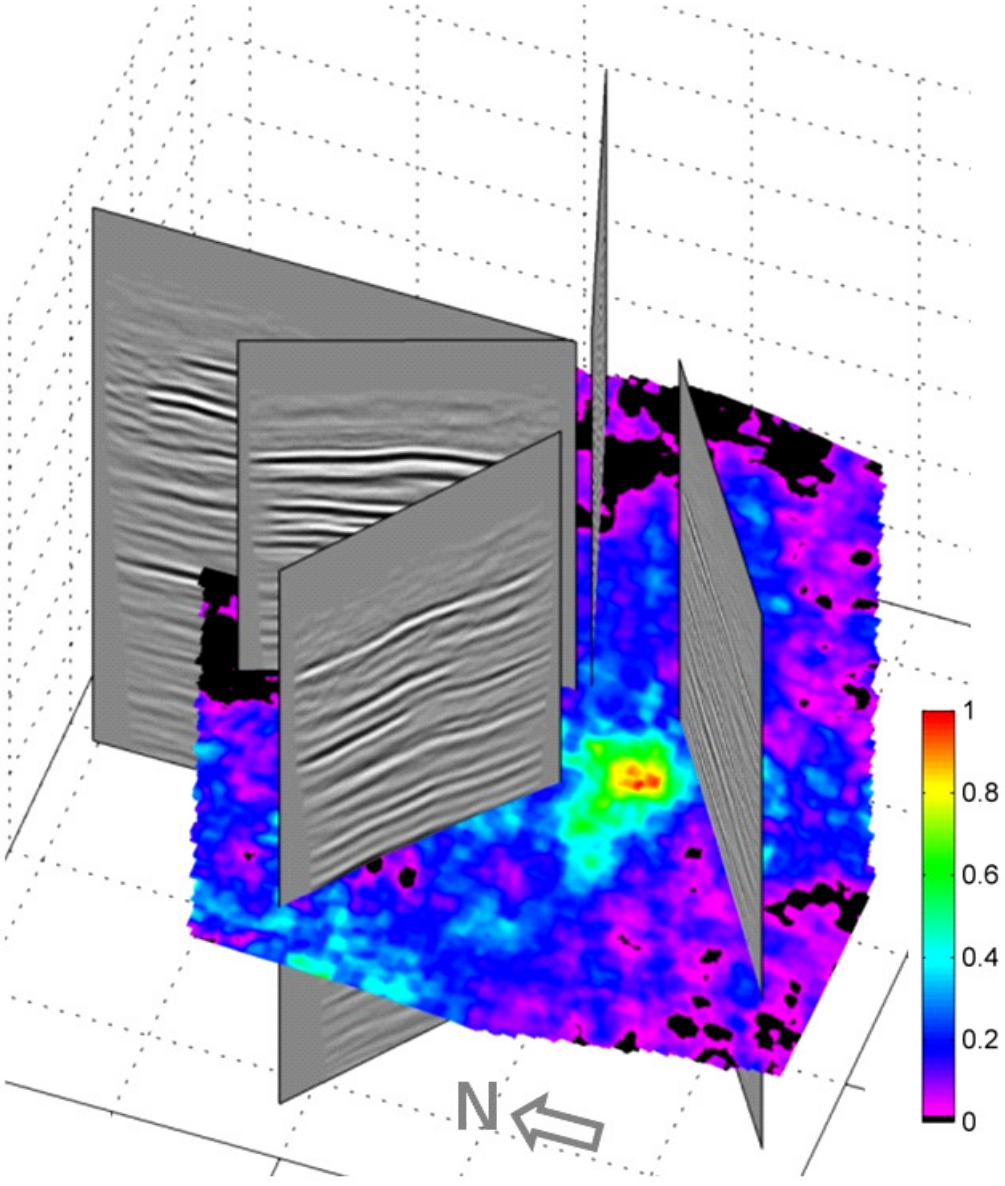

Figure 15. Independent time-lapse processing of 2D seismic profiles (Bergmann, 2011) is not suitable for imaging differences induced by the CO2 injection, as the extent of the plume (mapped by 3D, Juhlin, 2010) did not reach far enough in the regions covered by the 2D lines of the Star survey.

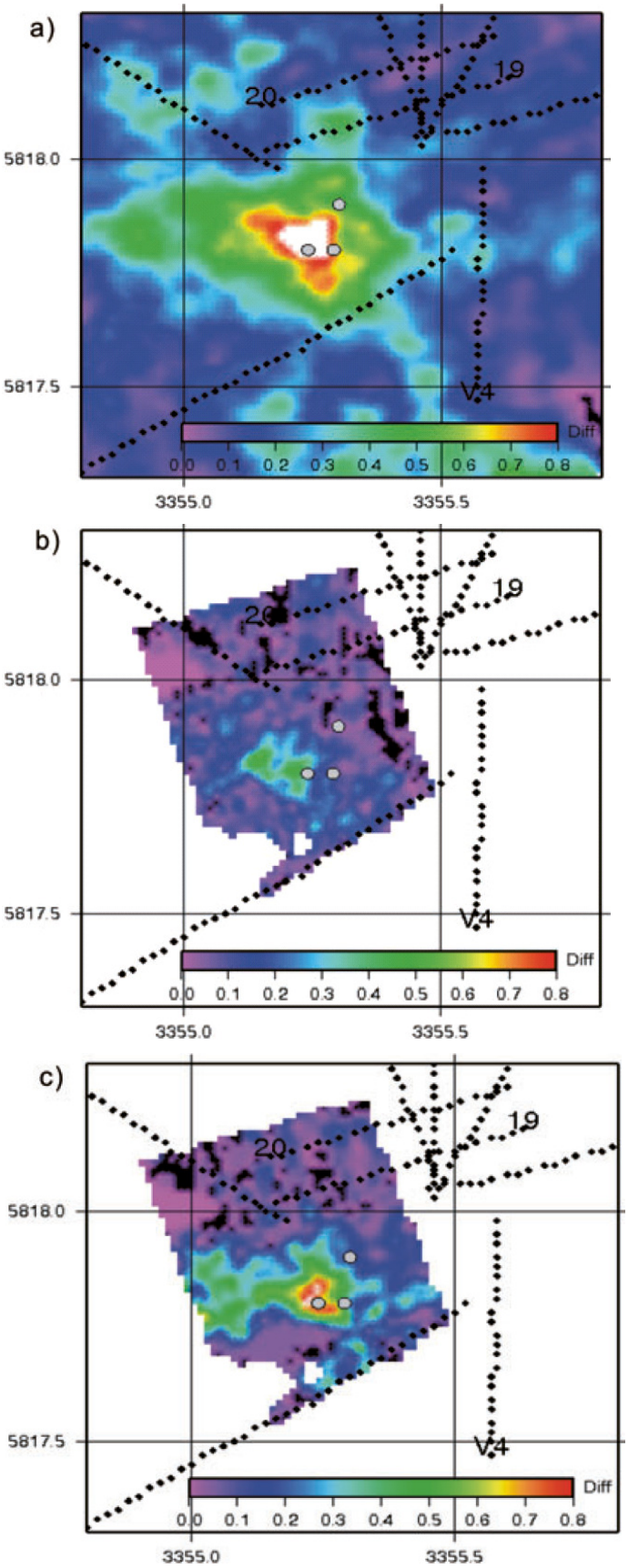

Figure 16 Amplitude difference horizon at the reservoir level for the a) mini-3D, b) 1st pseudo-3D repeat survey, and c) 2nd pseudo-3D repeat survey (Ivandic, 2012).

2 Time-lapse reservoir monitoring by MSP investigations

Moving Source Profiling (MSP) data was acquired at the same time with the 2D Star data, from all shot points on surface, along the 7 Star lines, by receivers placed from 470m to 540m in borehole KTZI-202. The detailed acquisition parameters are listed in Table 2 and the layout of the 2D Star, MSP and VSP surveys is shown in Figure 17.

2.1 Baseline & Repeat MSP surveys

The 1st 2D Star repeat survey was, like the baseline, carried out in close temporal succession to the respective 3D survey. The baseline 2D Star and MSP surveys were acquired with a VIBSIST-1000 source, whereas in the repeat surveys another type, but similar, source was used, the VIBSIST-3000. The VIBSIST is a swept impact seismic source (Park et al., 1996, Cosma, 2001) which combines the Vibroseis swept-frequency and the Mini-Sosie multi-impact techniques. Impulsive impacts are generated in a sequence with increasing impact frequency, with up to several hundred pulses.

The first repeat survey was acquired in 5 days in September 2009. A different borehole receiver string had to be used for the repeat, due to access limitations in the observation well, which had to be kept under pressure after the start of the injection. Baseline MSP data were acquired using the R8XYZ 3-component geophones chain, while for the repeat only two receivers could be used, in order to reduce the length or the string.

In February 2011, the second repeat MSP survey was acquired, and all the equipment and parameters were the same as in the 2009 campaign. The survey was acquired within 8 days. Because of weather conditions and permission issues, some shots were skipped.

Table 2. Acquisition parameters for the MSP baseline and repeat seismic surveys.

Parameter	**Value**		
Year & Month	**Baseline 2005 November**	**1st Repeat 2009 September**	**2nd Repeat 2011 February**
Source point spacing	12 m		
Receiver depth & spacing	470m to 540m at 5m	470m	470m and 480m at 10m
Number of shot points (7 lines)	V1–81, V2–81, V3–82 V4–28, V5–124 V6–81, V7–79	V1–84 V2–83, V3–82 V4–16, V5–121 V6–82, V7–83	V1–84 V2–84, V3–88 V4–14, V5–120 V6–84, V7–72
Recording length & sampling interval	30 s, 1 ms		
Source	VIBSIST-1000	VIBSIST-3000	VIBSIST-3000

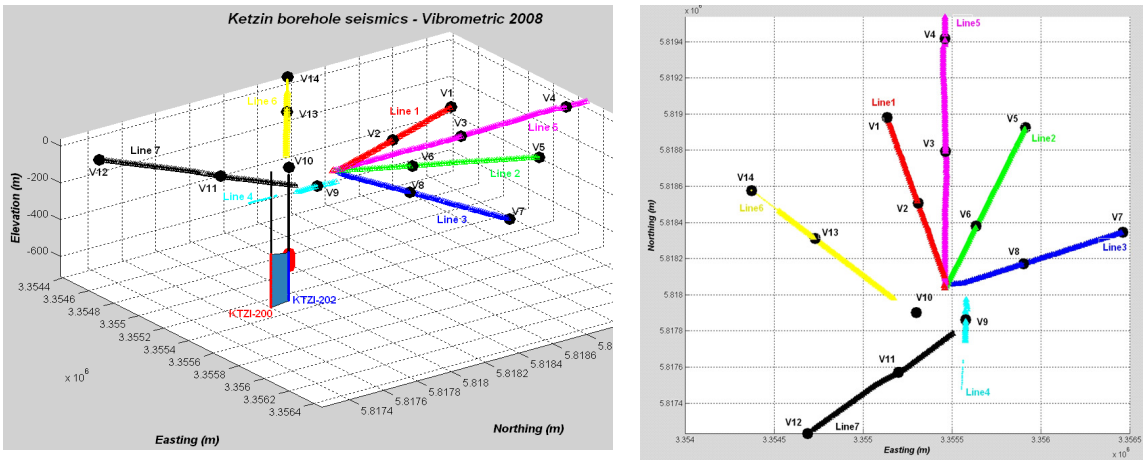

Figure 17. Geometry of the borehole seismic surveys used for site characterisation before and during CO_2 injection.

2.2 Conventional processing and analysis

Initial MSP analysis and processing was first done within the CO2SINK project, for the baseline and 1st repeat data sets. Based on the CO2 plume extent suggested by the 3D mapped difference (Juhlin, 2010) time-lapse analysis was done only for the MSP profiles recorded from lines 1, 5, 6 & 7 (Figure 18).

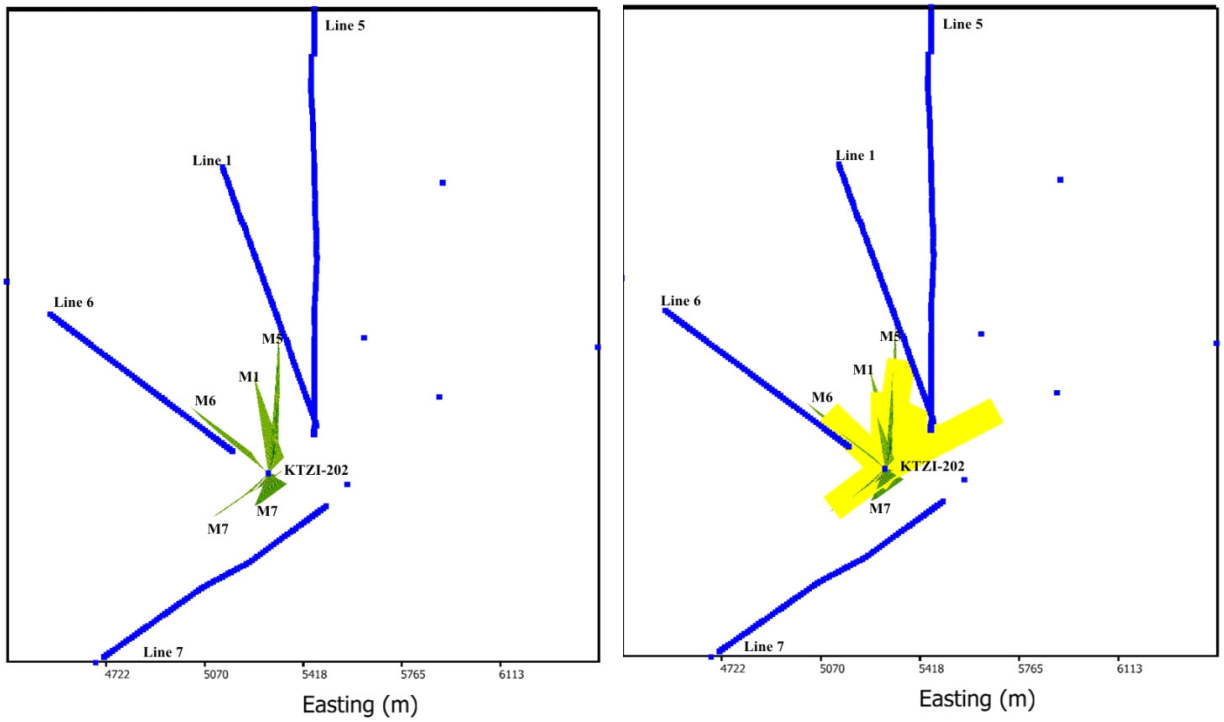

Figure 18. Geometry of the four MSP lines used for the first time-lapse analysis, together with horizontal plane projection of the 3D MSP migrations for each of these lines, labeled M1, M5, M6 & M7. Reflector elements interpreted at the reservoir level from the baseline VSP data are also shown on the right hand side as yellow rectangles.

Images shown in Figure 18 are relevant for the description of the actual coverage obtained by MSP observations at reservoir level. Any comparison between time-lapse images derived from different techniques can be made only where their respective coverage overlaps.

3D MSP migrated sections of the difference between the repeat and baseline MSP profiles, as derived during the initial processing stage are presented in Figure 19 and Figure 20. The difference profiles were calculated as “Repeat – Baseline”, for each MSP line, from data after removal of the direct wave-fields. Minimal processing was applied to each profile, in order to minimize possible processing artefacts. Detailed views are also shown in Figure 21, Figure 22 and Figure 23, where a coherent event at the injection level stands out on images from Line 7, Line 6 & Line 1 and part (nearer to KTZI-202) of Line 5.

The first approach in treating the Ketzin MSP profiles was to use the VSP-CDP transform, described in Appendix A.

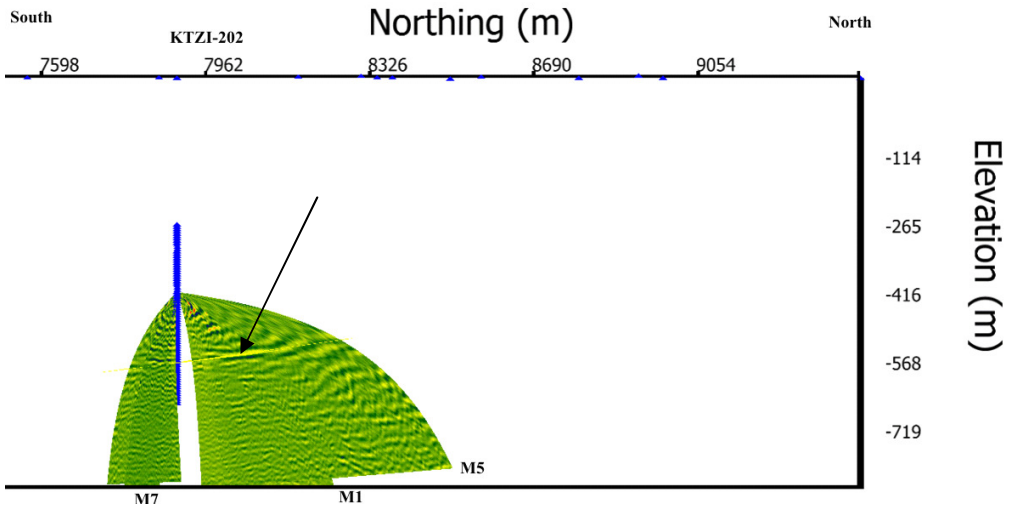

Figure 19. View from East of the difference 3D MSP migrated sections from lines 7, 1 and 5.

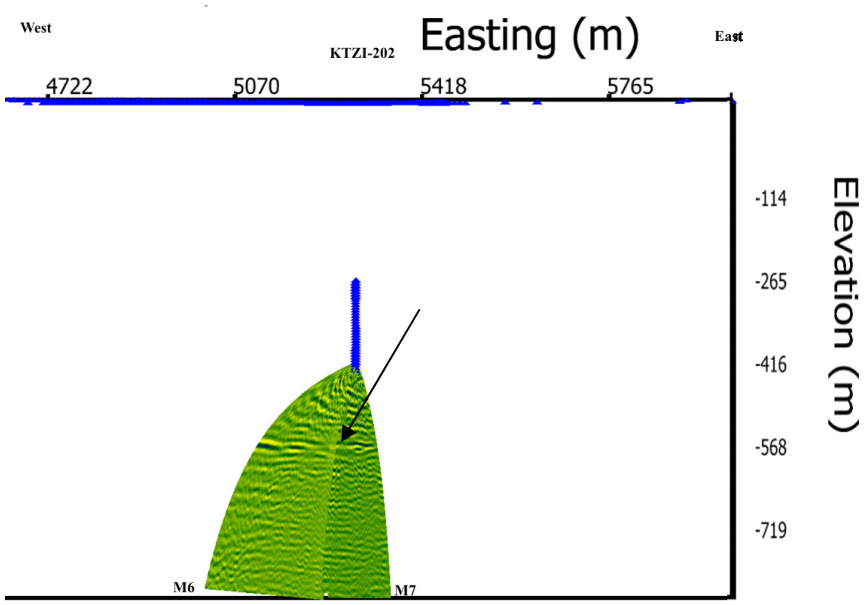

Figure 20. View from South of the difference 3D MSP migrated sections from lines 6 and 7.

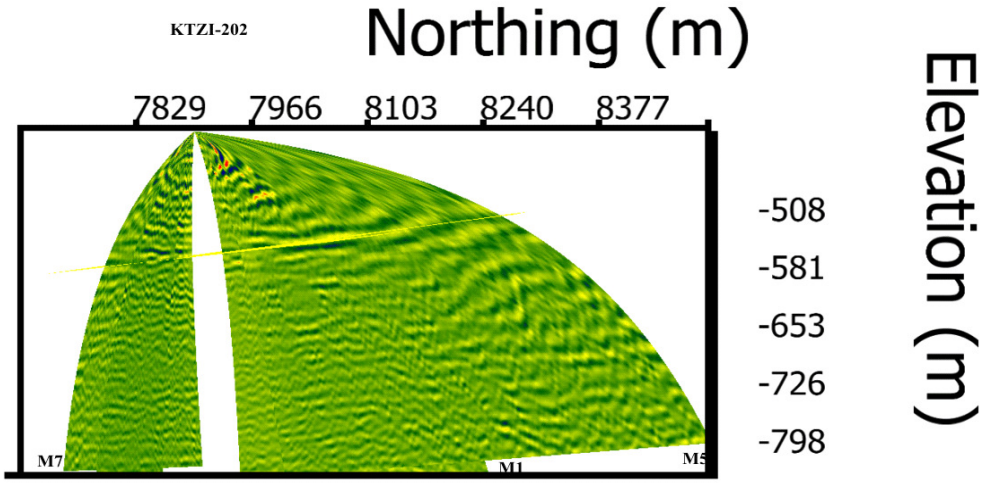

Figure 21. Detailed view from East of the difference 3D MSP migrated sections from lines 7, 1 and 5.

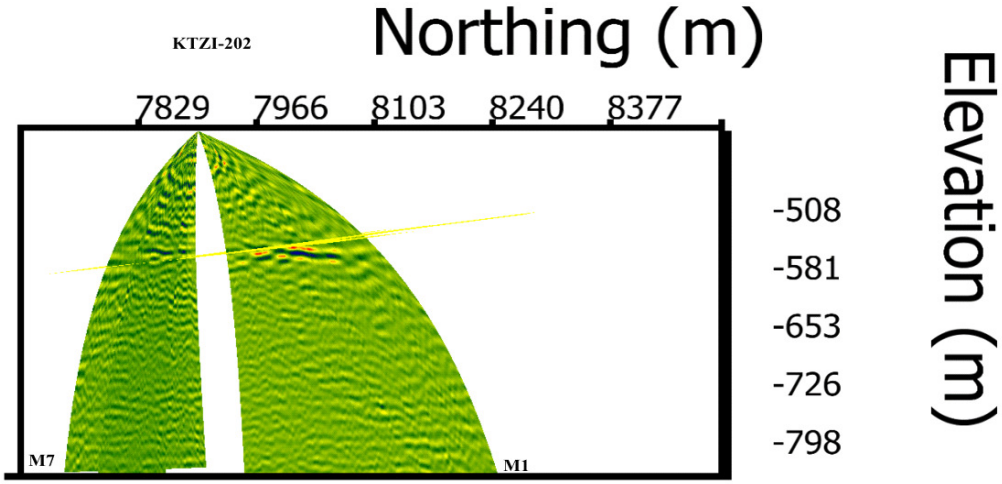

Figure 22. Detailed view from East of the difference 3D MSP migrated sections from lines 7 and 1.

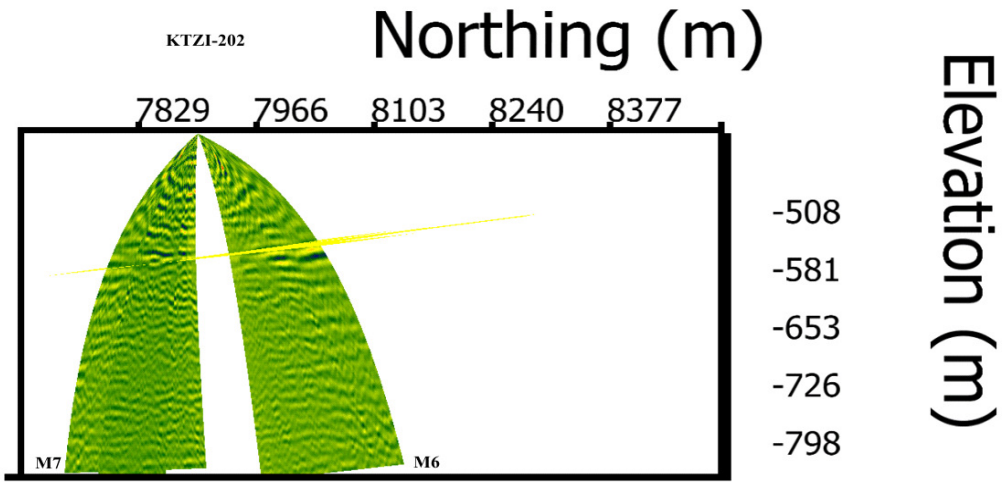

Figure 23. Detailed view from East of the difference 3D MSP migrated sections from lines 7 and 6. Images also display reflector elements (yellow) interpreted at the reservoir level from the baseline VSP data (Enescu, 2010).

2.3 Re-evaluation of Baseline and Repeat surveys

The initial time-lapse analysis of the MSP data revealed differences between baseline and repeats, mainly due to varying weather conditions. These included time lags, decreased amplitude and frequency content, as well as an apparent rebound of the source signature, which appeared due to changed near surface ground properties. Further processing was performed to remove the acquisition footprint as detailed below. Following that, work has been done within the CLEEN project to jointly analyze the entire MSP data set available from Ketzin, i.e. the baseline (BL), repeat 1 (R1) and repeat 2 (R2) surveys. The R2 data ha e been acquired after the completion of the CO2SINK project. Main processing steps and results obtained with this effort are illustrated by examples from MSP Line 7 (see Figure 17) in Figure 25 to Figure 34.

The spectra from Figure 25 show a definite trend: decreased frequency content of the R1 data and increased frequency content of R2 data, with respect to baseline. Cross-correlations of baseline and repeat profiles were used to evaluate the time lags between baseline and the two repeats. Figure 26 illustrates the improvement obtained, the cross-correlation lags being brought to zero after corrections had been applied. The result of the removing of the cross-correlation statics is illustrated in Figure 28.

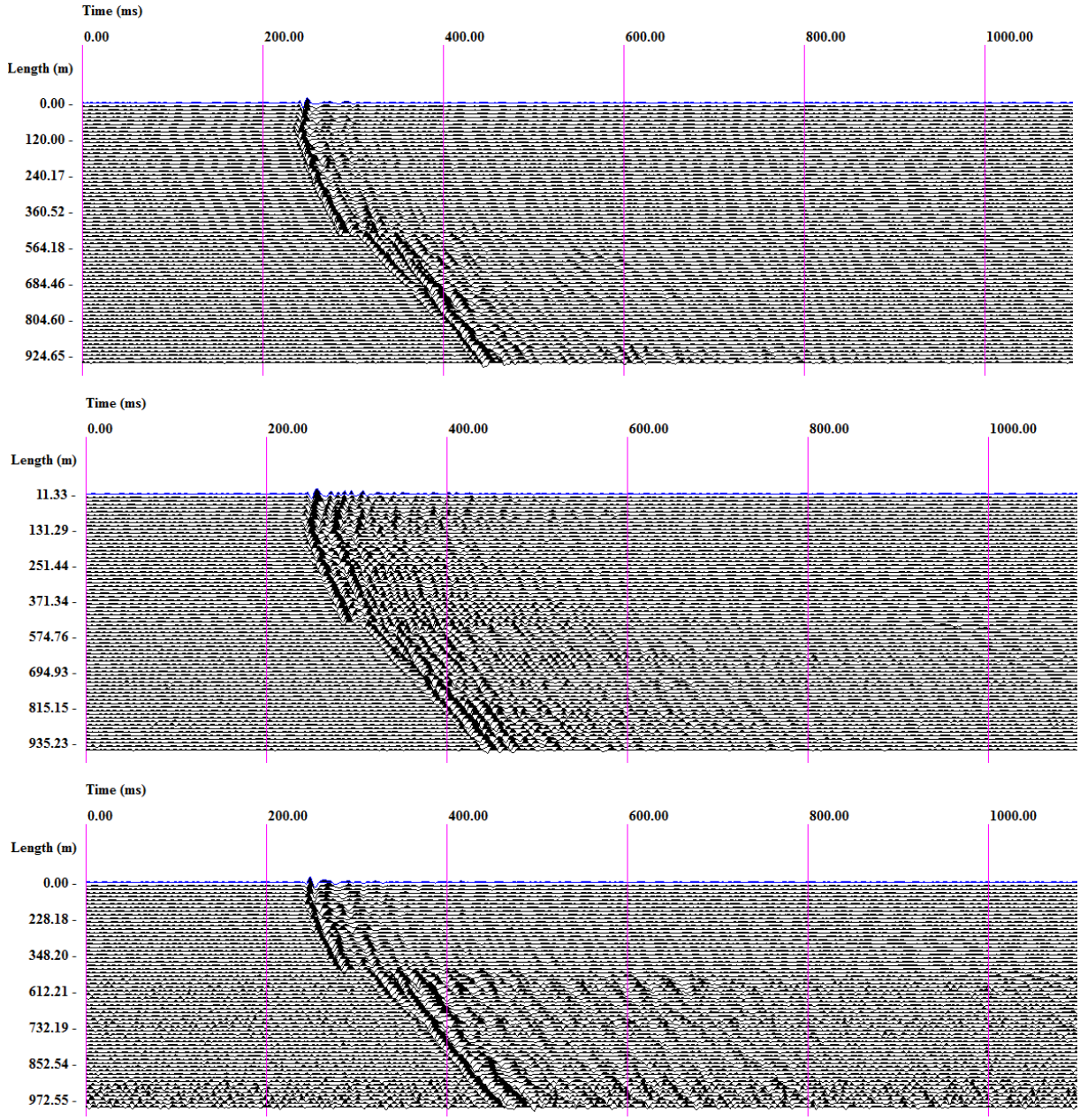

Figure 24. Baseline (top), first repeat (middle), second repeat (bottom) raw MSP vertical component data acquired along Line V7.

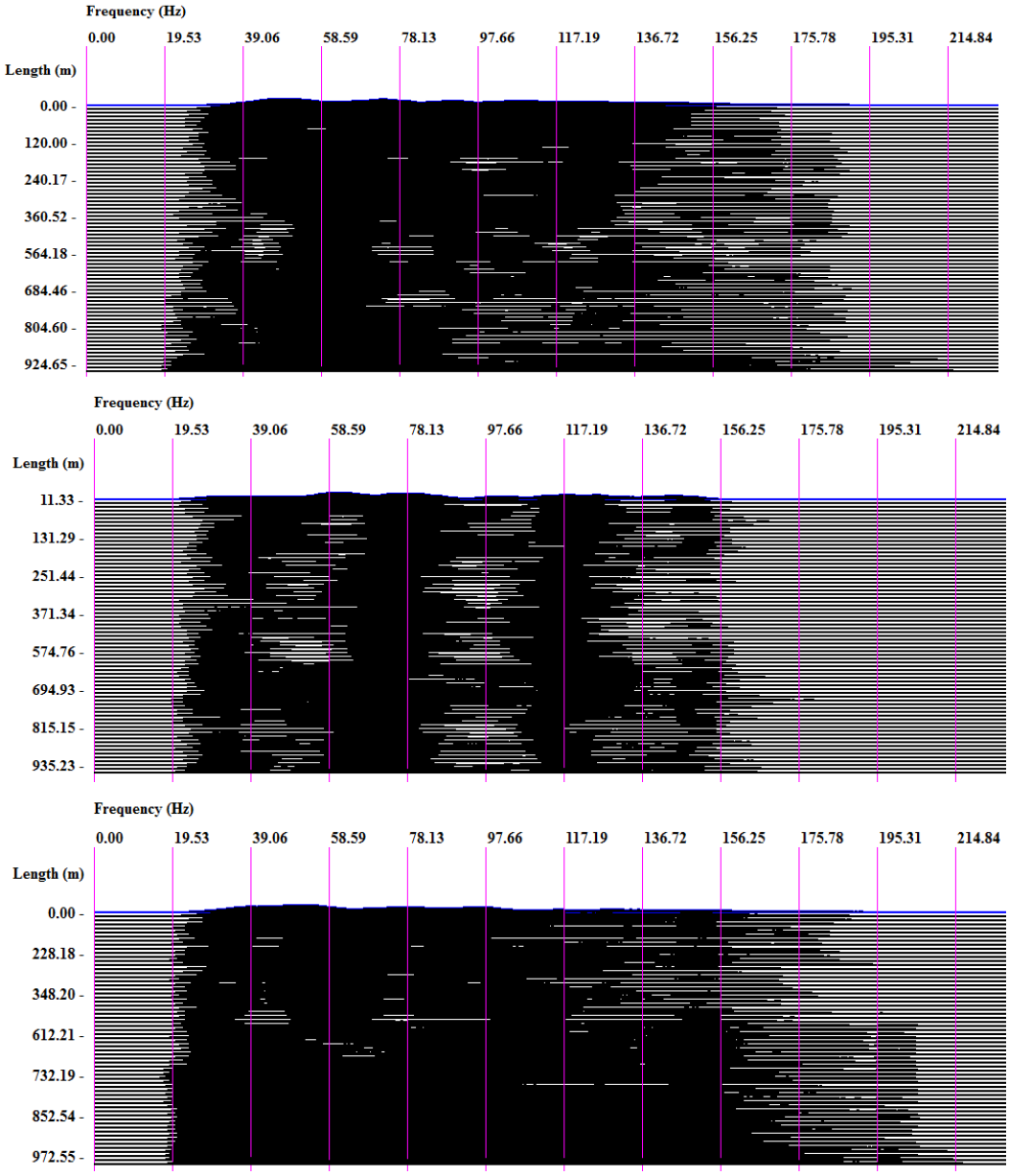

Figure 25. Spectra profiles of baseline (top), repeat 1 (middle) and repeat 2 (bottom) computed from the MSP profiles shown in Figure 24.

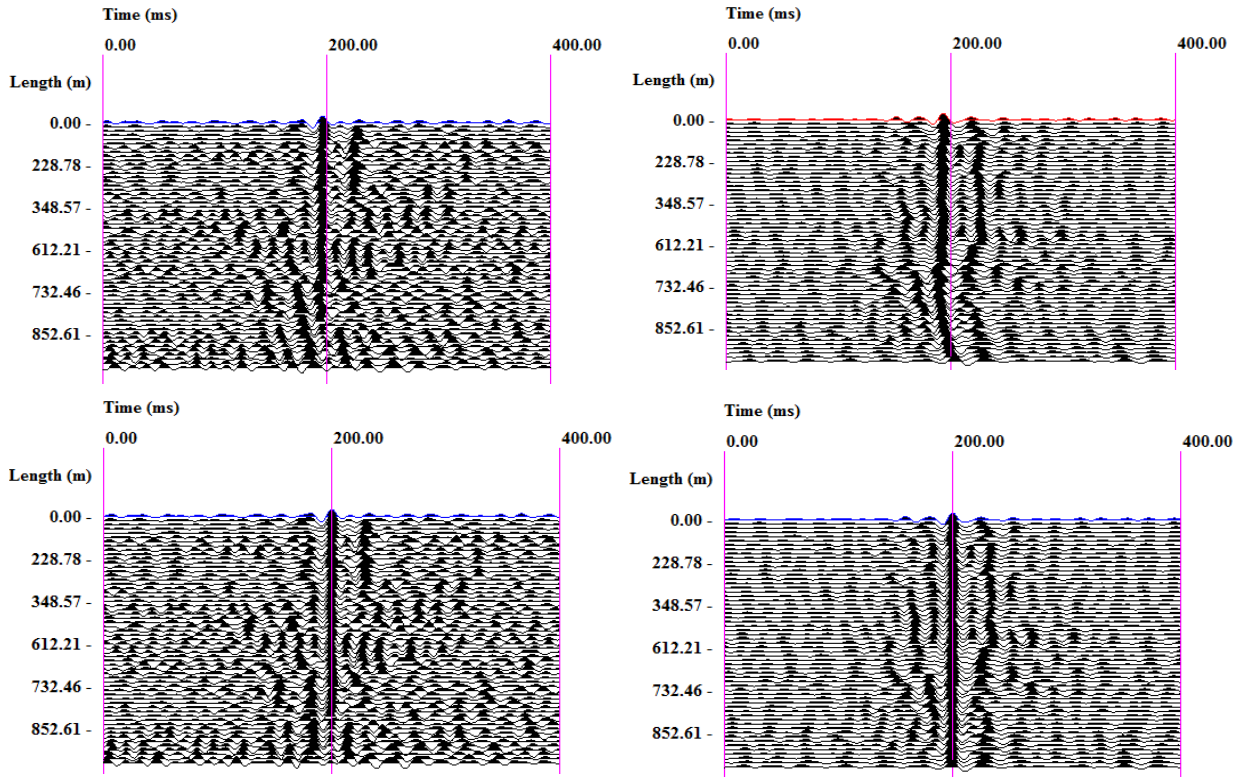

Figure 26. Cross-correlation profiles before (top) and after (bottom) shift corrections. Repeat 1 vs. Baseline is shown on the left side and Repeat 2 vs. Baseline is shown on the right side.

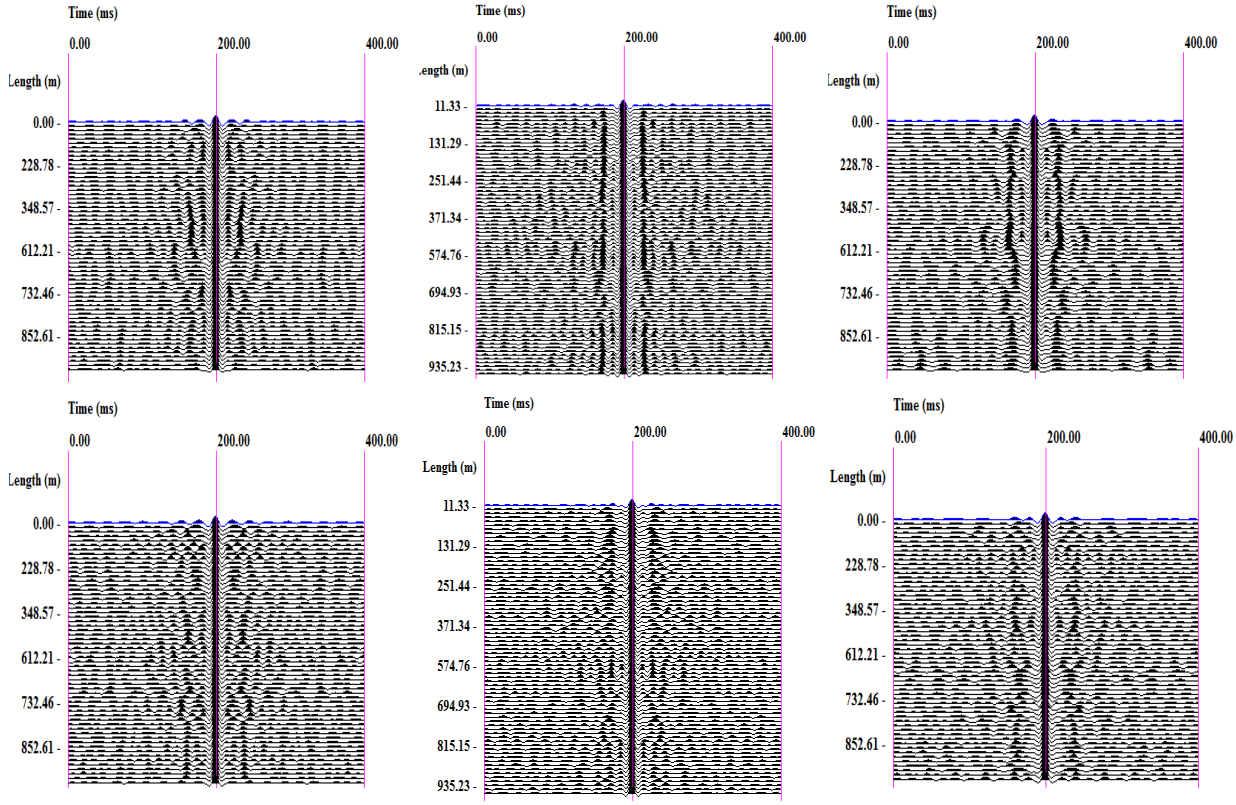

Figure 27. Auto-correlation profiles before (top) and after (bottom) harmonic filtering. Baseline (left), Repeat 1 (middle) and Repeat 2 (right).

The suppression of spurious multiples due to near surface changes was done by a time-domain interactive filter, which was found to be more stable than standard frequency domain wave-shaping. Excessive filtering was carefully avoided by careful comparison of the auto-correlation sections of each baseline and repeat profile.

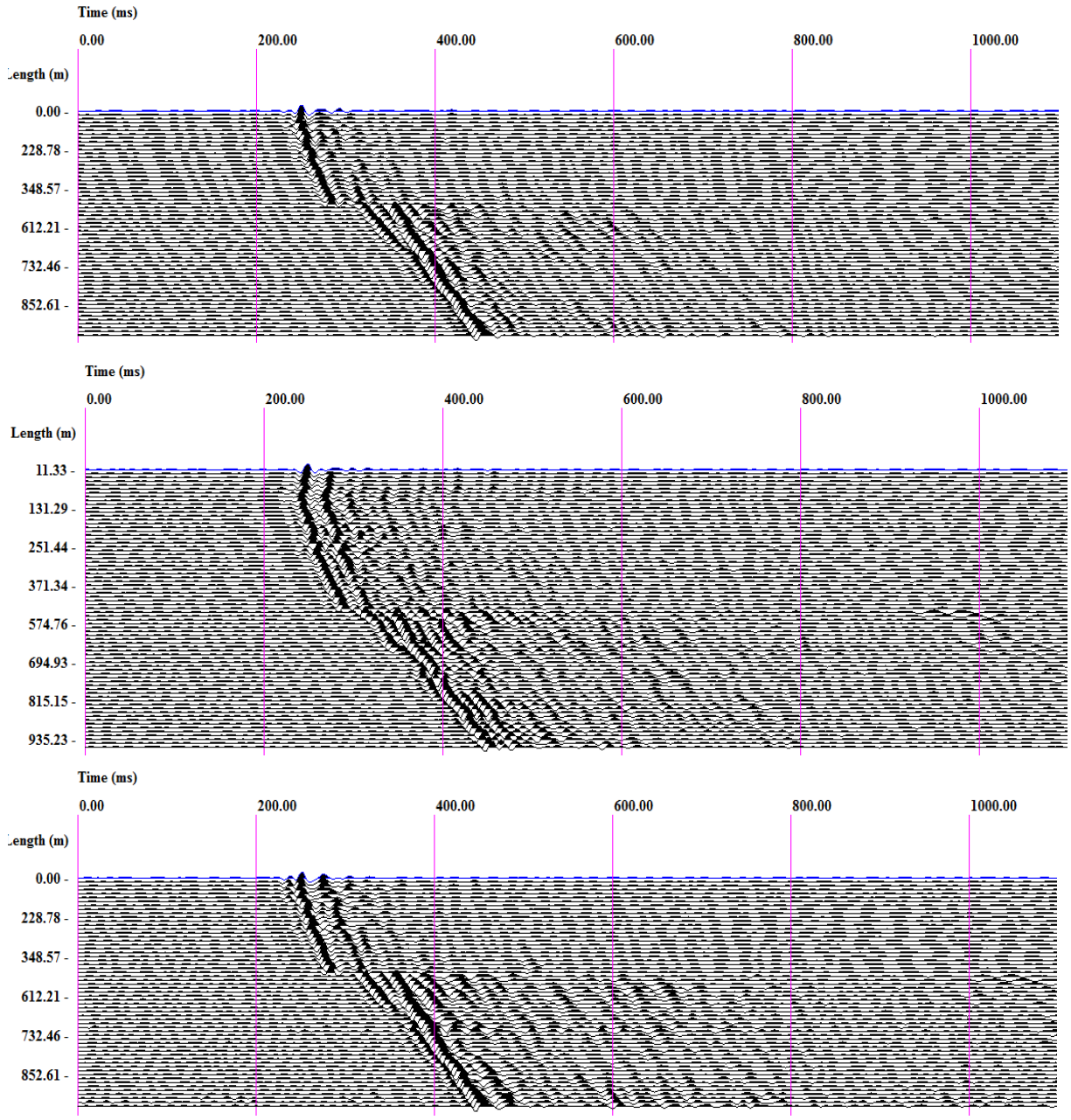

Figure 28. Same data profiles as in Figure 24, after band pass filtering (20 to 130 Hz) and shift correction with the time shifts determined by cross-correlation analysis.

Further, auto-correlation analysis (illustrated in Figure 27) and harmonic filtering were done, followed by amplitude normalization, in order to remove most of the differences related to acquisition particularities from all MSP time-lapse data sets. The result of this process is illustrated in Figure 29.

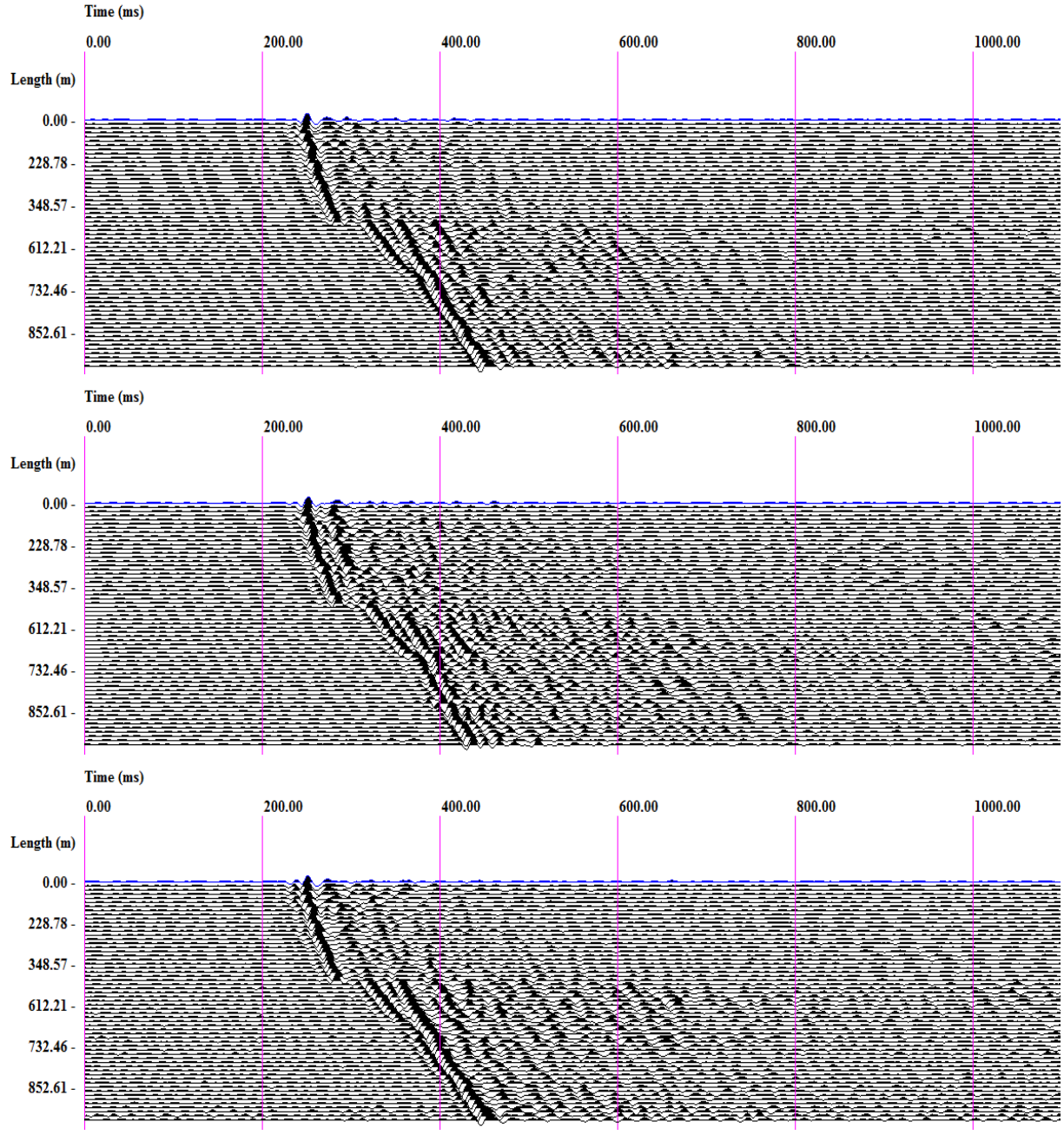

Figure 29. Line V7. Baseline (top), first repeat (middle) and second repeat (bottom) after harmonic filtering.

Figure 30 shows processed profiles for the baseline and the two repeat MSP data sets, after removal of direct P and S wave fields. Changes in amplitudes are found within the region of the injection layer at approximately 350ms (reflector marked with an arrow). The observed stronger reflections in the target area are interpreted as due to injected CO_2. The presence of CO_2 should enhance the impedance contrast of the internal layers in the aquifer (Kazemeini et al., 2010).

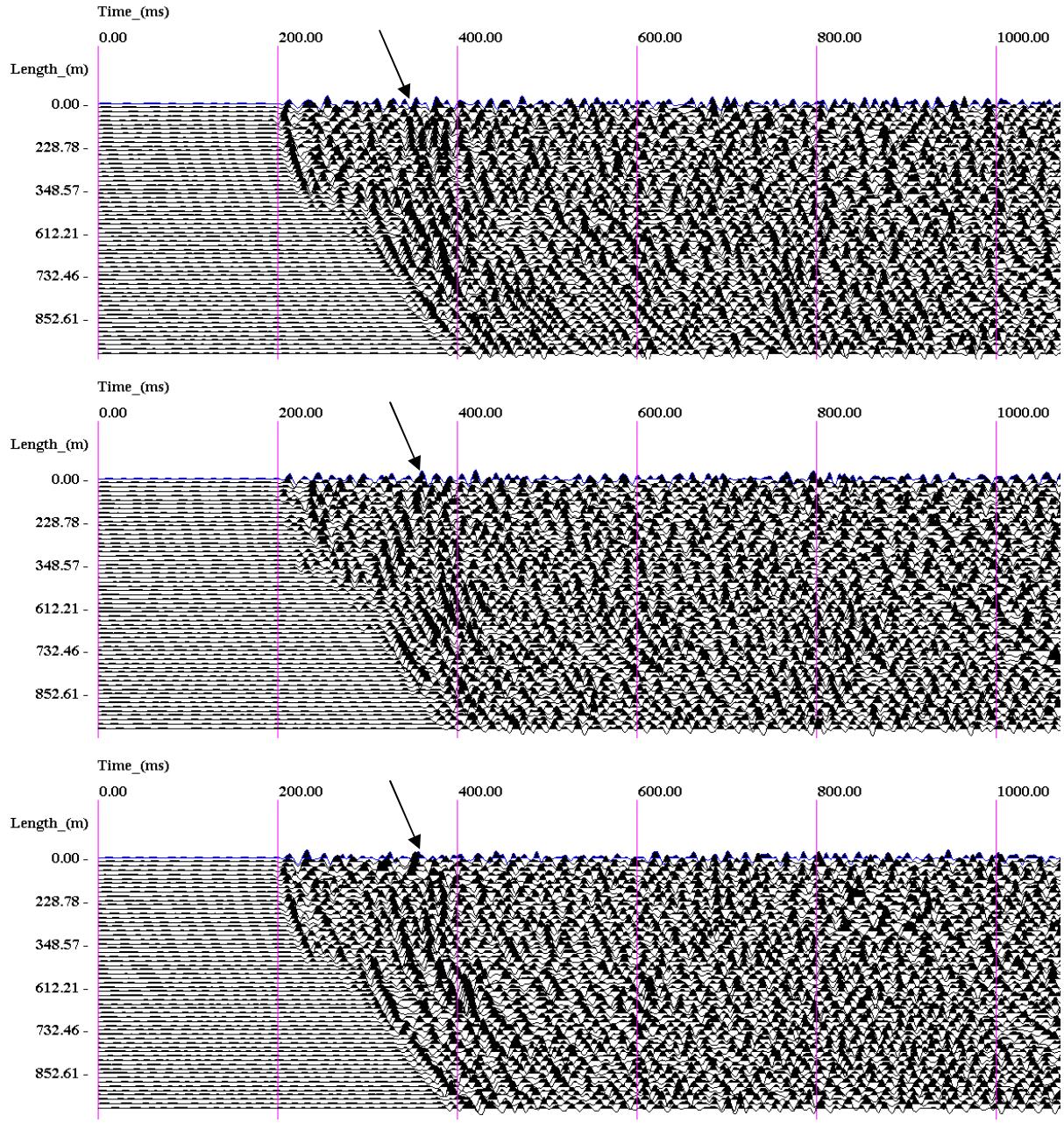

Figure 30. Line V7. Baseline (top), first repeat (middle) and second repeat (bottom) after removal of direct wave fields.

By comparing the baseline with the two repeat data sets potential changes related to CO_2 injection can be detected. Since time-discrepancies were minimized, the differences in the profiles shown in Figure 31 are considered relevant for the CO_2 monitoring process at Ketzin.

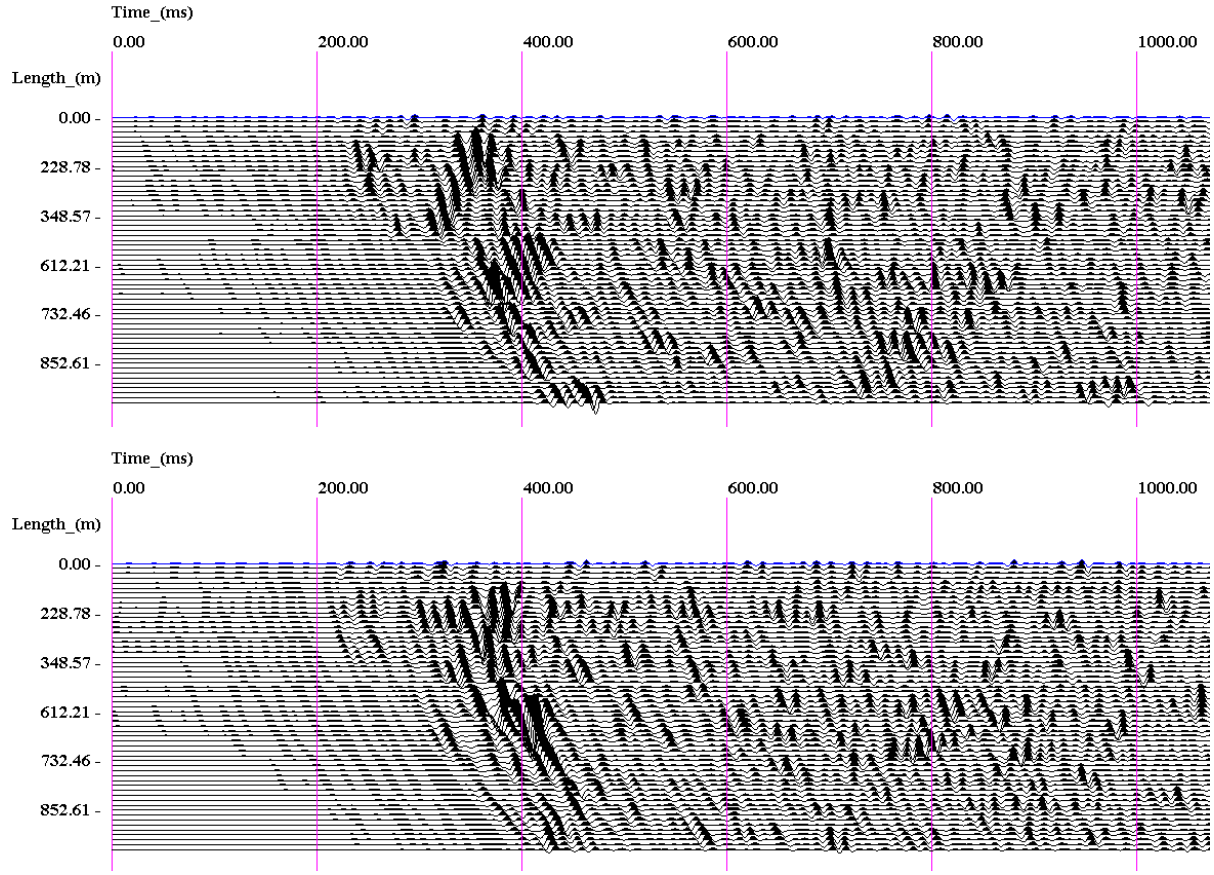

Figure 31. Differences computed for MSP Line7, from profiles shown in Figure 30. Baseline vs. first repeat (top) and baseline vs. second repeat (bottom).

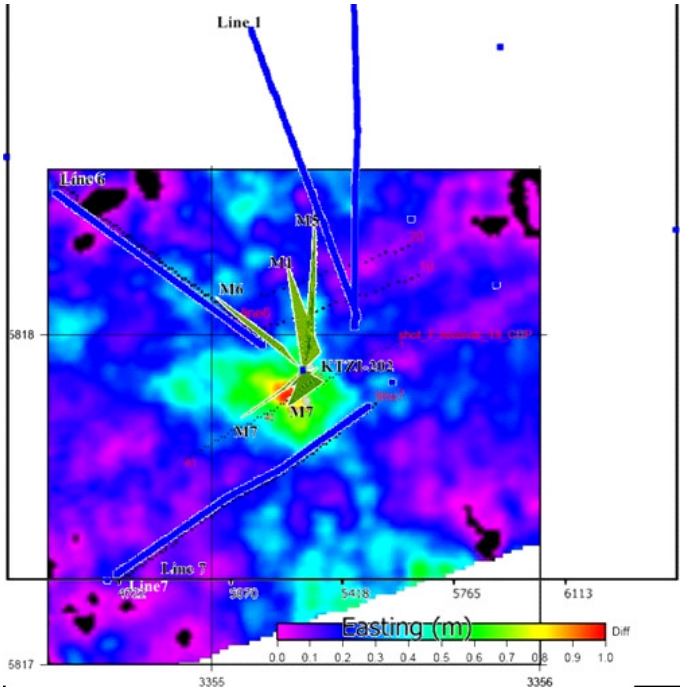

Figure 32. MSP coverage. View from above of the amplitude difference map at the reservoir level (Juhlin, 2010), overlain by MSP migrated sections (dark green, also shown in Figure 18), computed for imaging sub horizontal reflectors.

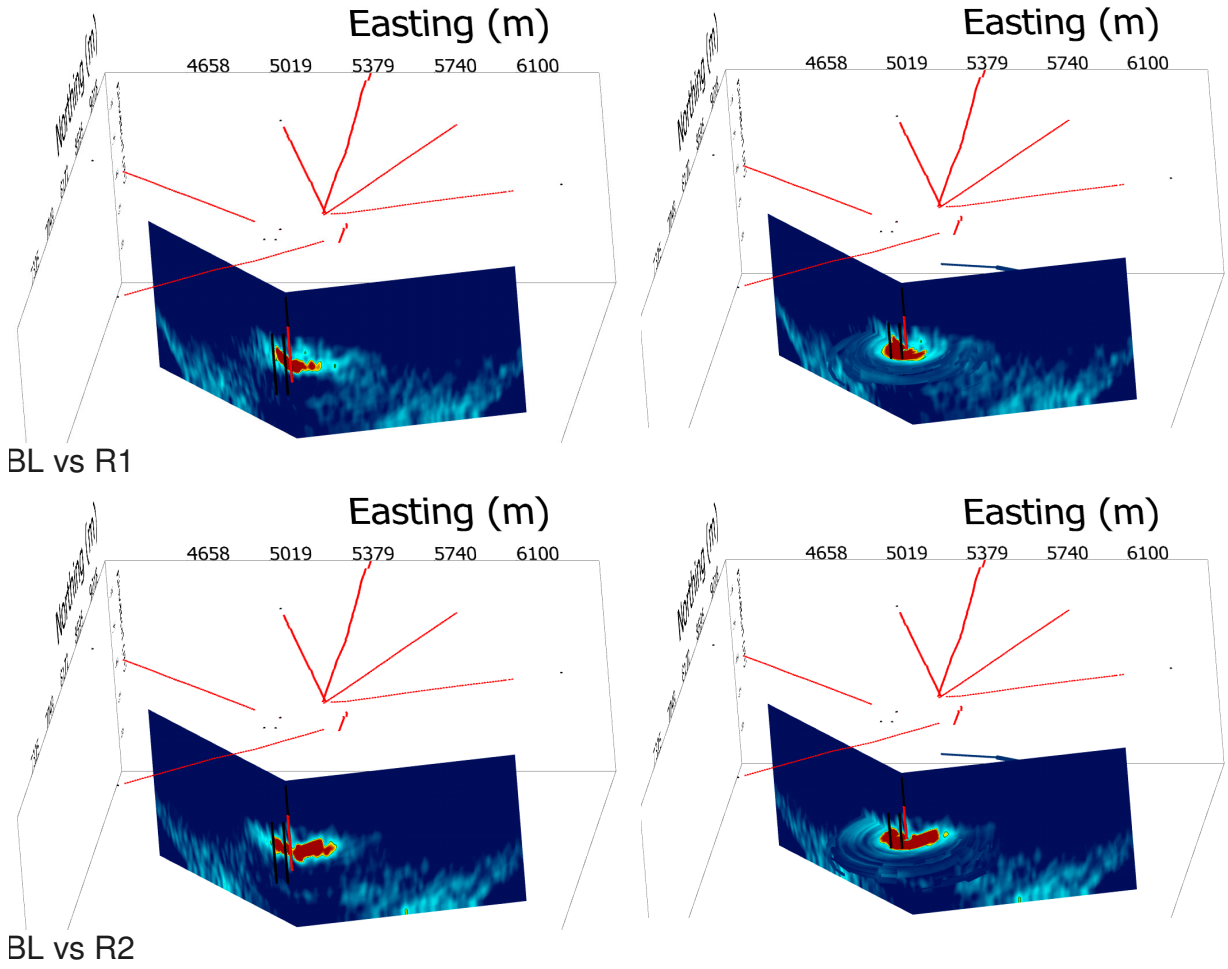

Figure 33. 3D view of two IP migrated vertical sections calculated at azimuths 75° and 315° from North on the left and the same, together with a time depth slice at the level of the reservoir (630 to 640m depth in KTZI-202). Baseline vs. first repeat appears in the top row and baseline vs. second repeat is shown in the bottom row.

Difference maps shown in Figure 34 and Figure 34 were computed from the time-lapse analysis of the MSP baseline and repeat surveys and can be compared with the difference maps computed from the 3D data by (Juhlin et. al. 2010, in Figure 14) and from the 2D star data by (Ivandic et. al., 2012, in Figure 16).

Comparison of difference maps obtained with different type of surveys is relevant only in the regions where coverage exists, considering intrinsec limitations caused by limited coverage for the 2D Star and MSP survey geometries.

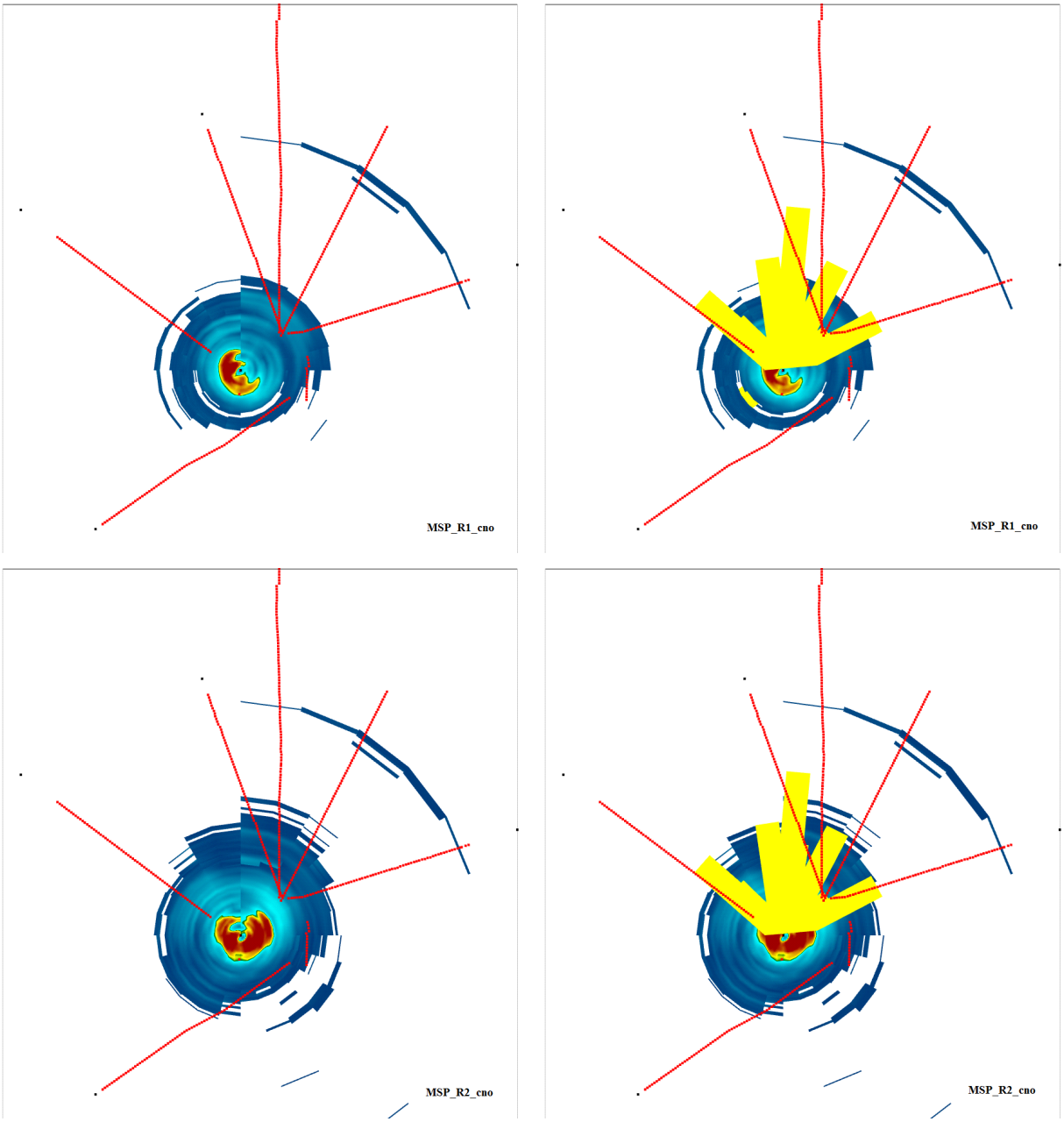

Figure 34. View from above of the time depth slice at the level of the reservoir (630 to 640m depth in KTZI-202) for baseline vs. first repeat (top) and baseline vs. second repeat (bottom). Images on the right side also display reflector elements (yellow) interpreted at the reservoir level from the baseline VSP data (Enescu, 2010).

3 Time-lapse reservoir monitoring by VSP investigations

The VSP layout, with the receiver array extended vertically, can produce images of the steep structures and the lateral coverage is significantly larger than with MSP. The gain of resolution is obtained by increased frequency and by more diverse view angles of the structure than achievable with surface stations only.

3.1 Baseline & Repeat VSP surveys

The VSP investigations at Ketzin were carried out in borehole KTZI-202. 3-component profiles were collected from 14 shot points, each profile comprising 80 levels, spaced at 5m intervals. The VSP surveys cover a region with an average radius of approximately 300m around the injection site.

The layout of the shot points is presented in Figure 17. The distances from the top of the borehole to shot points range from 5 to 1525m. The distances from shot points to the uppermost receiver in the borehole range from 325 to 1557m and to the deepest receiver in the boreholes from 720 to 1685 m.

The baseline VSP survey was carried out in 2007 with a VIBSIST-1000 source, whereas in the repeat survey another type, but similar, source was used, the VIBSIST-3000. Baseline data were acquired using the R8XYZ 3-component geophones chain, while for the repeat only two receivers could be used, in order to reduce the length or the string.

The repeat VSP survey was acquired in 2011, and the acquisition parameters varied slightly, as a reduced number of receiver positions were covered for some of the shot points. The reduction was necessary in order to speed up the survey, which was otherwise delayed because of weather conditions and permission issues. The detailed parameters are shown in Table 3.

Table 3. Acquisition parameters for the VSP baseline and repeat seismic surveys.

Parameter	**Value**	
Year & Month	**Baseline 2007 November**	**1st Repeat 2011 February**
Source points	12 m	
Receiver depth & spacing	325m to 720m at 5m	
Recording length & sampling interval	30 s, 1 ms	
Source	VIBSIST-1000	VIBSIST-3000

3.2 Conventional processing and analysis

The processing sequence aims to improve the signal-to-noise ratio, so that the later events, e.g. reflections, become visible. As the reflection coefficients may be low, the reflectors cannot normally be identified by an amplitude standout alone. Continuity and phase consistency have been found to be sensitive indicators.

The first stage of the processing sequence used for the Ketzin VSP data consisted of:

- Time stacking of the VIBSIST impact sequences
- Amplitude decay compensation using the function $Ac=A*t^{1.5}$
- Zero-phase band-pass filtering 10-150 Hz
- Component rotation: (X Y Z) to (R, T, Z)
- P- and S-wave arrival time picking and tomographic reconstruction of the P-wave velocity filed (illustrated in Figure 36, Figure 37 and Figure 38)
- Suppressing direct P- and S- wave arrivals by 21-trace hyperbolic medians for velocities of ~3500 m/s (P-wave) and ~2300 m/s (S-wave) with maximum coherency fit in a 20 ms window, to account for local velocity variations.
- Amplitude equalization (AGC in 50 ms running window, normalizing with the total 3-component amplitude, to conserve polarization information).
- Static corrections using tomographic reconstruction of velocities

The second stage of the processing sequence focused on reflector enhancing by Image Point filtering. The procedure has been applied on data from all three components. Non-linear enhancement of reflected energy has also been tested and used (Cosma et. al., 2002b).

Once all the profiles have been processed and the reflection events emphasized, the positions of the reflectors were determined by interactive interpretation. An example of processed profile, with interpreted reflectors is shown in Figure 39.

The data profiles were migrated along the mean azimuth of the interpreted targets, as exemplified in Figure 40.

The VSP migration applied with the Ketzin VSP data is assuming a given viewing direction (θ=dip, ϕ=azimuth) and a velocity field **V**(x,y,z) (Cosma et. al., 2010). Different assumptions for (θ,ϕ) and/or **V** produce different map points **A**(x',y',z'). A unique dip-azimuth solution is begotten by combining data from several shot-gathers. The procedure is robust and straightforward when applied to nearly planar features in a known velocity medium.

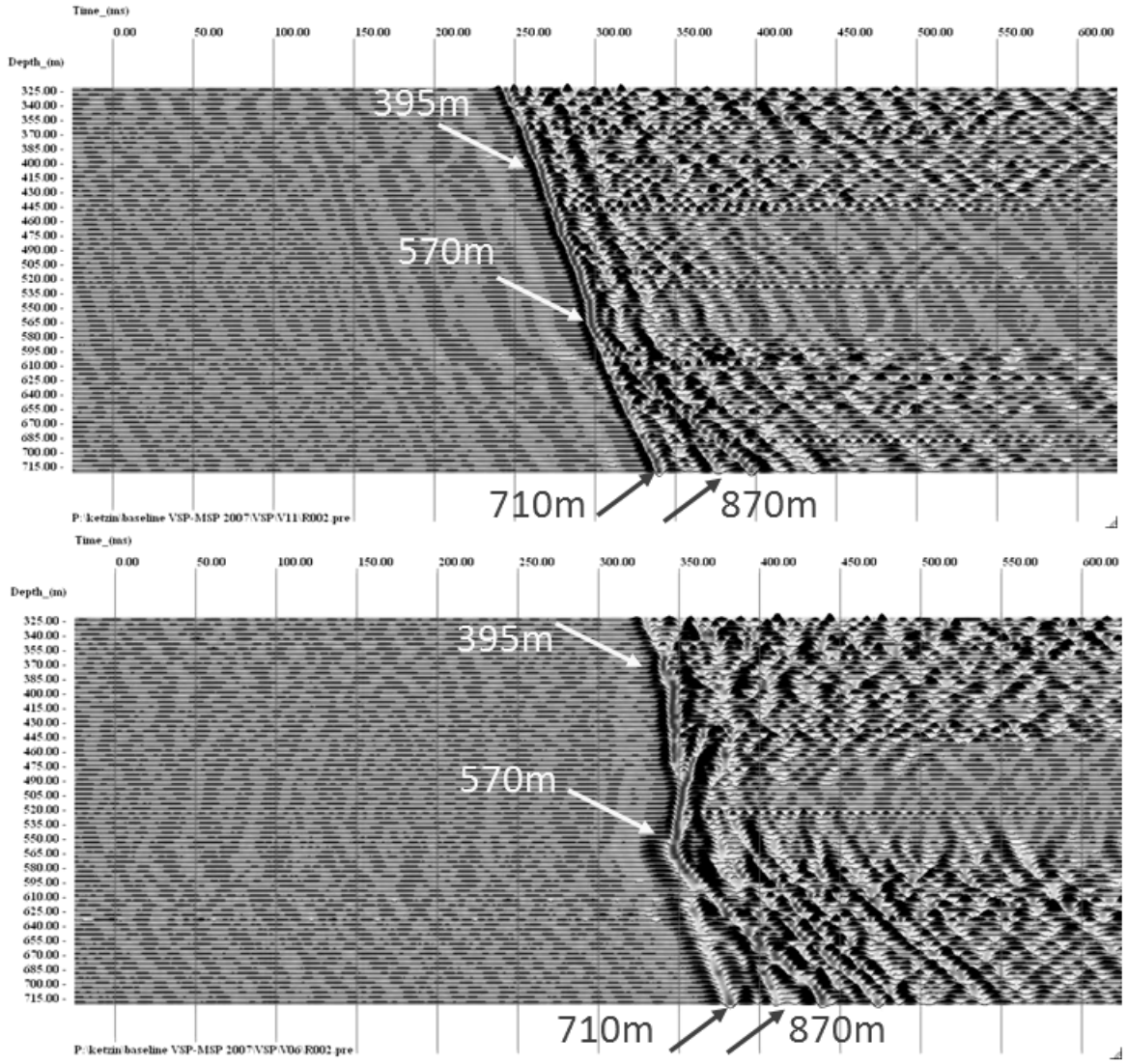

Figure 35. Top view: Shot V11, radial component. P-S conversions from sub-horizontal layers above Stuttgart formation: 395m, 570m and P-reflections from sub-horizontal layers below Stuttgart formation: 710m, 870m are observable on raw data. Bottom view: Shot V6, radial component. P-S conversions from sub-horizontal layers above Stuttgart formation: 395m, 570m and P-reflections from sub-horizontal layers below Stuttgart formation: 710m, 870m are observable on raw data.

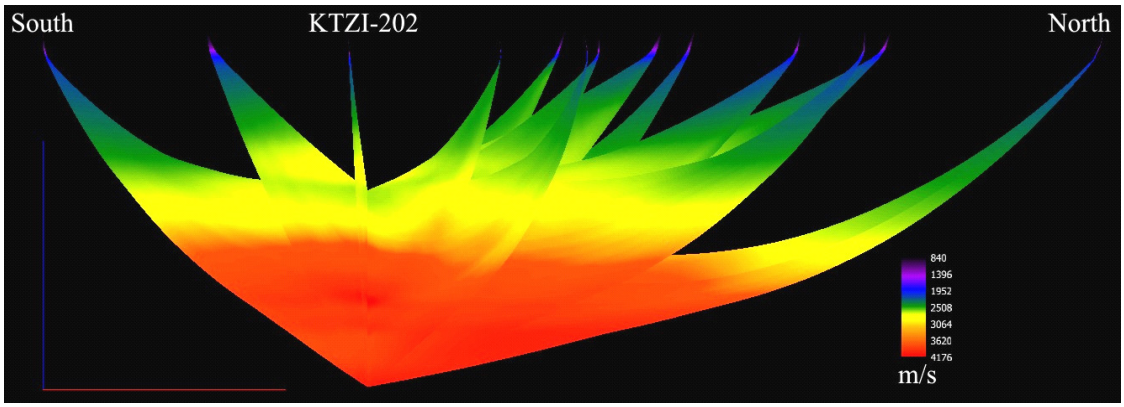

Figure 36 P-wave velocity field reconstruction from the first arrivals measured on all VSP profiles from borehole KTZI-202. View from East. Tomograms' velocity is scaled in the 800 – 4200 m/s range.

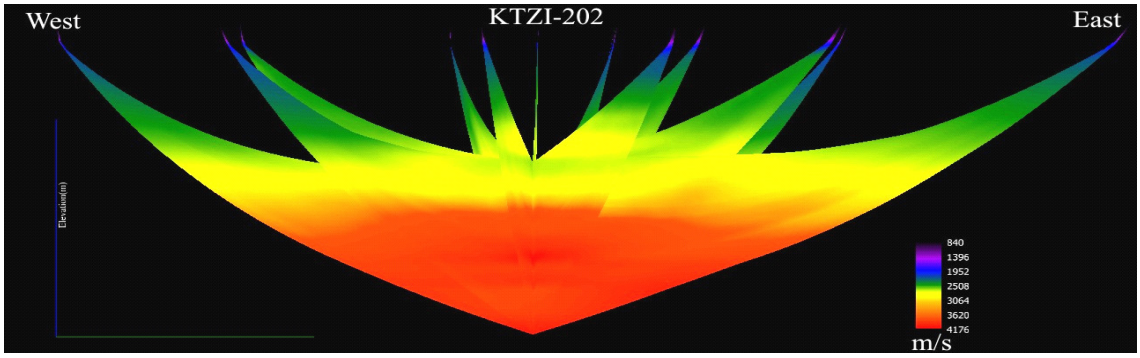

Figure 37. Same as in Figure 36, view from South.

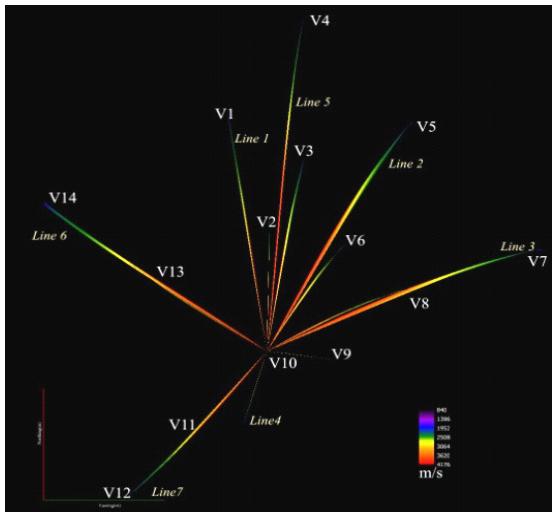

Figure 38. View from top of the 3D velocity distribution also shown in Figure 36 and Figure 37.

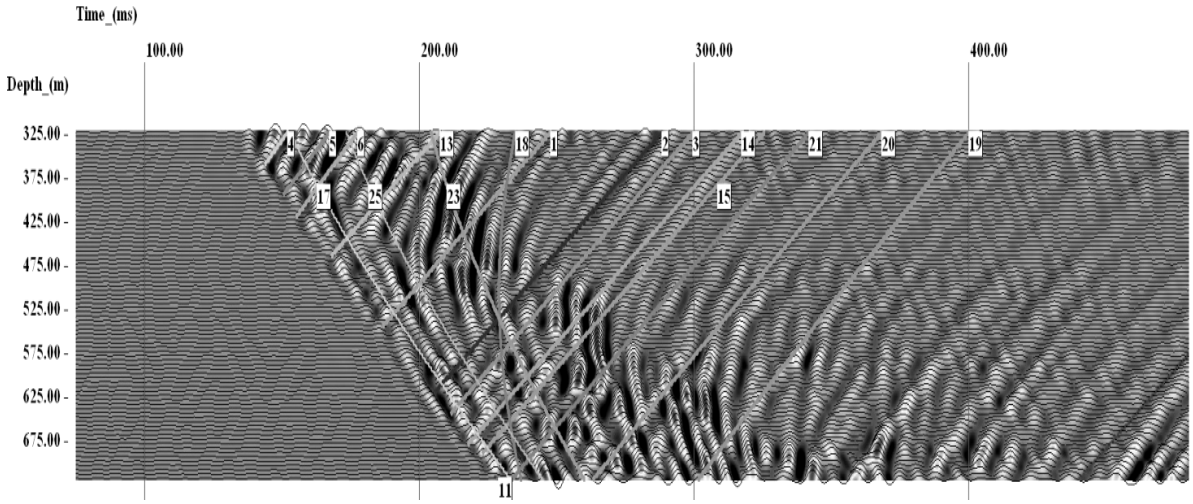

Figure 39. Axial component profile from SP11, with interpreted reflectors.

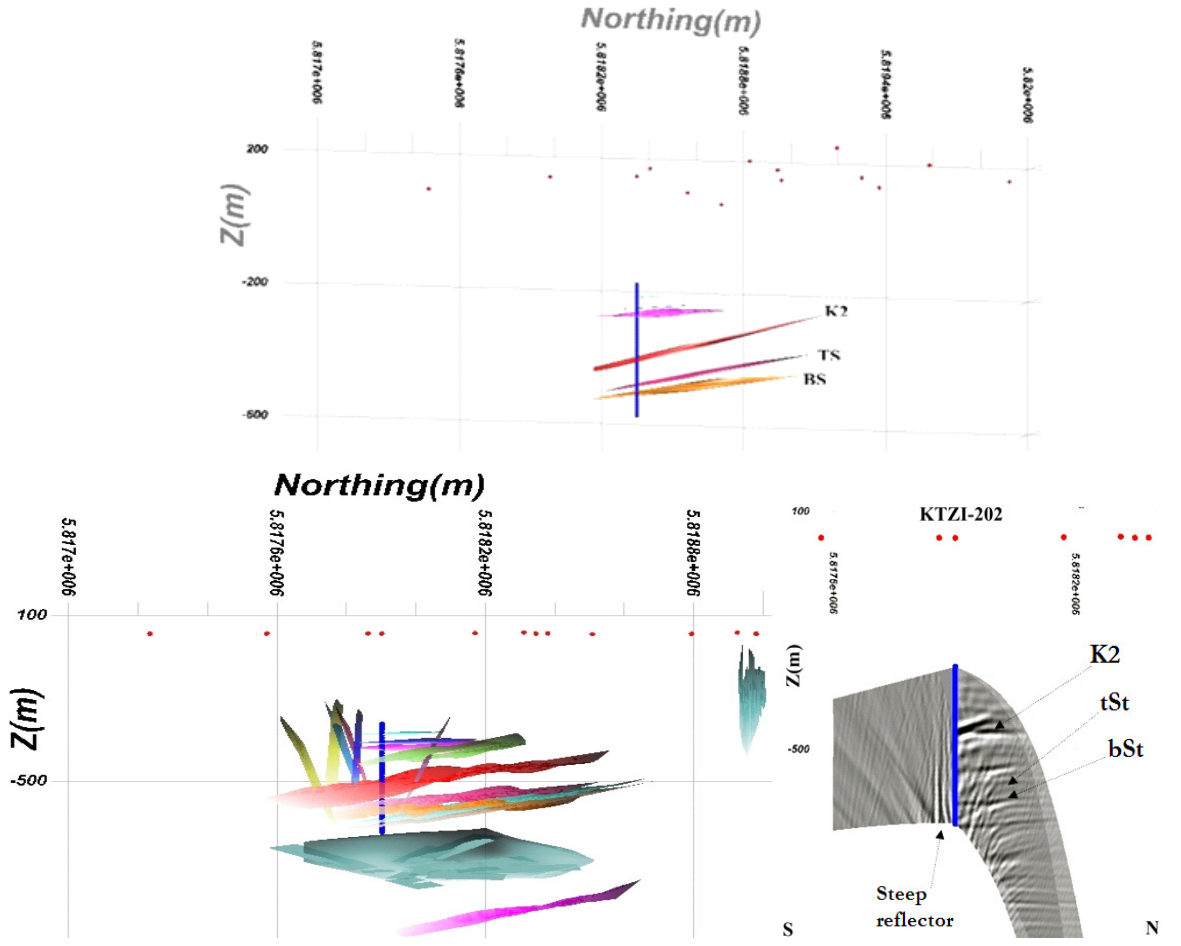

Figure 40. Top: The main targets, imaged as sub-horizontal reflectors: the K2 anhydrite layer, which intersects the KTZI-202 observation well at 550m, with dip 10° and azimuth 345°; the Top Stuttgart-Formation (TS), intersects the well at 626m, with dip 8° and azimuth 355°; the Bottom Stuttgart-Formation (BS), intersects the well at 650m, with dip 5° and azimuth 350°. Bottom: all 3D interpreted reflectors determined from the baseline VSP data, together with example of VSP-CDP migrated profiles, aimed at imaging the sub-horizontal target layers and also one steeply dipping reflector south of the investigation borehole.

3.3 Re-evaluation of baseline and repeat surveys

During the CO2SINK project only the analysis of the baseline VSP data has been done. In order to complete the time-lapse analysis of the VSP surveys, further processing needed to be done such that the two data sets benefit of the removal of the effect of different near surface conditions and amplitude equalization amongst different VSP shots. Work has been done within the CLEEN project to jointly analyze the entire VSP data set available from Ketzin.

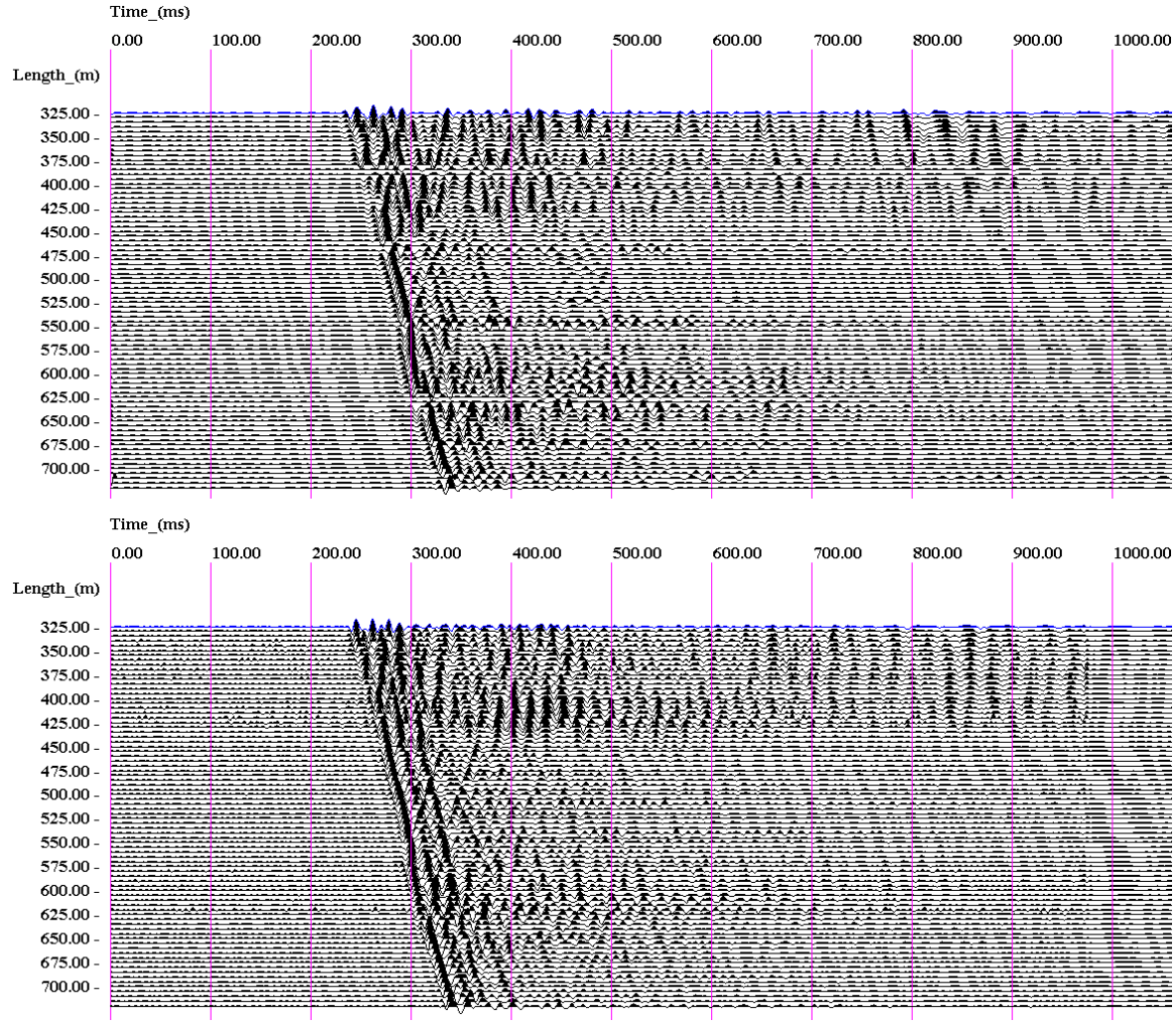

Figure 41. Baseline (top) and repeat (bottom) raw VSP vertical component data acquired from shot point V11, on line 7 of the 2D Star.

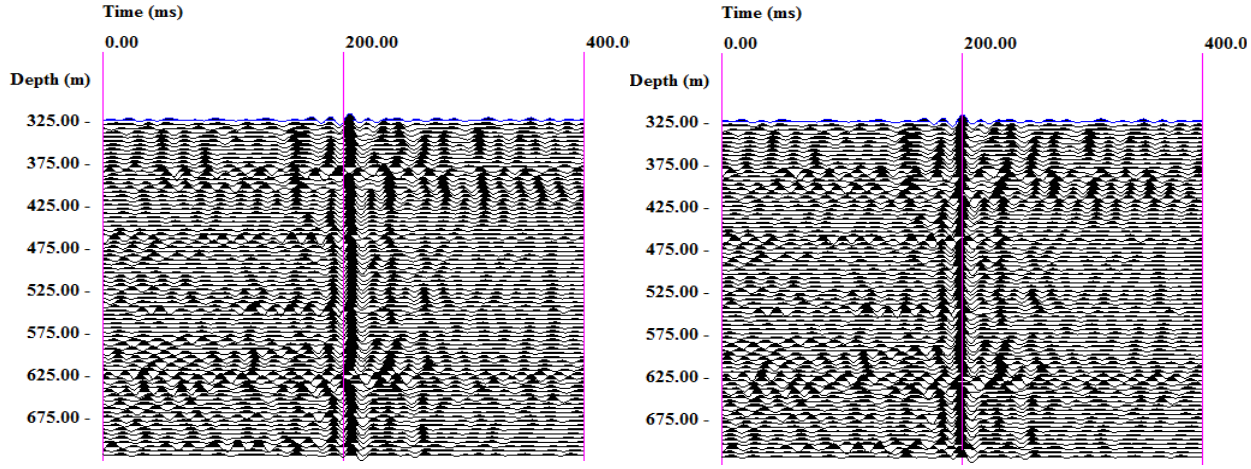

Figure 42. Cross-correlation profiles before (left) and after (right) shift corrections.

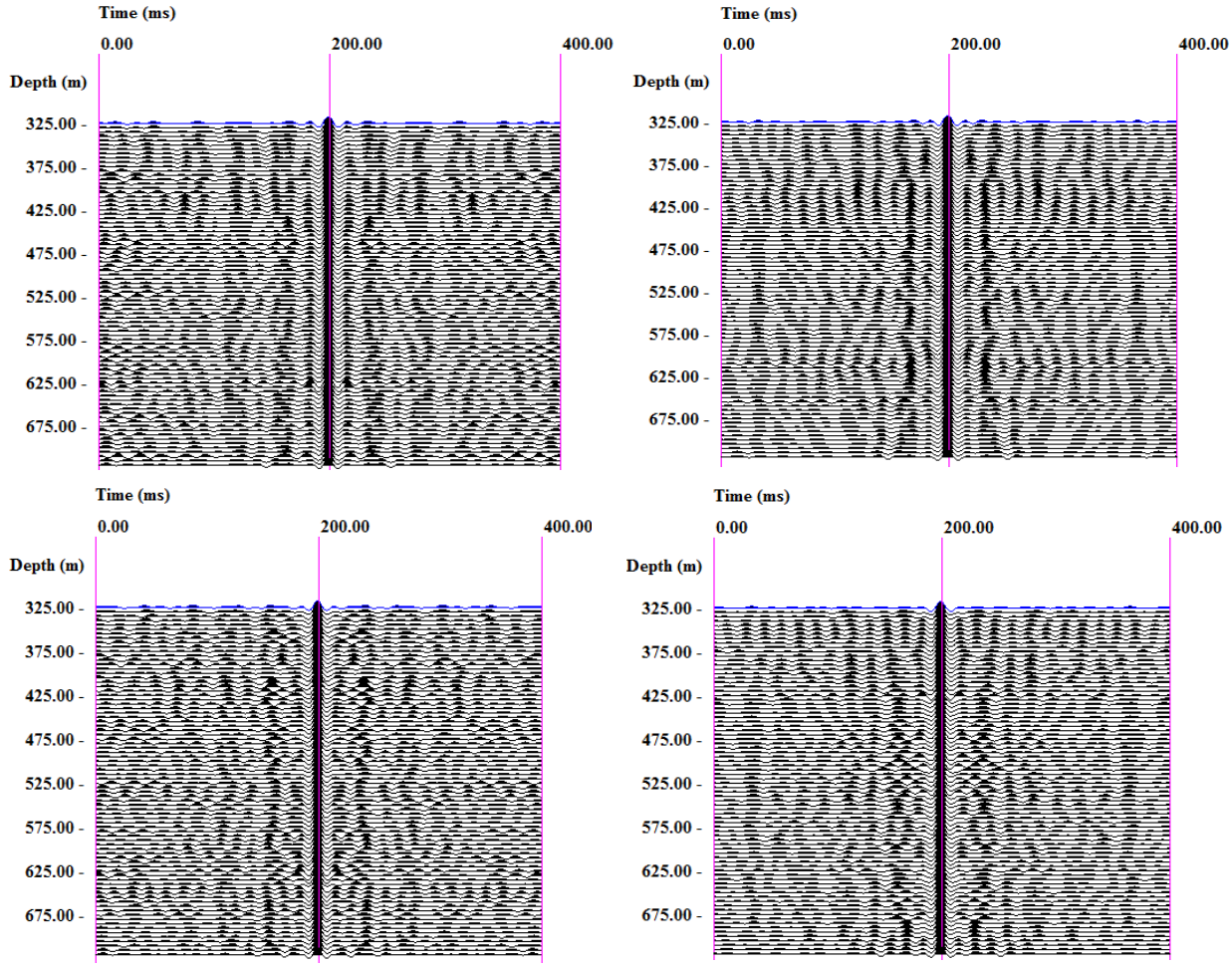

Figure 43. Auto-correlation profiles before (top) and after (bottom) harmonic filtering. Baseline (left), and Repeat (right).

By comparing the baseline with the two repeat data sets potential changes related to CO_2 injection can be observed, as seen in Figure 44.

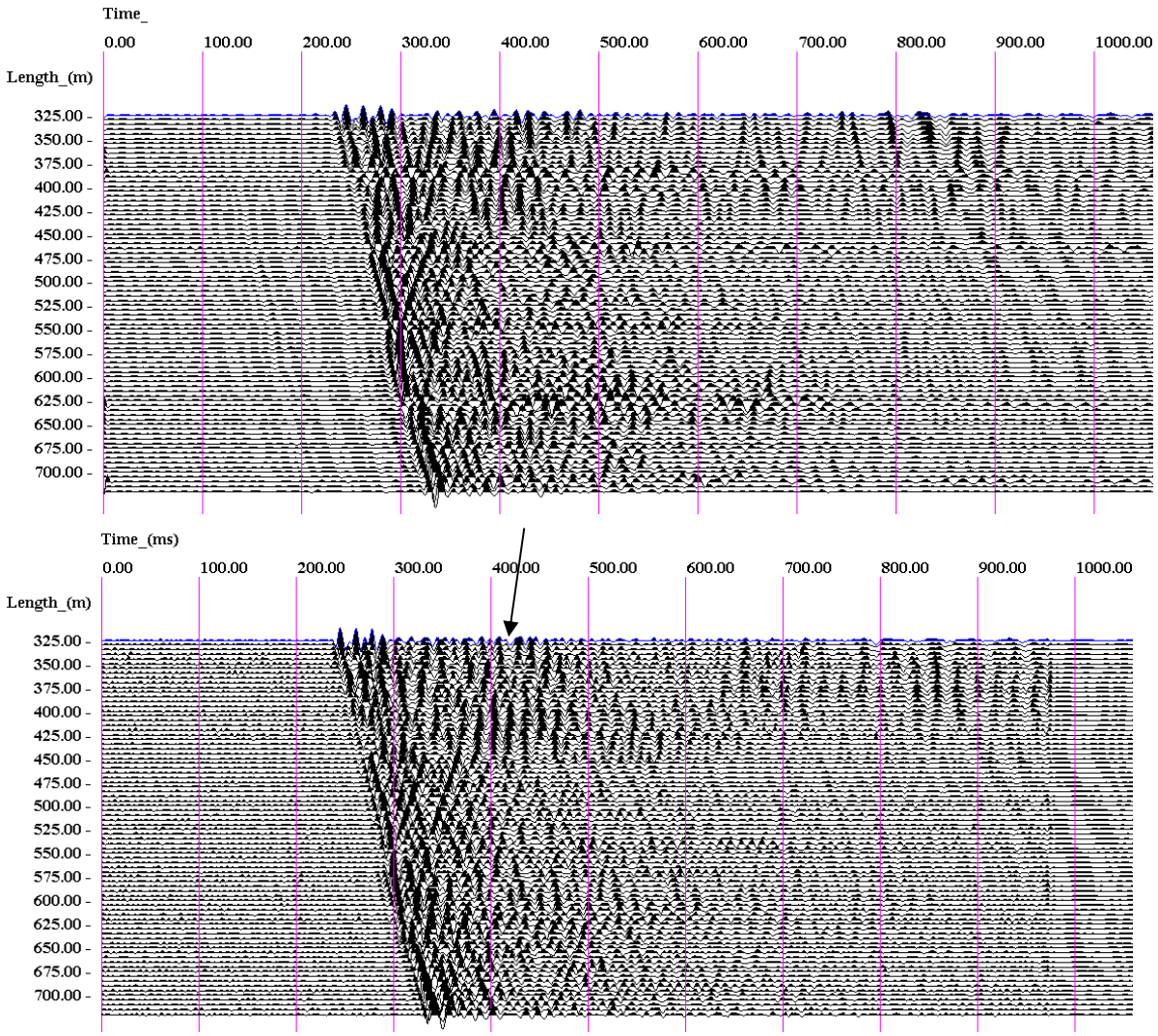

Figure 44. Vertical component shot V11, baseline (top) and repeat (bottom) after band pass filtering (10 to 150 Hz), shift correction with the time shifts determined by cross-correlation analysis and harmonic filtering.

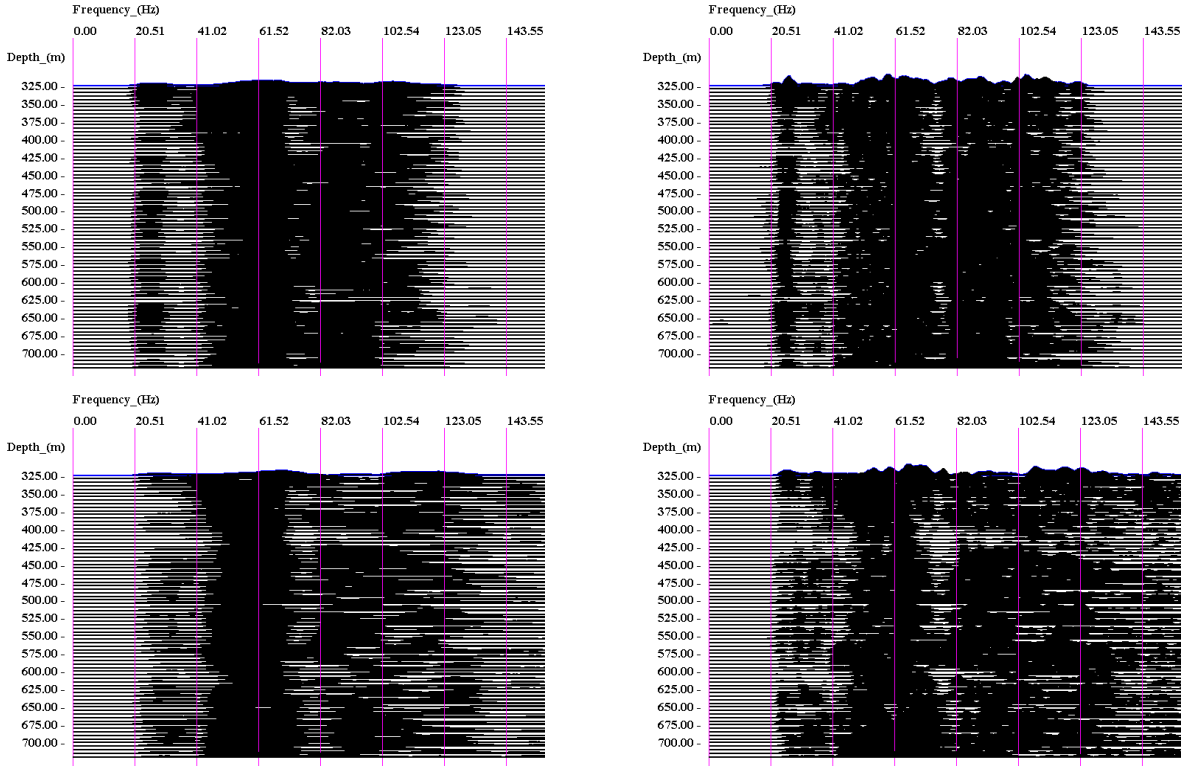

Figure 45. Spectra profiles of baseline (top) and repeat (bottom) computed from the MSP profiles shown in Figure 41 (right) and Figure 44 (left).

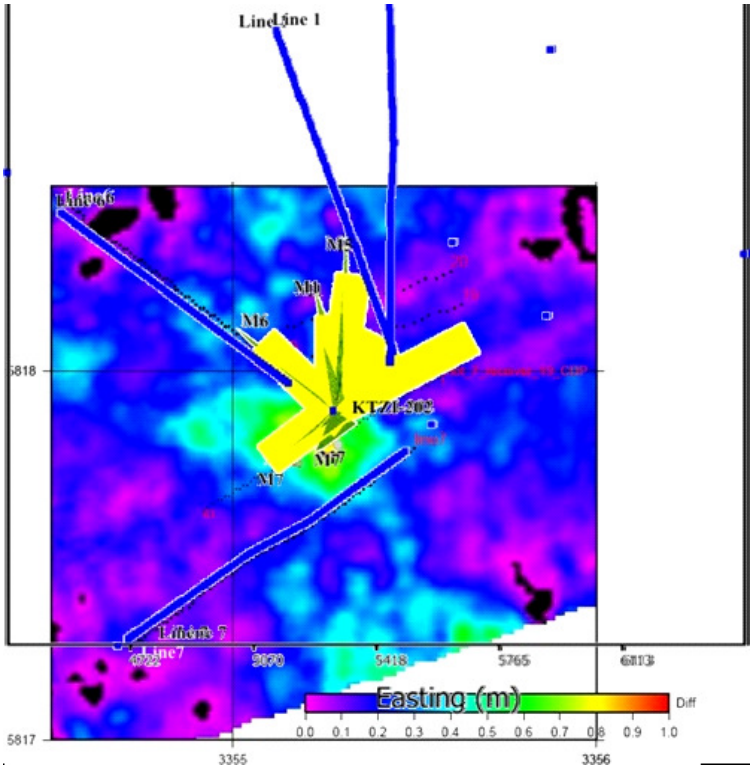

Figure 46. VSP coverage. View from above of the amplitude difference map at the reservoir level (Juhlin, 2010), overlain by VSP interpreted reflector elements (yellow rectangles, also shown in Figure 18), computed from all VSP shot points suitable for imaging the sub horizontal reflector at the reservoir level.

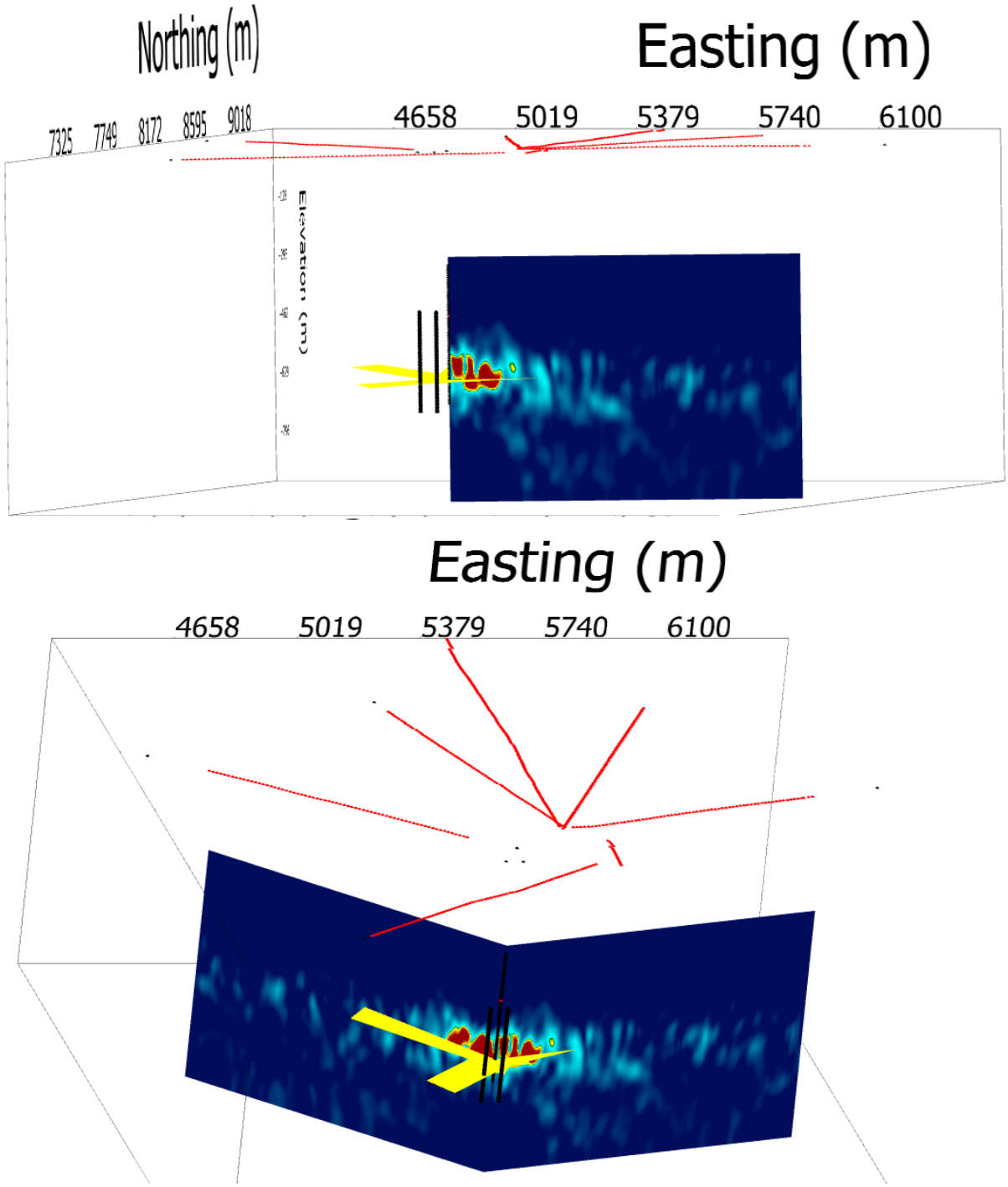

Figure 47. 3D view of two IP migrated vertical sections calculated at azimuths 75°(top) and 315° from North with receiver elements interpreted at the level of the reservoir (630 to 640m depth in KTZI-202), interpreted from the baseline VSP data.

Difference maps shown in Figure 48 were computed from the time-lapse analysis of the VSP baseline and repeat surveys and can be compared with the difference maps computed from the 3D data by (Juhlin et. al. 2010, in Figure 14) and from the 2D star data by (Ivandic et. al., 2012, in Figure 16) and the ones estimated from the MSP time-lapse data (shown in Figure 34).

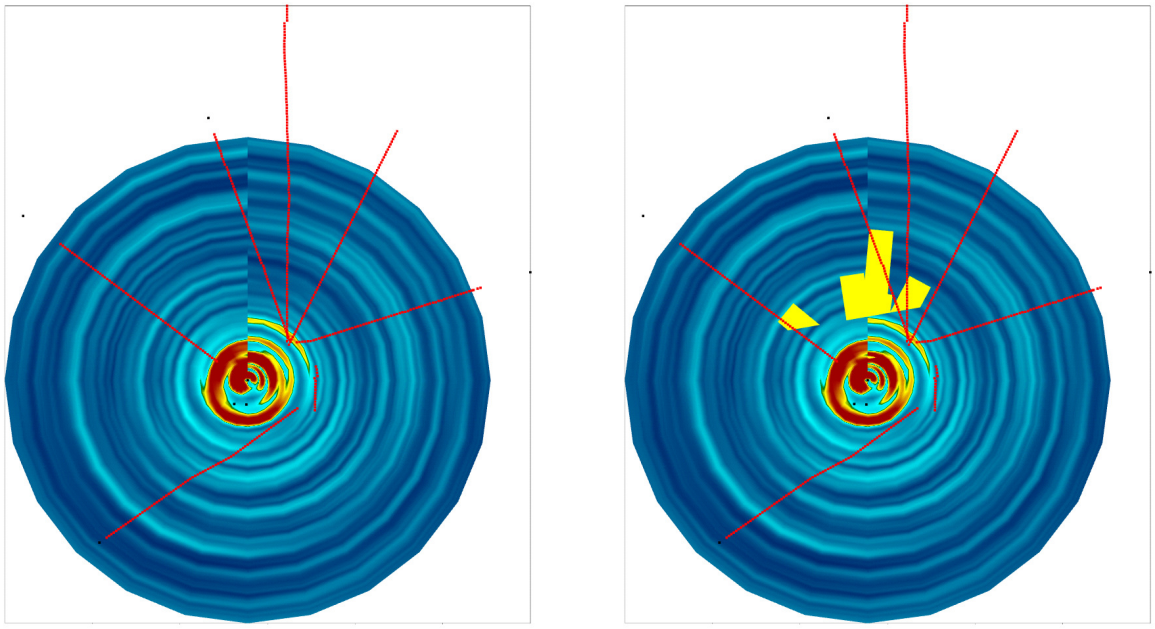

Figure 48. View from above of the time depth slice at the level of the reservoir (630 to 640m depth in KTZI-202) for baseline vs. first repeat VSP data set. Images on the right side also display reflector elements (yellow) interpreted at the reservoir level from the baseline VSP data (Enescu, 2010).

4 Time-lapse reservoir monitoring by crosshole investigations

A series of cross-well seismic surveys were acquired within the framework of the CO2SINK project at Ketzin, at various stages of an injection test.

4.1 Baseline & repeat crosshole measurements

The cross-hole seismic monitoring using the two observation wells close to the injection well (KTZI-200 at 50 m and KTZI-202 at 112 m distance to the injection well, KTZI-201) was designed to follow the migration of CO_2 at small scale close to the injection. Four time-lapse cross-hole seismic measurements were performed between the observation wells. The baseline survey was performed in May 2008. Two repeats followed in July and August 2008, after the breakthrough of the CO_2 in KTZI-200. A third repeat was performed in July 2009, following the breakthrough of the gas in KTZI-202 in March 2009. Timing of the surveys, in relation to the cumulative injected CO2 mass is illustrated in Figure 3.

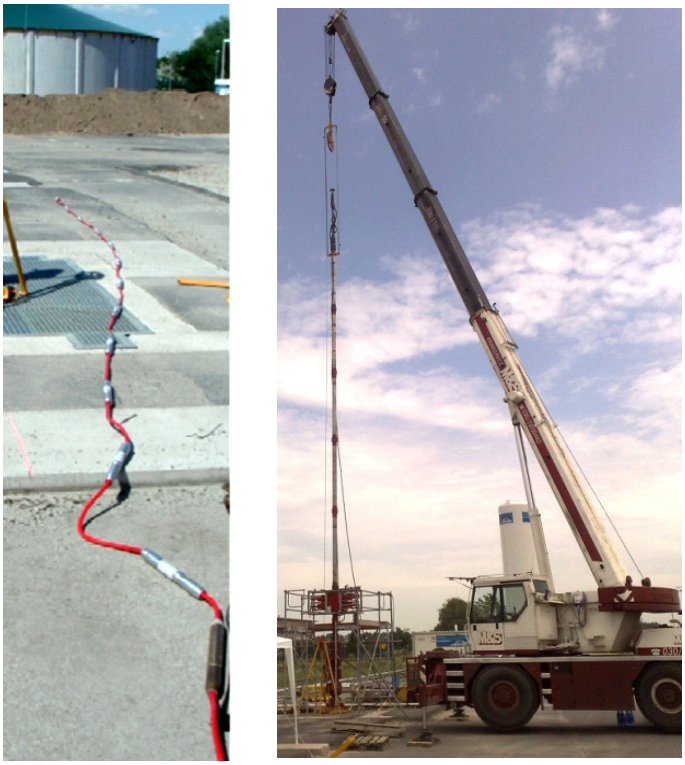

Figure 49. Receiver string used for cross-hole measurements and its installation in borehole KTZI-202.

The first three sets of measurements covered a depth range from 452m to 739m, at 1m intervals with sources in KTZI-200. The recording was performed in KTZI-202, from 464m to 726m, at 1m intervals.

In July 2009, the upper layouts were skipped due to the absence of liquid in the receiver hole KTZI-202, where the CO_2 had arrived and displaced the water. Both the source and the hydrophones were installed through lubricator towers (Figure 49) that allowed the tools to be moved while maintaining the boreholes pressure-tight.

4.2 Conventional processing and analysis

The frequency band selected for the filter is as wide as possible (250 – 1200 Hz), the rejected spectral components corresponding to clearly identified sources of noise. A data preparation and conditioning processing sequence was applied, consisting mostly of eliminating high amplitude tube-waves and spectral equalization.

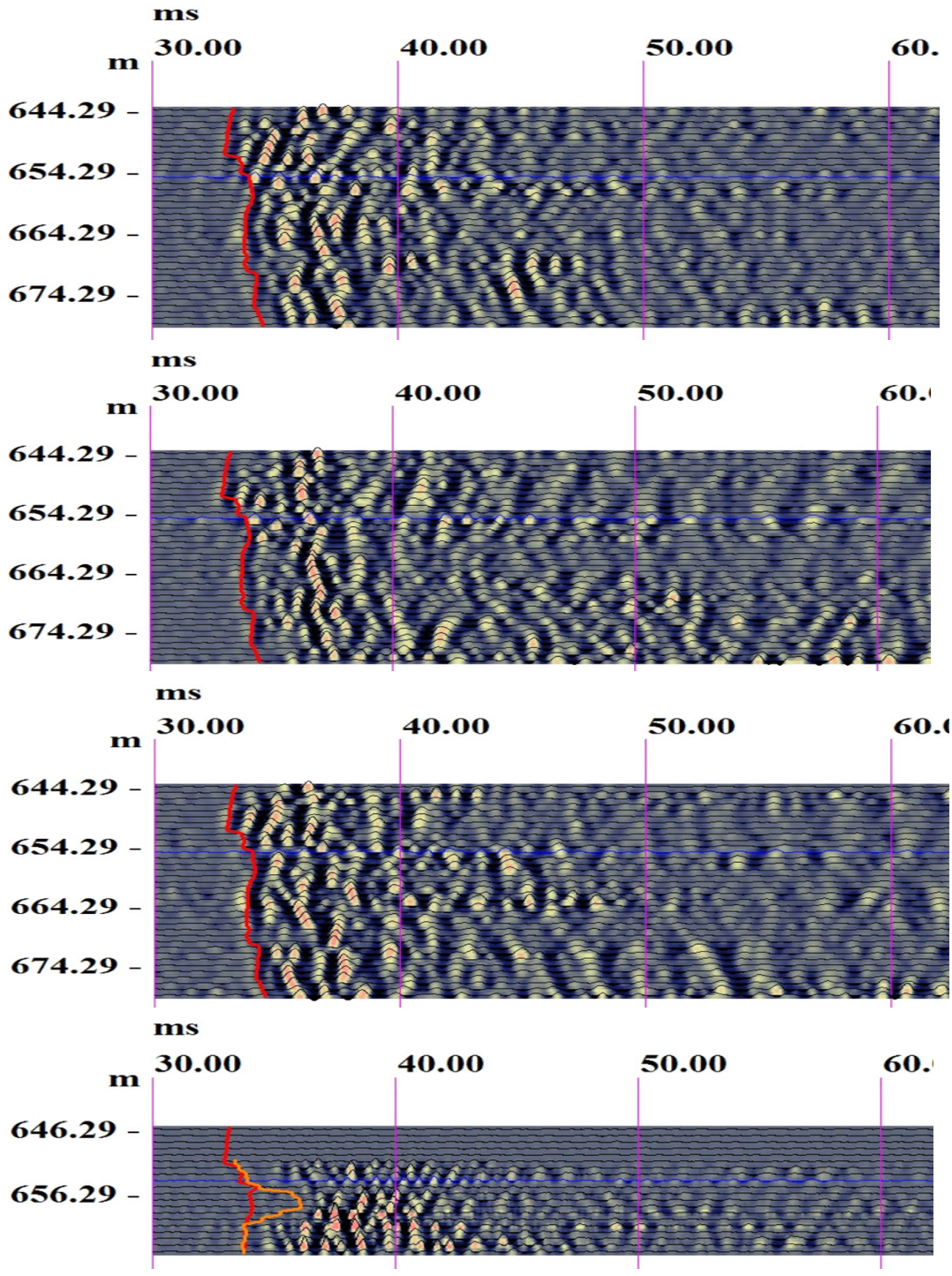

Figure 50. Baseline: May 2008 (top), 1st repeat: July 2008, 2nd repeat: Aug 2008 and 3rd repeat: July 2009 (bottom) shot gathers at injection layer level, after suppression of tube waves and band-pass filtering.

Picking of the first arrival times was done accurately and without problems on most of the traces. The time differences are minimal for the baseline and the two repeats done in 2008 (Figure 50). The red line follows the first arrivals picked on the baseline data set. The overall quality of the data is deemed good; all arrival times were picked. The picking errors are much smaller than the delay produced by the presence of the CO_2 in the 2009 measurements (see orange arrivals in Figure 51).

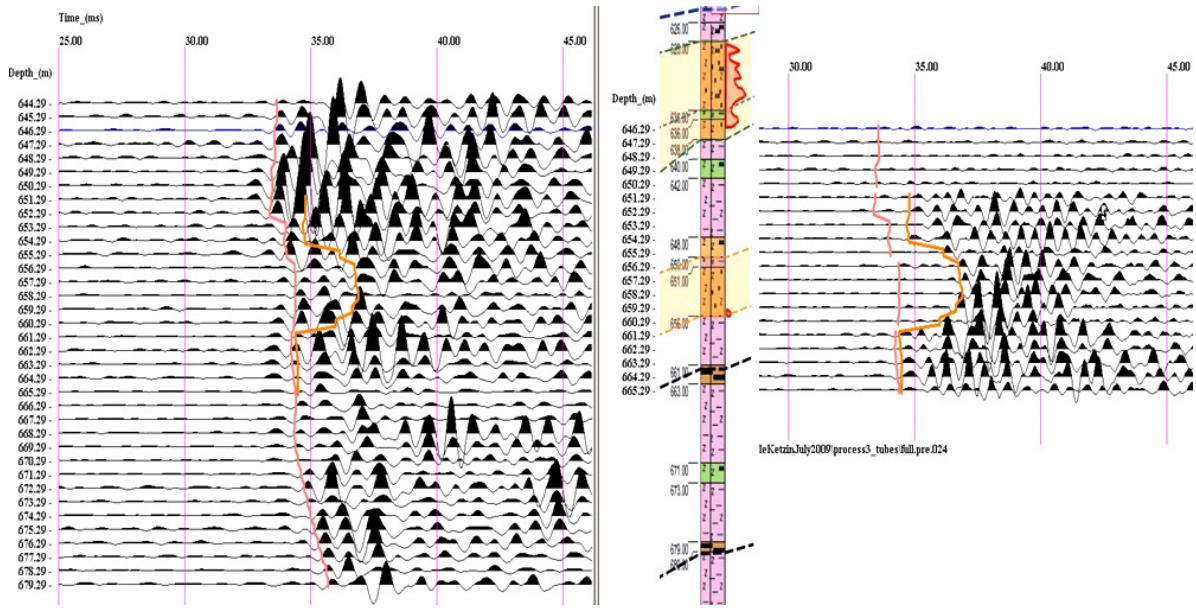

Figure 51. Shot gathers, at the level of the injection layer, baseline (left) is compared with the 3rd repeat (right), together with the relevant geologic log in hole KTZI-202.

With crosshole tomography, access to the region of interest is gained through boreholes, seismic signals being generated in one borehole and received in another. This makes the solution of the tomographic problem dependent on how accurately the coordinates of the boreholes and the position of the instruments along the boreholes can be determined.

To produce a resolved and reliable image, the crosshole tomographic method requires that the positions of the sources and receivers are determined with an accuracy of fractions of a meter at depths that may exceed hundreds of meters. In this case, it has been difficult to evaluate accurately borehole deviations as a part of the velocity inversion, due to the strongly refracted field components over the anhydrite (K2) layer, where P wave velocity is ~5500m/s. However, correcting for errors of the order of 1m of the actual distance between the holes can produce a better focused picture. The areas covered by less rays tend to attract accumulating artifacts.

Bent ray tracing was used for tomographic inversion of all crosshole data sets. Figure 52 displays the ray pattern derived from the baseline data. The K2 high velocity layer gathers refracted rays from a depth range of nearly 100m. The reservoir depth around 630 m is however well covered. Figure 52 (c) displays the same data as (a), with the color scale limited between 3000 m/s and 3300 m/s. Figure 52 (d) shows the second repeat (August 2008) data with the same color scale. Only very slight variation can be observed between the two sections, with no clear indication of differences induced by injection of the CO_2.

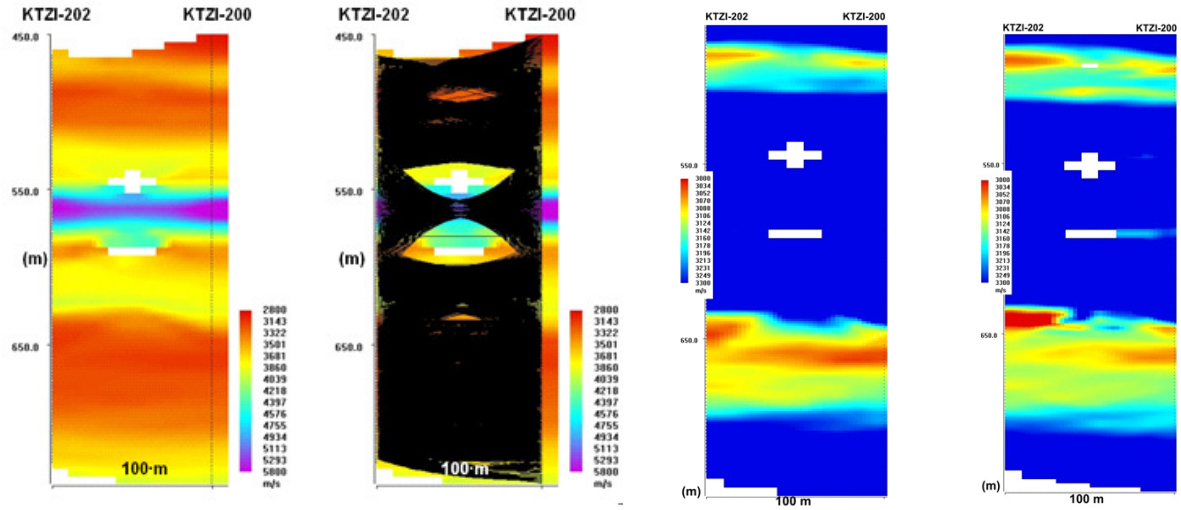

(a) (b) (c) (d)

Figure 52. (a) Tomographic inversion of the baseline crosshole data and (b) ray pattern; Baseline (May 2008, c) and second repeat (August 2008, d) velocity fields at the level of the injection layer. The velocity range has been limited for display from 3000 to 3300 m/s, to emphasize details of the target aquifer. The anhydrite layer, K2, becomes invisible, as its velocity is higher than the range selected. Charts (c) and (d) are not identical, but the different details are more likely attributable to time picking and ray path computation noise.

4.3 Re-evaluation of baseline and repeat surveys

Attenuation tomographic inversion (A=-Log(amplitude)) results are shown in Figure 53 for the baseline, repeat 1 and repeat 2 data sets. The progress of the CO_2 plume cannot readily be pointed out, but the aquifer could be outlined by higher attenuation.

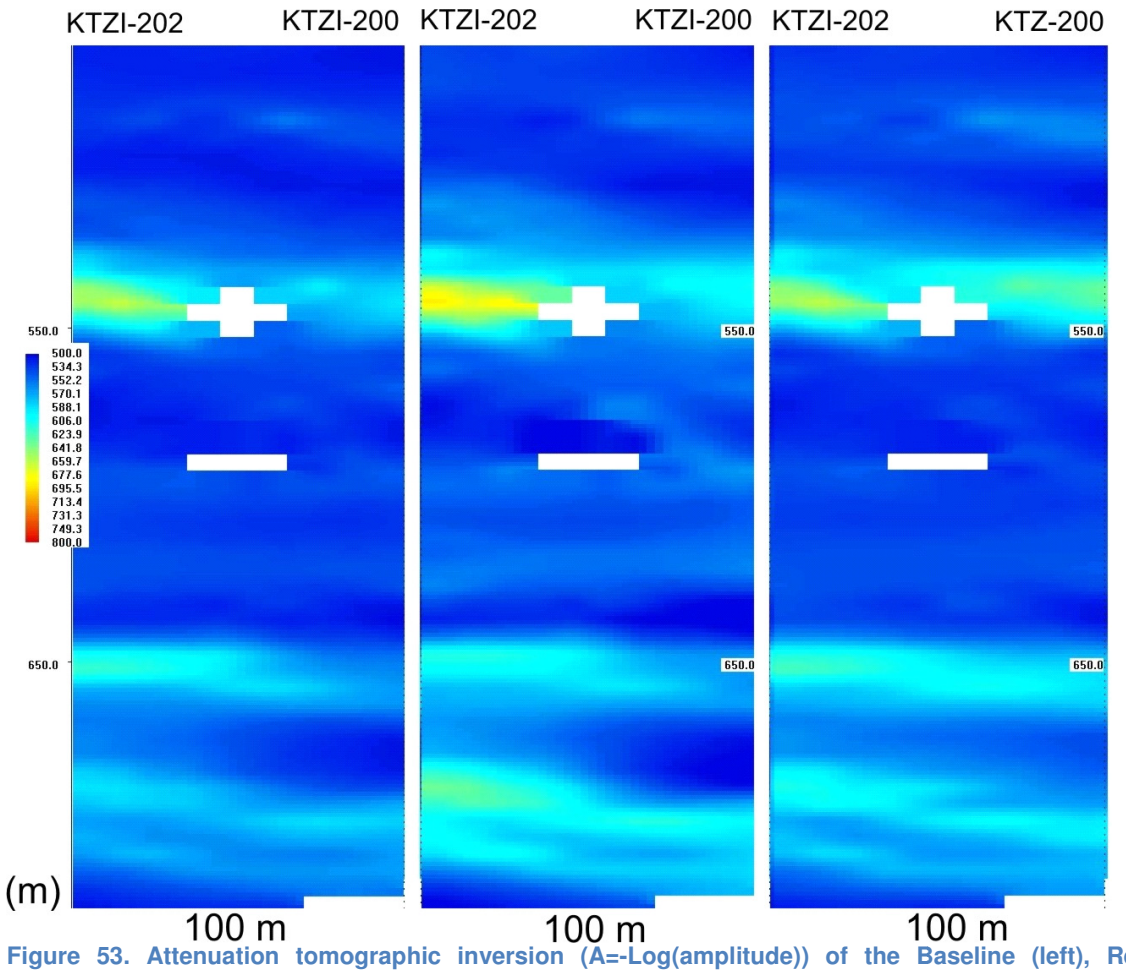

Figure 53. Attenuation tomographic inversion (A=-Log(amplitude)) of the Baseline (left), Repeat 1 (middle), Repeat 2 (right) crosshole data. The maximum attenuation is normalized to 1000. The progress of the CO_2 plume cannot readily be pointed out, but the aquifer could be outlined by higher attenuation. The low amplitude at depth 550 m is likely an artifact produced by ray path noise of the waves refracted through K2.

The first arrivals do not follow as well the low frequencies obtained by derivation of the Hilbert transform from Figure 54, but the gap at the reservoir level in the 2009 measurements remains clearly visible.

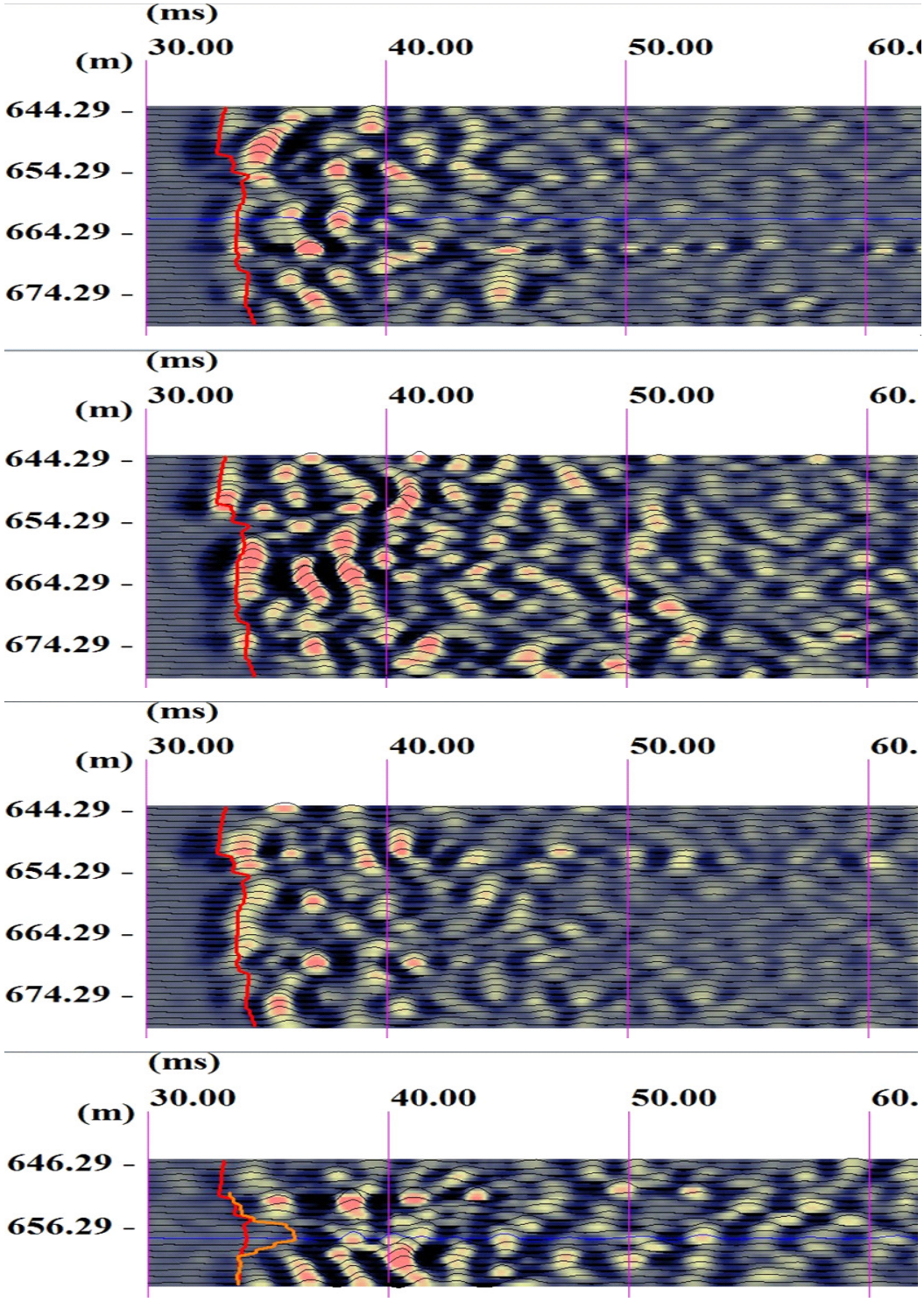

Figure 54. Same as in Figure 50, after taking the derivative of Hilbert transform.

Covariant tomographic inversion of difference sets are also in Figure 55. The correlation coefficient has been multiplied with a symmetric function depending on the amplitudes of two data sets, estimated of in window after the P wave arrivals.

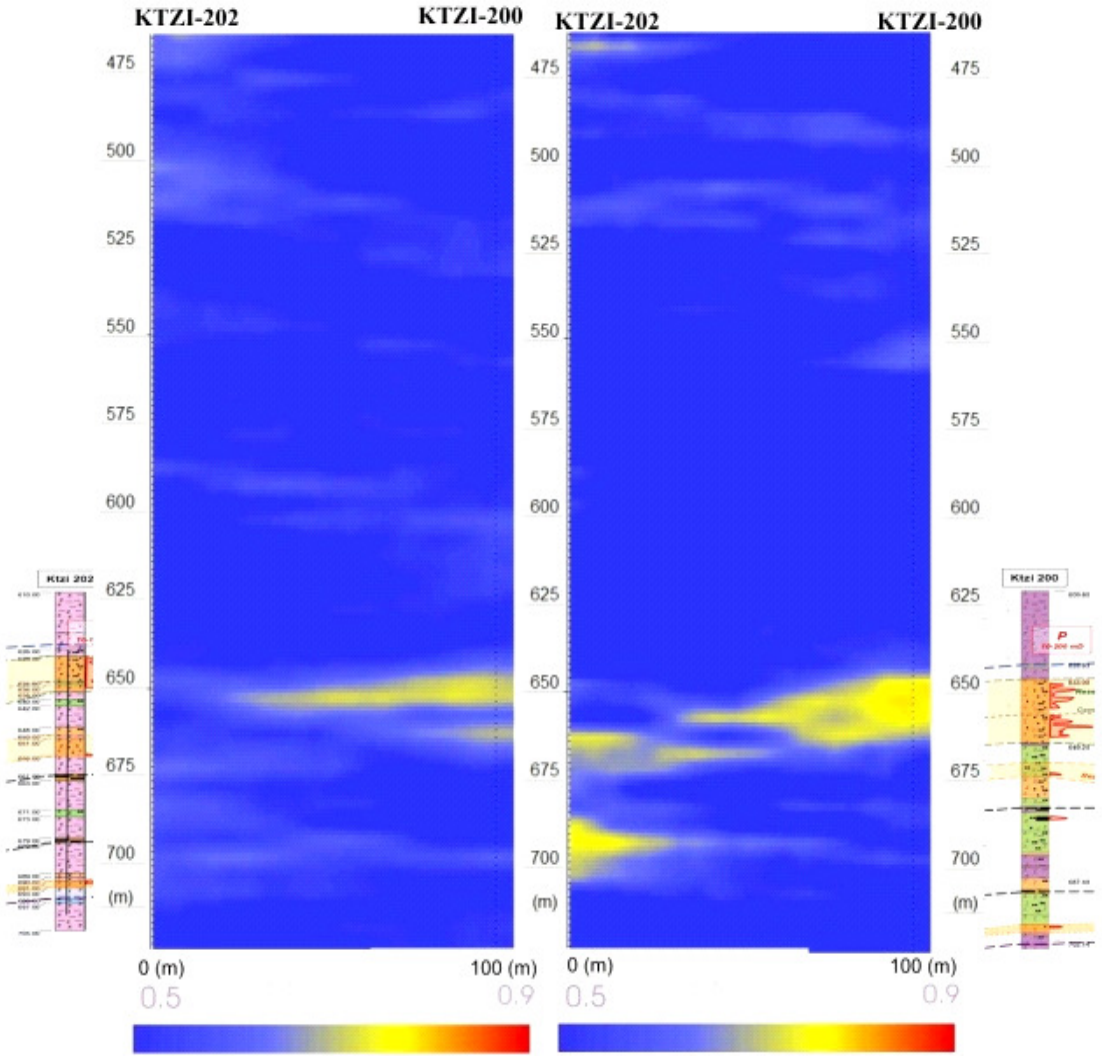

Figure 55. Covariant tomographic inversion of sets: difference July–May 2008 (left) and difference August–May 2008 (right), together with the geological interpretation at the reservoir layer. The term covariance is not entirely properly used, as the amplitude modulation of the correlation coefficient is not obtained by multiplying with the variances of the amplitudes of two sets, but by symmetric function depending on the amplitudes.

The left panel of Figure 55 is also shown on the left side of Figure 56 and compared with the IP-migrated difference of the Repeat 1 (July 2008) and Baseline (May 2008) data sets.

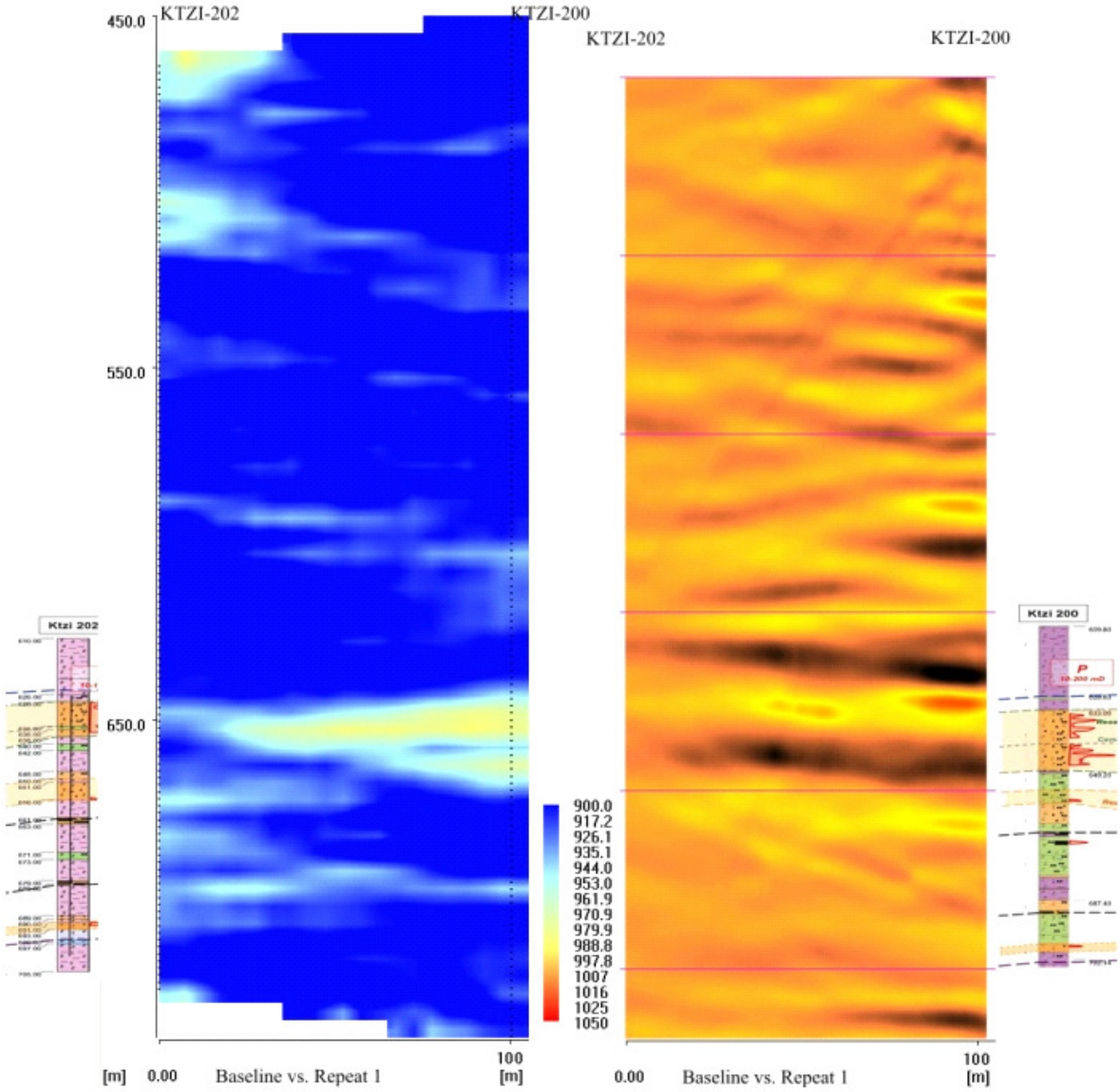

Figure 56. Covariance inversion and Difference IP migration of First Repeat and Baseline data.

The crosshole time-lapse surveys were meant to follow the migration of the CO_2 during injection. As modeling assumptions lead to the accurate prediction of the CO_2 breakthrough in KTZI-200, the baseline and two repeat surveys were carried out over a three-month span in 2008, when the quantity of CO_2 injected was approximately 1000 tons. The small quantity injected and the evolution of the plume mainly outside the plane of the crosshole section measured were a serious challenge to routine techniques, e.g. travel time and amplitude inversion, which could not present convincing evidence of the CO_2 plume intersecting the crosshole plane.

The covariance inversion method exemplified here uses changes in the character of the wavelet, including its coda, which apparently increases significantly the sensitivity of the inversion.

The IP pre-stack migration identifies a quite similar finger-shaped area at the same depth as the covariance inversion. The amplitude calibration prior to subtracting the

data has been performed based on the response of K2 and extrapolated. Indeed the K2, at 550 m depth, vanishes almost completely, but shot footprints can steel be seen near KTZI-200. Nonetheless, the most important feature of the difference migration remains the one that can be associated with a CO_2 plume touching KTZI-200 but avoiding KTZI-202, which is consistent with the situation at the time of the repeat measurements. A forth crosshole repeat made in 2009, after the CO_2 breakthrough in KTZI-202, not presented here, showed clear travel time delays associated with the CO_2 plume.

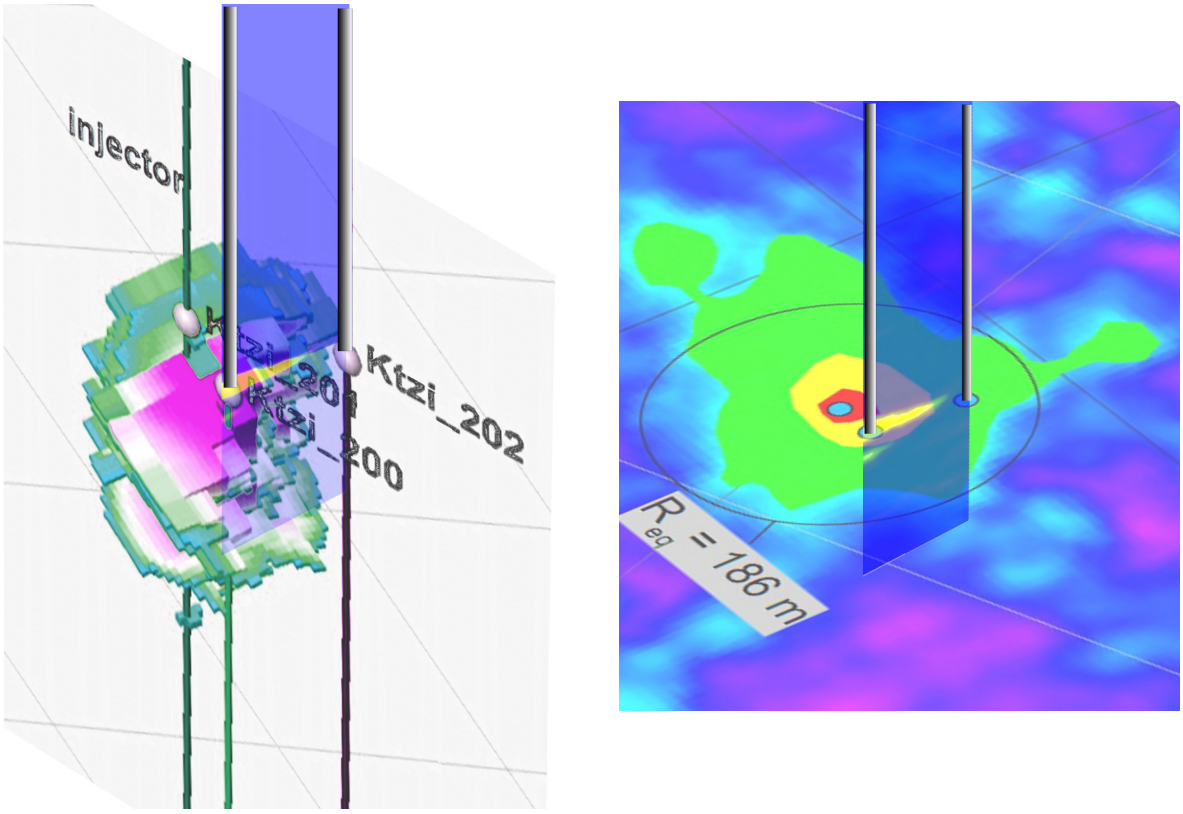

Figure 57. Left: Covariance tomogram together with the updated CO2 plume propagation model /Frykman, 2010/ derived in conformity with the delayed propagation of the CO2 from the injection well to the second observation well. Right: Covariance tomogram together with the difference amplitude map determined from the baseline and repeat 3D data sets /Juhlin, 2010/ at the level of the injection layer.

From crosshole data, in 2008, we could tell that the plume did not propagate towards North, as expected. Without any other crosshole section, we could not tell more at the time. One year later this has been confirmed by the repeat 3D seismics which determined that preferential propagation was mainly towards West.

5 Discussion and conclusions

A CO_2 monitoring programme should be designed to encompass several experimental scales. Analysis of the time-lapse VSP data analysis shows that it is possible to detect changes in the subsurface caused by injection of CO_2, however the method is not particularly suitable for imaging sub-horizontal layers. Better suited for that are MSP surveys and analysis of the MSP time-lapse data from Ketzin proves the suitability of this method for timely monitoring of CO_2 injection in gently dipping aquifers. The cross-well imaging method used is able to identify very small quantities of CO_2. Focused surveys inherently lack the wide coverage of site-scale 3D surveys; however, these can monitor the evolution of the CO_2 plume accurately and in a timely manner.

Models must be built having in mind the possibility of validating them by a real life experiment. After all the practical details are clarified, planned experiments should be modeled with the highest accuracy possible with respect to the layout and with a maximum of available data regarding the geology, hydrogeology, structure and physical properties at the experimental site.

With any storage site, including a CO_2 sequestration one, the most challenging issue is to demonstrate that containment of the disposed substance will be effective in the short and long term. In our case, this involves firstly determining the spatial extent and geometry of the seal and predicting (and subsequently monitoring) the size of the injected plume of CO_2. It must also be demonstrated that the seal is not compromised by faults, fractures or thinning over the entire potential footprint of the CO_2 plume. The detection of steep structures before injection can be difficult solely by surface methods but the VSP layout, with a receiver array extended vertically in a borehole, can accomplish this task (Enescu and Cosma, 2010).

The 4D time-lapse seismic technology is useful and is an efficient technique for reservoir monitoring. Various aspects of sparser than full 3D geometries were investigated in detail and proven to be effective for CO_2 injection monitoring.

Time-lapse analysis of 2D seismic data, done independently on each of the seven 2D lines at Ketzin, showed that in 2009 no CO_2 related time-lapse signature was observable where the 2D lines allowed monitoring of the reservoir (Bergmann, 2011). This agreed with the time-lapse results of the 3D surveys imaging (Juhlin, 2007), where a reflectivity increase was mapped just centered at the injection well, but which did not reach the area monitored by the 2D lines.

When analyzing the 2D star array as a pseudo-3D seismic survey, time lapse processing provided a good qualitative image of the amplitude changes due to the CO_2 injection (Ivandic, 2012). Although the size of the amplitude anomaly due to the CO_2 was smaller in the pseudo-3D than in the 3D data, a similar pattern was observed. Therefore, at least at the Ketzin site, it is possible to use low and variable fold seismic surveys to image the distribution of the CO_2. The pattern of the amplitude anomaly indicated that the lateral heterogeneity of the Stuttgart Formation strongly affected the plume geometry. The preferential movement of CO_2 plume towards the west direction, as opposed to the expected north direction, prevented observation of the CO_2 plume evolution when the “star” lines were processed as

individual 2D lines. Both repeat surveys showed that no CO_2 leakage was observed at the time of the surveys.

The main role of the MSP has been to map the 3D velocity field and the velocity field inferred by MSP can be used e.g. to increase the resolution of the 3D surveys. The geometry of the MSP layout, allows for limited lateral imaging of the CO_2 plume and the horizontal profiles obtained (each profile consists of multiple source lines on surface and one receiver down-hole) produce high-resolution images confined to the vicinity of KTZI-202.

The VSP layout, with the receiver array extended vertically, can produce images of the steep structures and the lateral coverage is significantly larger than with MSP. The VSP surveys cover a region with an average radius of approximately 300m around the injection site. The gain of resolution is obtained by increased frequency and by more diverse view angles of the structure than achievable with surface stations only.

The crosshole time-lapse surveys have been meant as a means to follow the migration of the CO_2 during and after injection. Following modeling assumptions that lead to the accurate prediction of the CO_2 breakthrough in KTZI-200, the baseline and two repeat surveys were carried out over a three-month span in 2008. A forth crosshole repeat made in 2009, after the CO_2 breakthrough in KTZI-202, showed clear travel time delays associated with the CO_2 plume, but the depth interval of the measurements was limited due to poor hydrophone coupling, as the borehole water had been replaced by gaseous CO_2. Repeating the post injection crosshole with modified equipment able to work in dry holes is seen as a necessary conclusive step.

5.1 Recommendations for further development

Since the reservoir at the Ketzin site proved to be heterogeneous (Förster, 2008) and generally less than 20 m thick, conventional 2D/3D seismic data could not resolve it with good enough detail to characterize in detail the CO_2 plume evolution (Cosma, 2009; Zhang 2012). Borehole measurements are therefore instrumental in order to achieve better resolution. However, in the Ketzin case the initial design of the source and receiver layouts has been made with the assumption that the expected migration of the CO_2 plume would be towards North, while it actually took a preferential path towards West. The Ketzin site geological model was correct at large scale, while details of heterogeneity, especially at the reservoir level were not fully understood before investigations began within the CO_2SINK project.

In the case of a new site characterization programme for a potential CO_2 storage facility, baseline seismic investigations from surface and boreholes should be made well in advance of the infrastructure construction and from more than one borehole, such that the results of the baseline surveys may be used for selection of the most suitable location of the injection well. Also, the design of the baseline surveys should cover a larger area than what may be necessary for subsequent time-lapse monitoring and no strong assumptions should be made on a preferential migration path for the injected CO_2. One of the lessons learned at Ketzin is that local heterogeneity of the reservoir plays an important role in the migration of the injected CO_2 and only very high resolution measurements that sample the space close to the reservoir may be used to characterize the reservoir at a relevant scale.

6 References

Arthur C., Lianjie H., Jim R., 2010. Time-lapse VSP data processing for monitoring CO_2 injection. *The Leading Edge,* 29: 196-199.

Bergmann, P., Yang, C., Lüth, S., Juhlin, C. and Cosma, C., 2011. Time-lapse processing of 2D seismic profiles with testing of static correction methods at the CO_2 injection site Ketzin (Germany). Journal of Applied Geophysics, Volume 75, Issue 1, pp. 124–139, DOI 10.1016/j.jappgeo.2011.05.005

Cosma, C, Balu, L. and Enescu, N., 2010. 3D VSP migration by image point transform, Geophysics, ISSN 0016-8033, Volume 75, Issue 3, p. S121.

Cosma, C. and Enescu, N., 2010. Report on crosshole seismic survey, Time-lapse crosshole investigations from boreholes KTZI-200 and KTZI-202 at Ketzin, Germany. CO2SINK report D6.3-2, June 2010.

Cosma, C., Enescu, N., Cosma M. & the CO2SINK Team, 2009. Borehole Seismic Monitoring at CO2SINK Site, The 9th International Workshop on the Application of Geophysics to Rock Engineering, Hong Kong, China.

Cosma, C and Enescu, N., 2001. Characterization of fractured rock in the vicinity of tunnels by the swept impact seismic technique. International Journal of Rock Mechanics and Mining Sciences: 38, 815-821.

Eaton, D., 1998. Description of the BMOD3D program. Private communication.

Enescu, N., Juhlin, C. and Cosma, C., 2011a, Seismic modelling results for optimal source and receiver depths for detecting CO2 leakage and the potential of passive monitoring using ambient noise. MUSTANG report D033, Oct. 2011.

Enescu, N., Cosma, C., Juhlin, C. and Zhang, F., 2011b,Seismic Methodology for Characterization of Deep Saline Aquifers for CO2 Storage. Geophysical Research Abstracts, Vol. 13, EGU2011-9687, EGU General Assembly, May 2011

Enescu, N. and Cosma, C., 2010. Report on baseline and repeats VSP/MSP and 2D Star, VSP & MSP investigations from borehole KTZI-202 at Ketzin, Germany. CO2SINK report D6.3-3, June 2010.

Förster, A., Norden, B., Zinck-Jørgensen, K., Frykman, P., Kulenkampff, J., Spangenberg, E., Erzinger,J., Zimmer, M., Kopp, J., Borm, G., Juhlin, C., Cosma, C. and Hurter, S., 2006. Baseline characterization of the CO2SINK geological storage site at Ketzin, Germany, Environmental Geosciences, v. 13, no. 3 (September 2006), pp. 145–161.

Förster, A., Giese, R., Juhlin, C., Norden, B., Springer, N. and CO_2SINK Group, 2008, The Geology of the CO_2SINK Site: From Regional Scale to Laboratory Scale, Elsevier, Energy Procedia, GHGT-9.

Giese R., Henninges J., Lüth S., Morozova D., Schmidt-Hattenberger C., Würdemann H., Zimmer M., Cosma C., Juhlin C., and CO2SINK Group, 2009. Monitoring at the CO2SINK Site: A Concept Integrating Geophysics, Geochemistry and Microbiology. Energy Procedia, 1, 2251-2259.

Kazemeini, H. S., Yang, C., Juhlin, C., Fomel, S. and Cosma, C., 2010. Enhancing seismic data resolution using the prestack blueing technique: An example from the Ketzin CO2 injection site, Germany. SEG GEOPHYSICS Volume 75, Issue 6, pp. 1942-2156, DOI 10.1190/1.3483900

Kazemeini H., Juhlin C. and Fomel S., 2010. Monitoring CO2 response on surface seismic data; a rock physics and seismic modeling feasibility study at the CO2 sequestration site, Ketzin, Germany. J. Applied Geophysics, 71, 109-124. doi:10.1016/j.jappgeo.2010.05.004

Kazemeini, H., Juhlin C., Zinck-Jørgensen K., Norden, B., 2009. Application of the Continuous Wavelet Transform on seismic data for mapping of channel deposits and gas detection at the CO2SINK site, Ketzin, Germany, Geophysical Prospecting, 57,111-123, doi: 10.1111/j.1365-2478.2008.00723.x

Ivandic, M., Yang, C., Lüth, S., Cosma, C and Juhlin, C., 2012. Time-lapse analysis of sparse 3D seismic data from the CO_2 storage pilot site at Ketzin, Germany. Journal of Applied Geophysics, Volume 84, pp. 14–28, DOI 10.1016/j.jappgeo.2012.05.010

IEAGHG, 2012. "Quantification Techniques forCO2 Leakage", 2012/02.

Juhlin, C., Bergmann, P., Giese, R. Götz, J., Ivanmova, A., Juhojuntti, N., Kashubin, A., Lüth, S., Yang, C. and Zhang, F., 2010. Preliminary Results from a Repeat 3D Seismic Survey at the CO2SINK Injection Site, Ketzin, Germany, EAGE 2010, Barcelona.

Juhlin, C., Giese, R., Zinck-Jørgensen, K. , Cosma, C., Kazemeini, H., Juhojuntti, N., Lüth, S., Norden, B., and Förster, A., 2007, 3D baseline seismics at Ketzin, Germany: the CO_2SINK project. Geophysics 72, 5, B121–B132.

Juhlin, C., 1995. Finite-difference elastic wave propagation in 2D heterogeneous transversly isotropic media, Geophysical prospecting, 43, 843-858.

Lüth, S., Bergmann, P., Cosma, C., Enescu, N., Giese, R., Götz, J., Ivanova, A., Juhlin, C., Kashubin, A., Yang, C., Zhang, F., 2011. Time-lapse seismic surface and down-hole measurements for monitoring CO2 storage in the CO2SINK project (Ketzin, Germany). Energy Procedia, 4, 3435–3442, doi:10.1016/j.egypro.2011.02.268.

Norden, B., Forster, A., Vu-Hoang, D., Marcelis, F., Springer, N., & LeNir, I., 2008. Lithological and petrophysical core-log interpretation in the CO2SINK, the European CO2 onshore research storage and verification project, Society of Petroleum Engineers SPE 115247.

Yang,C., Juhlin, C., Enescu, N., Cosma, C. and Lüth, S., 2010. Moving source profile data processing, modelling and comparison with 3D surface seismic data at the CO_2SINK project site, Ketzin, Germany. Near Surface Geophysics, Issue: Vol 8, No 6, pp. 601 – 610, DOI 10.3997/1873-0604.2010022

Yang C, Juhlin C, Fan W, Ivandic M, Luth S, Cosma C., 2012. Estimation of changes in the zero-offset reflection coefficient due to CO_2 injection at Ketzin, Germany. http://urn.kb.se/resolve?urn=urn:nbn:se:uu:diva-163004

Zhang F, Juhlin C, Cosma C, Tryggvason A, Pratt R G., 2012. Cross-well seismic waveform tomography for monitoring CO2 injection : a case study from the Ketzin Site, Germany. Geophysical Journal International. Vol.189(1): pp. 629-646. DOI 10.1111/j.1365-246X.2012.05375.x

Zhang F, Juhlin C, Ivandic M, Luth S., 2012. Application of seismic waveform tomography to monitoring of CO_2 injection: modeling and a real data example from the Ketzin site, Germany. In Press Geophysical Prospecting (ISSN 0016-8025)(EISSN 1365-2478);

Zhang F, Juhlin C, Enescu N., 2011. A feasibility and efficiency study of seismic waveform inversion for time-lapse monitoring of onshore CO2 geological storage sites using reflection seismic geometry. Internal communication, UU.

Zhang F., Juhlin C. and Enescu N., 2010, Seismic waveform inversion as a method for reducing the seismic monitoring effort at CO2 geological storage site. SEG summer research workshop 2010, Snowbird, Utah, USA, Expanded abstracts.

APPENDIX A. Image Point Transform and 3D Image Point Migration

The reflecting interfaces in the rock mass are generally from lithological contacts but can also be from faults, fracture zones and dissolution features. Those reflections from faults and fracture zones usually display relatively weak seismic characters and extensive processing is needed to obtain information on the position of the reflectors from the seismic profiles.

It is necessary to improve the signal-to-noise ratio, so that the later events (e.g. reflections) become visible. As the reflection coefficients are expected to be low, the reflectors cannot usually be identified by amplitude contrast. Phase consistency is a more sensitive indicator.

The Image Point transform is a technique developed for both filtering and interpretation of VSP profiles. Like the τ-*p* method, it is based on the Radon-transform, but while in the τ-*p* transform the traces are stacked along straight paths across the section, in the Image Point transform the stacking is done along paths lining up with travel times corresponding to possible real reflectors. This gives to the Image Point transform two advantages: the signal coherence can be used as effectively as possible to enhance the weak reflections and the transformed section in Image Point Space can be directly used as an interpretation tool, to estimate the strength and position of the reflectors. The approach permits the determination of both the 3-D position and local orientation of the observed reflectors. The physical meaning of the procedure is that each reflection event can be considered as being produced by an “image source” from which the signal propagate to each receiver on a direct path, much like the mirror effect in optics. The mirror on which the image source is formed is a reflecting rock feature, e.g. a fracture zone, as shown in *Figure A-1*.

The Image Point transform of a depth-time profile g(z,t) is obtained by stacking along paths, all possible values of ζ and ρ, i.e. to all possible orientations of the reflecting planes.

The direct transform is expressed as:

$$\Gamma(\zeta,\rho)=\int_{z_{\min}}^{z_{\max}} g(z,t=t_r(\zeta,\rho;z))dz.$$

The function $t_r(\zeta,\rho;z)$ gives the travel times corresponding to the planar reflector specified by ρ and ζ , to the detector at the depth z:

$$t_r=\sqrt{\rho^2+z^2-2z\zeta}/c$$

where

$$\rho=\sqrt{\zeta^2+\xi^2}$$

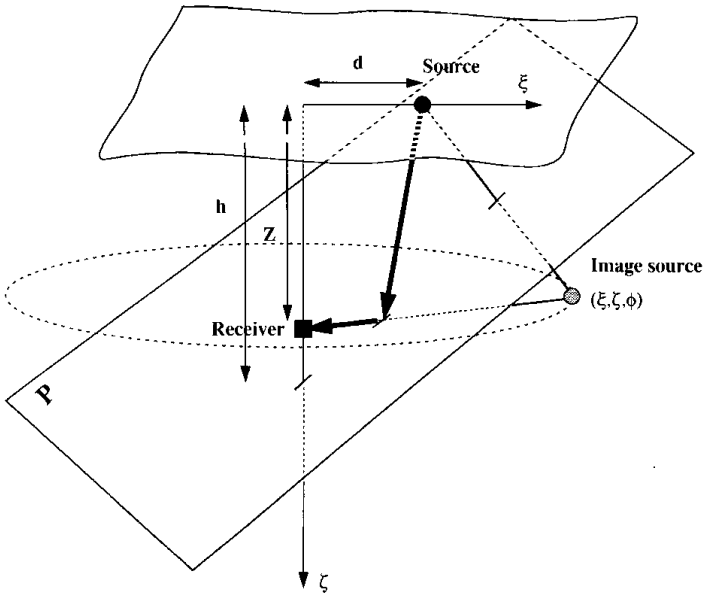

Figure A-1. **Schematic presentation of the Image Point Transform.**

The inverse transform has the following expression:

$$g(z',t') = \frac{d}{dt'} H \int_{\zeta_1}^{\zeta_2} \Gamma(\zeta, \rho = \rho_r(z',t';\zeta))d\zeta$$

where

$$\rho_r = \sqrt{c^2 t^2 - z^2 + 2z\zeta}$$

The derivation and the Hilbert transform H restore the original signal shape.

In the Image Point transform, coherent reflection events collapse to points. Therefore, the signal coherence can be used as effectively as possible to enhance the weak reflections.

Within a certain range for the propagation velocity c, only real reflectors produce coherent patterns along their integration paths. Therefore, the inverse transform from the Image Point space to the depth-time space always leads to a filtered version of the reflection profile.

With the Image Point method, two of the three parameters defining the 3-D position of a reflector can be determined. The reflectors with image points located on a circle perpendicular to the borehole generate equal travel times to all detectors. In order to determine uniquely the 3D position and orientation of a reflector, means should be found to estimate the dip direction. An effective method is to use polarisation analysis.

The reflected signals do not stack constructively along the image point integration path if the reflector is not a plane. This problem is solved by dividing the time-depth section into several overlapping panels, each containing a subset of the traces. For each panel, the Image Point transform is computed independently.

A novel 3D vector imaging technique, the IP (Image Point) pre-stack migration was introduced (Cosma et. al., 2010), which can combine and integrate uneven and sparse data sets measured on surface and in boreholes. Sharper 3D images of both bedding and faults are obtained by this technique.

IP migration is based on a curved-path Radon transform, which characteristically reconstructs reflected wave fields from oriented plane elements instead of point diffractors. The defining property of the IP migration is its ability to resolve images of targets of widely diverse orientations while strongly suppressing or eliminating 'smiling' artifacts characteristic to unevenly covered layouts.

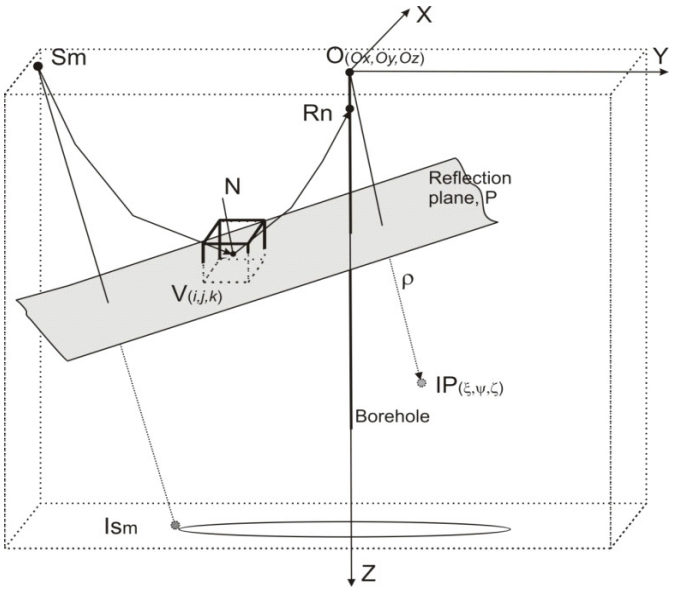

$$\mathbf{\Gamma}(\rho_x,\rho_y,\zeta)=\int \mathbf{G}(V,P(\rho_x,\rho_y,\zeta))\,\mathrm{d}v$$

Direct 3D Image Point transform

$$\mathbf{G}'(V)=\mathrm{H}\frac{\partial}{\partial p}\int \mathbf{\Gamma}(P(\mathbf{N},V))\,\mathrm{d}p$$

Inverse 3D Image Point transform

Figure A-2. Geometry of the 3D Image Point Transform.

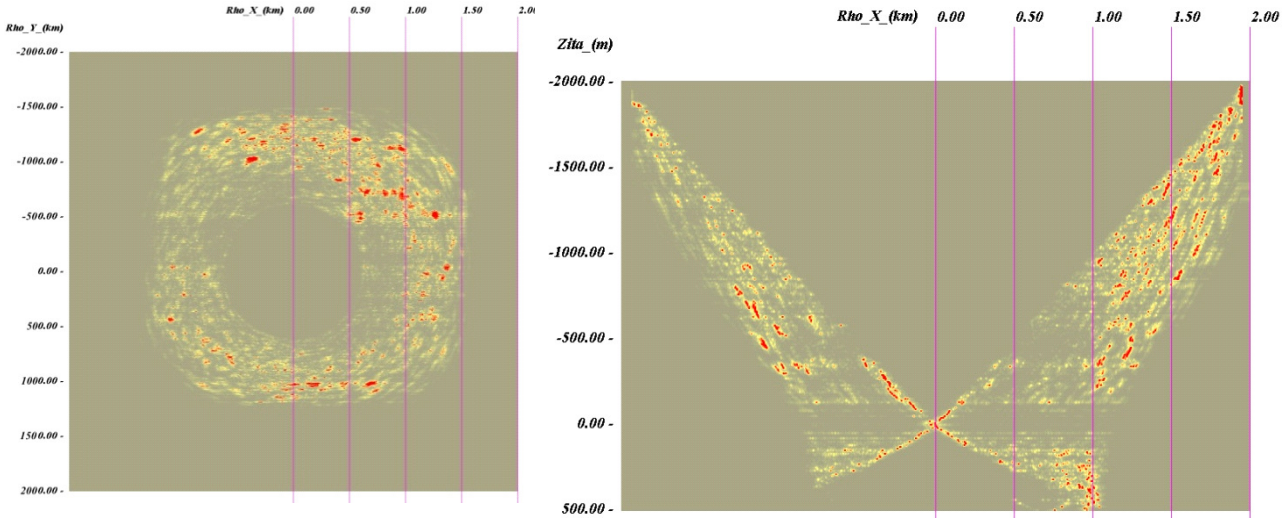

Figure A-3. Image Point Space: View along Z-axis (left), View along X-axis (right).

An accurate velocity model is required, provided by 3D tomographic inversion of all available seismic data: surface, VSP and side-scan.

IP Migration and the 3D CDP Transform

By comparison, to 2-D and 3-D seismic, the offset vertical seismic profiles (OVSP) - be those acquired as VSP or MSP - are more difficult to interpret because they are not usually displayed as a zero-offset sections or volumes. The approach followed so far has been to compute reflector positions and orientations from the travel time functions in depth-time representations and to display them in 3-D as reflection elements. A possible difficulty that this approach may run into is that the decision on what is a true reflector and what it isn't is made before the 3-D display and the interpretive advantage of the perspective view is thus lost.

The IP migration attempts to compute 3-D coordinates of the reflection points corresponding to a class of reflectors defined e.g. by the same strike and dip. The main difference between the IP migration and the VSP-CDP transform explained by (Wyatt and Wyatt, 1984) lays in the fact that with the IP migration the reflection points are computed directly in 3-D, by firstly constructing a 1-dimensional variety to represent the locus of a class of image sources. The locus of the reflection points associated with the set of images and the linear array of detectors forms a 2-dimensional variety, which may, but does not necessarily, follow a plane. If a projection plane is chosen, it can in particular be the one containing the CDP (common depth points), in which case the projection of the IP migration becomes identical with the VSP-CDP transform.

The CDP Transform has been extensively used in petroleum exploration as one of the few imaging methods for OVSP data sets (Gras and Craven, 1998). Similar applications in the hardrock environment are rare. One example is the imaging of steeply dipping volcanic stratigraphy in the vicinity of the Kidd Creek deposit in North – Eastern Ontario by (Eaton et al., 1996).

Unlike with the VSP-CDP transform, with the IP migration the trajectory reconstruction is done directly in 3-D and a constant velocity is not required, the travel time functions being computable, in principle, for any velocity model. Another serious limitation with CDP, namely that the transform does not handle properly data corresponding to other dips and strikes than the value assumed, is elegantly solved by the IP migration, because other orientations than the ones permitted are suppressed by IP filtering. The same applies to diffractors.

Like the general IP transform, the IP Migration is essentially 2-Dimensional and the 3-D geometry of the reflectors cannot be resolved with data from a single profile. The major utility of IP migration lies in the possibility that it opens for interpreting reflectors of a lesser character, belonging to the same orientation classes as a major event used to define the respective class.